MODELING THE BEHAVIOR OF MULTIPATH COMPONENTS PERTINENT TO INDOOR GEOLOCATION

A Dissertation
Submitted to the Faculty
of

WORCESTER POLYTECHNIC INSTITUTE

In partial fulfillment of the requirements for the

Degree of Doctor of Philosophy

in

Electrical and Computer Engineering

by

_____

Ferit Ozan Akgül

May 2010

APPROVED:

_____   _____
Prof. Kaveh Pahlavan, Major Advisor   Prof. Berk Sunar

_____   _____
Prof. Allen H. Levesque   Dr. Bardia Alavi

_____
Prof. Fred J. Looft, Department Head

To my family

Abstract

Recently, a number of empirical models have been introduced in the literature for the behavior of direct path used in the design of algorithms for RF based indoor geolocation. Frequent absence of direct path has been a major burden on the performance of these algorithms directing researchers to discover algorithms using multipath diversity. However, there is no reliable model for the behavior of multipath components pertinent to precise indoor geolocation.

In this dissertation, we first examine the absence of direct path by statistical analysis of empirical data. Then we show how the concept of path persistency can be exploited to obtain accurate ranging using multipath diversity. We analyze the effects of building architecture on the multipath structure by demonstrating the effects of wall length and wall density on the path persistency. Finally, we introduce a comprehensive model for the spatial behavior of multipath components. We use statistical analysis of empirical data obtained by a measurement calibrated ray-tracing tool to model the time-of-arrival, angle-of-arrival and path gains. The relationship between the transmitter-receiver separation and the number of paths are also incorporated in our model. In addition, principles of ray optics are applied to explain the spatial evolution of path gains, time-of-arrival and angle-of-arrival of individual multipath components as a mobile terminal moves inside a typical indoor environment. We also use statistical modeling for the persistency and birth/death rate of the paths.

Acknowledgements

Every researcher looks up to a certain person in his/her own field in order to shape one's own thoughts and determine his/her directions into the future. For me this person has been my advisor, Prof. Kaveh Pahlavan. I would like to express my utmost gratitude for his guidance and support not only in research and in my technical field but also in the matters of life. I believe this is the true meaning of becoming a Doctor of Philosophy and the words uttered by him summarizes this marathon in the best way possible:

'Being a PhD is like being in the olympics. You have to fight for the gold medal! But at the end of the day, it is being at the olympics that matters.'

–Prof. K. Pahlavan on 3/13/2009

I would like to thank Worcester Polytechnic Institute for providing the environment and support, Draper Laboratory and Skyhook Wireless for their funding that made most parts of this thesis possible.

I also would like thank the members of my thesis committee, Prof. Allen H. Levesque for always being kind enough to give valuable comments on various parts of my thesis, Dr. Bardia Alavi for his continual assistance on the improvement of this thesis and his quick response whenever I needed support and Prof. Berk Sunar for his guidance and support both technically and socially throughout my studies at WPI. Thanks are also due to Prof. Fred J. Looft for his generous support that made it possible for me to present my work in various technical conferences throughout the world.

I would like to extend my sincere thanks to former and current members of CWINS namely Dr. Mohammad Heidari, Dr. Nayef Alsindi, Dr. Muzaffer Kanaan for introducing me to a new field of research as well as helping me get familiar with the lab, and Yunxing Ye for the extensive measurements we took at WPI and for the times we spent in the lab.

I am also indebted to my friends Kaan Yuksel, Erdinc Ozturk at Intel Corporation and Kahraman Akdemir, Cengiz and especially Deniz Karakoyunlu at WPI for making the time I spent here in Worcester a very memorable one.

Finally, words would be insufficient to express my indebtedness to my family: my brother Onur, my father Azat and my mother Hatice for their moral and physical support through the years that made all this possible.

Contents

List of Figures

List of Tables

Abbreviations and Acronyms

AK	Atwater Kent
AP	Access Point
AOA	Angle-of-Arrival
CDF	Cumulative Distribution Function
CDMA	Code Division Multiple Access
CIR	Channel Impulse Response
DDP	Detected Direct Path
DME	Distance Measurement Error
DOA	Direction-of-Arrival
DP	Direct Path
EKF	Extended Kalman Filter
FCC	Federal Communications Committee
FDP	First Detected Path
FP	First Path
GPS	Global Positioning System
GSM	Groupe Spécial Mobile
IFT	Inverse Fourier Transform
ISI	Inter-Symbol-Interference
K-S	Kolmogorov-Smirnov
LOS	Line-of-Sight

LS	Least Squares
MIMO	Multiple Input Multiple Output
ML	Maximum Likelihood
MPC	Multipath Component
MSE	Mean Squared Error
NLOS	Non Line-of-Sight
OLOS	Obstructed Line-of-Sight
PDF	Probability Density Function
QoS	Quality-of-Service
RF	Radio Frequency
RMSE	Root-Mean-Squared-Error
RP	Reference Point
RSS	Received Signal Strength
RT	Ray Tracing
SDP	Strongest Detected Path
SP	Strongest Path
TDOA	Time-Difference-of-Arrival
TOA	Time-of-Arrival
UDP	Undetected Direct Path
UKF	Unscented Kalman Filter
UWB	Ultra-Wideband
VNA	Vector Network Analyzer
WLAN	Wireless Local Area Network
WPAN	Wireless Personal Area Network
WPI	Worcester Polytechnic Institute
WSN	Wireless Sensor Network

Chapter 1

Introduction

The application of wireless technology in the realm of indoor systems has been one of the popular concepts due to recent advances in high speed communication networks and the interoperability and ubiquity of capable wireless terminals. For achieving high speed communication in indoor areas, higher bandwidth, limited coverage systems have been proposed as opposed to narrow bandwidth, long range outdoor wireless systems. The need for communicating and conducting business within confined areas has created a unique set of challenges for the design and analysis of wireless systems.

Earlier wireless systems aimed at long range communications needed very limited bandwidth just enough to convey the information for the primary application: voice service. Following the advances in digital technology and high speed computers, it has become a necessity to optimize the wireless systems for higher data rates as well as maintaining reasonable coverage to end users. Besides voice, data applications have shown a steep rising trend thanks to faster electronics and smarter hardware design. In order to achieve these high speeds various challenges need to be addressed, especially for indoor environment. The behavior of a wireless channel is much more complex and requires rigorous treatment to be able to develop systems that can perform satisfactorily in these RF

hostile environments. The primary distinction of the indoor environment from outdoor is the confined space cluttered with various materials that give rise to numerous and closely spaced MPCs. The presence of these MPCs very close to each other necessitates the use of much larger bandwidths and advanced equalization techniques in order to minimize the effect of ISI, which makes communication less reliable.

Indoor wireless channel modeling has thus been the focus of recent studies and paved the way for advanced high rate wireless systems such as IEEE 802.11 and MIMO. Although communications applications were at the core of research for both outdoor and indoor systems, the need for locating and tracking assets and people has turned the research direction towards location based systems and the challenges involved when deploying these systems in indoor areas.

The following table gives an overview of both outdoor and indoor channel for wireless communication and localization/positioning applications.

Table 1.1: Overview of indoor and outdoor wireless channel

	Outdoor	Indoor
Channel	- Low number of MPCs	- High number of MPCs
	- Sparse CIR	- Closely spaced CIR
	- Distance-power gradient usually ≤ 2	- Distance-power gradient usually > 2
	- τ_{RMS} high, w_c low	- τ_{RMS} low, w_c high
Communications Applications	- Low bit rate applications	- High bit rate applications
	- Wider coverage	- Limited coverage
e.g	CDMA, GSM	WLAN, MIMO
Localization Applications	- Low bandwidth required	- High bandwidth required
	- Low UDP probability	- High UDP probability
e.g	GPS	UWB TOA

In table 1.1, τ_{RMS} is the delay spread of the wireless channel and w_c is the coherence bandwidth, which are important channel indicators for wireless system design for both communications and localization applications, and UDP is the undetected direct path condition which will be introduced in detail in the coming chapters.

Since the study presented in this thesis is related to indoor localization, our focus will

be on the localization aspects of the indoor wireless channel and we will present channel modeling challenges in the light of these applications.

1.1 Location Awareness

The question "where" might seem simple at first but the answer might not. Throughout the centuries, mankind has always tried to find the right answer to this question in his quest for exploring new lands and navigating the unknown seas. The first sailors relied on particular water currents, landmarks and positions of the celestial bodies to navigate through the waters. With the discovery of compass about 700 years ago, mariners were able to identify their directions. However, the need to get precise position and navigation, primarily for military purposes, led the nations and researchers to develop systems closer to achieving this goal. After the first developments in radio navigation starting in the first half of the 20th century [1], the first successful implementation of such a system came in the form of a global positioning system or GPS, developed by the US military.

1.2 GPS and Outdoor Geolocation

In its 40 years of development and maturity, GPS [2] has become a reliable location finding and tracking system for use not only by military but also by the civilian world. Today, after various advancements in the field such as differential-GPS (DGPS) and Wide Area Augmentation System (WAAS) typical commercial grade GPS receivers can achieve accuracies of 1-5m with DGPS and 3 meters with WAAS. The study in [3] reports DGPS accuracies in the centimeter range. Higher end geodetic and surveying GPS units using carrier phase, dual frequency methods and sophisticated algorithms can achieve centimeter and even sub-centimeter accuracy through GPS ambiguity resolution techniques [4,5].

Following GPS, other countries also started their own satellite positioning projects (EU's Galileo and Russia's GLONASS [6]). Owing to its accurate positioning capability, most industries rely on GPS and the position information obtained via GPS (such as anchor node position information) serves as reference for other small scale localization systems.

Although GPS is a proven and reliable technology, it falls short of expectations for some terrestrial applications where the GPS signals cannot be detected due to obstructions. Satellite signals are attenuated heavily through the atmosphere and further obstruction by trees, heavy fog or manmade structures such as building tops prevent this system to be useful especially for densely populated urban settlements and inside buildings. In order to overcome this issue, researchers turned their attention to land-based positioning and tracking systems such as cellular networks for situations that cannot make use of satellite signals. After the proliferation of cellular based radio communications systems, the FCC mandated mobile phones be located within a certain accuracy using this technology [7]. According to this report, mobile operators should be able to locate phones with 50m accuracy 67% of the time and 150m accuracy 95% of the time for handset based positioning, and 100m accuracy 67% of the time and 300m 95% of the time for network based positioning. Appendix C presents a study conducted in suburban and dense urban areas for the performance analysis of outdoor cellular positioning systems. For the dense urban area we obtained 70m accuracy at 50th percentile and 240m at 90th percentile.

The fundamentals of locating and tracking RF emitting devices differ greatly from those of data communications. In communications, information is transferred from one entity to another and the information carrier might be RF, sound or light. A single link, as long as it is reliable, will be enough to transfer data between the entities. However, locating a device whose location is completely unknown requires a completely different approach than transmitting data.

Localization might be realized in two ways:

1. Geometric methods (Trilateration, triangulation, hyperbolic methods)

2. Fingerprinting methods (Signal mapping)

Geometric methods include techniques that can locate or track devices based on signal properties that are estimated. TOA/TDOA, RSS and AOA are examples of geometric measurement techniques.

Fingerprinting methods require a two-phase approach. In the first phase (also called the off-line phase), a database is formed based on signal parameters and this database is utilized in the second phase to estimate the location. Nearest-neighbor mapping and artificial neural networks are examples of such methods [8]–[11].

The following section focuses on indoor geolocation and presents the challenges engineers face in indoor specific localization systems.

1.3 Indoor Geolocation

In the late 1990s, motivated by a variety of envisioned applications in commercial, public safety, and military settings, indoor geolocation began to attract considerable attention [12, 13]. In commercial applications for residences and nursing homes, there is an increasing need for indoor geolocation systems to track people with special needs, the elderly, and children who are away from visual supervision. Other applications include systems to assist the sight-impaired, to locate instrumentation and other equipment in hospitals, to locate surgical equipment in an operating room, and to locate specific items in warehouses. In public safety and military applications, indoor geolocation systems are needed to track inmates in prisons, and to guide policemen, firefighters, and soldiers in accomplishing their missions inside buildings. More recently, localization has found applications in location-based handoffs in wireless networks, location-based ad hoc network routing, and location-based authentication and security [14]. Given the growing interest

in sensor networks and radio frequency identification (RFID) technologies, one can also envision wider-ranging applications such as locating unwanted chemical, biological, or radioactive material using sensor networks, and tracking specific items such as controlled pharmaceuticals in their containers using RFID tags. The most popular emerging indoor location and tracking systems use information about RF signal properties in large indoor areas. However, location sensing using multiple cameras and ultrasound is also becoming popular for line-of-sight applications within a room.

To implement low-cost RF localization systems, the target object should be an existing traceable device that radiates RF signals and is connected in some manner to a backbone network. There are tens of millions of IEEE 802.11 WLAN network cards, billions of RFID tags, a growing number of IEEE 802.15 WPANs using Bluetooth, UWB, and ZigBee technologies, and several billion cellular phones that are connected in various ways to the Internet and can be used for RF localization. The bandwidths of these devices range from close to 100 kHz in traditional RFID tags to several GHz for emerging UWB devices, providing numerous technical opportunities to implement localization systems with various degrees of precision. The accuracy required for indoor localization also depends on the application, and in indoor areas it varies from a few millimeters for locating surgical equipment in an operating room to as much as a few meters for locating a person or an item of equipment inside a specific room in a large building. RF localization systems locate the target based on the features of the received signal radiated from the device. There are two popular metrics for this purpose: the RSS, which is easy to measure but provides less accurate positioning [15], and the TOA of the DP, which can potentially provide more accurate localization [12, 13, 16, 17].

Currently, robust precise TOA-based localization in multipath-rich indoor areas has remained a challenge facing the research community. The core of this challenge is to understand the cause of unexpected large ranging errors in estimating the TOA of the

DP between the transmitter and the receiver, and finding algorithms that can cope with these errors. Results of wideband measurement and modeling in a variety of indoor areas obtained in the past decade have revealed that large ranging errors are caused by severe multipath conditions and frequent absence of DP in the received signal giving rise to the UDP condition, which will be introduced in chapter 2 [12, 18].

1.4   Motivation

The study presented throughout this dissertation is related to wireless channel modeling pertinent to indoor RF geolocation. Particular emphasis is given to the spatial behavior of the indoor multipath channel when the receiver is in motion with respect to a fixed transmitter and how multipath diversity can be exploited for precise RF ranging and geolocation, especially in UDP environments.

Accurate modeling of indoor propagation for positioning applications would require as much information as possible regarding the features of MPCs. Individual TOAs of MPCs relative to the LOS arrival together with their AOAs, path gains (amplitudes), the total number of MPCs as a function of transmitter-receiver separation and path persistencies along with path birth/death rate need to be known to employ channel aware precise positioning systems that can exploit multipath diversity.

1.5   Contributions and Outline

The primary contribution of this thesis is the modeling of spatial behavior of multipath components for indoor geolocation using multipath diversity. We used the results of dynamic UWB measurements and measurement calibrated RT to model dynamic changes in TOA, AOA and path gain. The existing RF models were primarily designed for com-

munication applications without specific attention to characteristics of MPCs pertinent to indoor geolocation applications such as transmitter-receiver distance. In our model we also include receiver-transmitter distance in the modeling of number of MPCs for a more accurate channel description.

We introduce the concept of "path persistency" together with "path birth" as part of our complete spatial channel model and as a potential tool to aid in precise ranging under harsh RF conditions.

Additionally we have studied the effect of different building architectures to show its effect on path persistency and how system designers can use building specific information to employ site-aware positioning systems to achieve more accurate results.

In summary the contributions of this thesis are:

- System engineering aspects of a typical positioning system

    - Effect of node density on the performance of a typical positioning system

    - MSE profiling as a performance metric for the performance of a typical positioning system

- Channel aspects of a positioning system

    - Multipath diversity as a potential tool for precise ranging in UDP conditions

    - AOA assisted NLOS error mitigation for TOA based systems

    - Complete spatial modeling of MPCs in a typical indoor area (TOA, Path gain, AOA, Distance dependent number of MPCs, Path persistency and path birth)

    - Effect of UDP, system bandwidth and peak detection threshold on number of MPCs and path persistency using an empirical UWB measurement system

    - A new method for UDP identification

The outline of this thesis is as follows: Chapter 2 gives an overview of system engineering and channel modeling aspects of localization. TOA based ranging and localization is also introduced here as well as the bipolar DDP/UDP channel characteristics. We also present a study of the system engineering aspects of positioning systems under UDP conditions and how node density affects TOA estimation and how MSE profiling can be used to obtain a certain positioning goal. Chapter 3 presents a new method in UDP identification. Chapter 4 introduces the concept of path persistency and ranging in the absence of DP. Chapter 5 discusses the effect of building architecture on path persistency. Chapter 6 introduces a study of sensitivity analysis and modeling of MPC characteristics using the results of an empirical measurement campaign. Chapter 7 gives the complete spatial indoor wireless channel model. Finally, chapter 8 concludes the work with some possible future directions.

Appendix A derives the dependency of path persistency on wall lengths and appendix B presents a method to generate floorplans using the slicing tree method. They are a part of chapter 5.

Additionally, appendix C presents the cellular positioning study performed during the author's internship at Skyhook Wireless of Boston.

This thesis draws substantially from results presented previously in:

1. F. O. Akgul, M Heidari, N. Alsindi, K. Pahlavan, "Overview of RF Location Sensing Techniques and Algorithms for WSNs", in Localization Algorithms and Strategies for Wireless Sensor Networks, G. Mao, B. Fidan Eds. Hershey: IGI Global, pp.54-95 [19]

2. K. Pahlavan, F. Akgul, M. Heidari, H. Hatami, J. Elwell and R. Tingley, "Indoor Geolocation in the Absence of Direct Path", IEEE Wireless Magazine, Vol. 13, Issue 6, December 2006 [20]

3. M. Kanaan, F. O. Akgul, B. Alavi, K. Pahlavan, "Performance Benchmarking of TOA-based UWB Indoor Geolocation Systems Using MSE Profiling", 64th Semi-annual IEEE Vehicular Technology Conference, IEEEVTC, fall 2006, Montral, Canada, September 25-28, 2006 [21]

4. M. Kanaan, F. O. Akgul, B. Alavi, K. Pahlavan, "A Study of the Effects of Reference Point Density on TOA-Based UWB Indoor Positioning Systems", 17th Annual IEEE International Symposium on Personal Indoor and Mobile Radio Communications (PIMRC06), Helsinki, Finland, 11-14 Sept. 2006 [22]

5. Heidari, M., Akgul, F. O., and Pahlavan, K., "Identification of the Absence of Direct Path in ToA-Based Indoor Localization Systems", International Journal of Wireless Information Networks, Volume 15, Numbers 3-4, pp. 117-127, December 2008 [23]

6. F. O. Akgul, K. Pahlavan, "AOA Assisted NLOS Error Mitigation for TOA-based Indoor Positioning Systems", IEEE MILCOM, Orlando, FL, 29-31 Oct. 2007 [24]

7. F. O. Akgul, K. Pahlavan, "High Precision Ranging using Temporal TDOA and Multipath Tracking in the Absence of Direct Path", ION GNSS 2007, Fort Worth, TX, 25-28 Sept. 2007 [25]

8. F. O. Akgul, K. Pahlavan, "Path Persistency for High Precision Ranging in Different Building Architectures", 18th Annual IEEE International Symposium on Personal Indoor and Mobile Radio Communications (PIMRC07), Athens, Greece, 3-7 Sept. 2007 [26]

9. Y. Ye, F. Akgul, K. Pahlavan, "Dynamic Behavior of UWB Channel Pertinent to Indoor Geolocation", IEEE ICUWB, Vancouver, CA, Sept. 2009 [27]

10. Y. Ye, F. Akgul, K. Pahlavan, "Effect of Bandwidth Multipath Parameters Pertinent to Indoor Geolocation", IEEE Wamicon, Clearwater, FL, April 2009 [28]

11. F. O. Akgul, K. Pahlavan, "A New Ray Optical Statistical Model for Multipath Characteristics Pertinent to Indoor Geolocation", IEEE WCNC, Budapest, Hungary, April 2009 [29]

12. F. O. Akgul, K. Pahlavan, "A Novel Statistical AOA Model Pertinent to Indoor Geolocation", Journal of Geographic Information System, vol.2, no.1, pp.45-48, January, 2010 [30]

13. F. O. Akgul, K. Pahlavan, "A Model for Spatial Behavior of Multipath Components Pertinent to Indoor Geolocation Using Ray Optics", Submitted to IEEE Vehicular Transactions [31]

14. F. O. Akgul, K. Pahlavan, "A New Spatial Path Persistency Model for TOA-based Indoor Geolocation", IEEE Communication Letters, vol.13, no.4, March 2009 [32]

15. F. Akgul, K. Pahlavan, "Location Awareness for Everyday Smart Computing", ICT'09, Marrakech, Morocco, May 2009 [33]

Chapter 2

Background

In this chapter, we discuss the system engineering and channel aspects of indoor positioning systems. A brief survey of channel models is also presented. This chapter draws substantially from results presented previously in: [19]–[22].

2.1 System Engineering Aspects

2.1.1 Overview of a Localization System

A typical localization system consists of mobile terminals that need to be located/tracked, beacon or anchors serving as RPs, a central processing station that implements the positioning algorithm and keeps track of all the terminals as well coordinates data communications and a higher layer system that shows the results of positioning or tracking, such as an LCD panel. Figure 2.1 shows the components of such a localization system. The system might use different ranging metrics for obtaining the position information. The most common of these metrics are RSS, TOA/TDOA and AOA. RSS and TOA might be considered as ranging metrics since ranging information can be obtained from these signal parameters. The nodes will need at least three ranging estimates from different an-

chors to be able to obtain a position fix. In the case of AOA, two different AOA estimates from two anchors will suffice to obtain a location fix. More details will be given for each of these techniques in the coming sections.
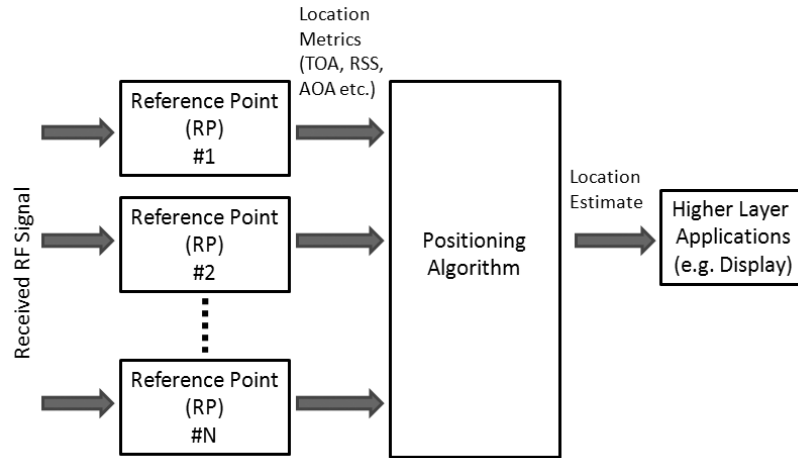
Figure 2.1: High level architecture of a typical positioning system

2.1.2   Distance and Position Estimation Metrics

As mentioned in the previous section, a localization system needs to obtain range estimates from fixed anchors or reference points in order to estimate the location of a node. Ranges estimates can be obtained using different metrics. RSS and TOA/TDOA are examples of such techniques whereas AOA is a position estimation metric.

RSS

As the RF signal is radiated by a transmitter, its energy experiences loss that is proportional to the distance the signal travels. A common model based on single-path radio propagation is given by

$$P_r(dB) = P_t(dB) - 10\alpha log_{10}d \tag{2.1}$$

13

where P_r (dB) and P_t (dB) denote the received and transmitted signal powers in dB. α is the distance-power gradient (or equivalently path-loss coefficient) and is dependent on the propagation environment. For free space, $\alpha = 2$. A wide range of values are possible for α, i.e. for a brick construction office environment α is reported to be 3.9 or for a laboratory environment with metal-faced partitioning it is found to be 6.5 [14].

Other empirical models have also been developed based on extensive measurements in various environments. The author in [34] proposed a path-loss model for multi-floor buildings. Technical working group of TIA/ANSI JTC recommended an indoor path loss model [35] for PCS applications. Apart from the indoor model, the same group proposed micro and macro-cellular models for outdoor applications. Other popular models for outdoor environments are the models in [36]–[38].

Either by using the simple radio-propagation model or the more complicated empirical models, distance information can be obtained from the received signal power given the transmitted signal power. Although this method can be easily applied since almost all RF wireless devices can report received signal strength, its accuracy is not always acceptable due to the stochastic variation of the channel. The path loss models discussed in this section are deterministic models that do not consider the fading and shadowing effects. At any time instant, the signal level experiences slow and fast fading caused by local scatterers and the movement of the receiver node. Slow fading is also called "Shadow fading" and it is generally modeled as a zero-mean normal variable, X(dB), in the logarithmic scale. Hence shadows are log-normally distributed. The pdf for the log-normal distribution is given as:

$$f(x) = \frac{1}{x\sigma\sqrt{2\pi}}e^{-\frac{(ln(x)-\mu)^2}{2\sigma^2}} \tag{2.2}$$

where μ and σ are the mean and standard deviation respectively. Hence the received power can be given as

14

$$P_r(dB) = P_t(dB) - 10\alpha log_{10}d + X \qquad (2.3)$$

Due to this fluctuating behavior of received signal power, accurate ranging measurements are not always possible hence leading to lower accuracy position estimation. In fact, the accuracy of such estimation is lower bounded by its Cramer-Rao lower bound (CRLB). CRLB basically specifies the lower bound on the variance of estimation. For the simplistic RSS model this bound has been given by [39] as:

$$\sigma_{RSS} \geq \frac{ln(10)}{10}\frac{\sigma_{sh}}{\alpha}d \qquad (2.4)$$

Here, σ_{RSS} is the standard deviation of RSS estimation, σ_{sh} is the variance for shadow fading, d is the actual distance between the transmitter and the receiver and α is the power-distance gradient.

AOA

AOA information from two different anchors might be used to determine the position of a node by using triangulation as shown in figure 2.2. AOA estimation is also referred to as DOA estimation, direction finding or bearing estimation in many contexts and has been researched extensively in the literature [40]–[45]. A common method for AOA estimation is by using special structures called uniform linear arrays (ULA) [46]. The n elements of an ULA with spacing d can be used to estimate the DOA of an RF signal based on the following relation:

$$\theta = arcsin(\frac{c\Delta t}{d}) \qquad (2.5)$$

where θ is the angle at which the signal is impinging upon the ULA, c is the speed of light, Δt is the time difference between the arrivals of the signal at consecutive array

elements and d is the spacing between consecutive elements.
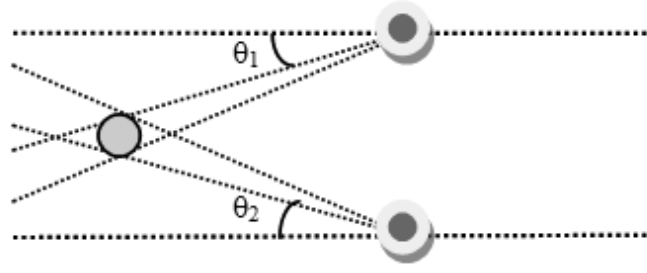
Figure 2.2: Triangulation of a node by two anchors

To achieve finer results by using a certain antenna array configuration, one can employ super-resolution techniques. Although various methods are available in literature, most common ones are MUSIC [47] and ESPRIT [48] and their variations [49, 50]. Authors in [51] report angular estimation variance of $1°$ with 0dB SNR and down to $0.01°$ with SNRs of about 40 dB.

The performance bounds for AOA estimation can also be studied to derive the CRLB. The bound for AOA is formulated to be [52]

$$\sigma_{AOA} = \frac{c\sqrt{2BN_0}}{N\Delta 2\pi f_c sin(\theta)AA_T} \tag{2.6}$$

where σ_{AOA} is the standard deviation for AOA estimation, c is the speed of light, B is the bandwidth of the signal, N_0 is the noise spectral density, N is the number of elements of the ULA, Δ is the spacing between the elements and A is the channel coefficient. A_T and f_c are respectively the amplitude and carrier frequency of the source signal $x(t)$ denoted as

$$x(t) = A_T cos(2\pi f_c t) \tag{2.7}$$

The SNR of the signal can be expressed as

16

$$SNR = \frac{A^2 A_T^2}{BN_0} \tag{2.8}$$

so we can rewrite equation (2.6) as

$$\sigma_{AOA} = \frac{c\sqrt{2}}{N\Delta 2\pi f_c sin(\theta)\sqrt{SNR}} \tag{2.9}$$

From equation (2.9), it can be seen that the CRLB is inversely proportional to the number of elements N, f_c and SNR. Thus having a high SNR and high frequency signal like an UWB signal as well as a high number of array elements give higher resolution AOA estimation.

TOA

Another distance estimation method is the TOA method in which the range is estimated based on the time the signal spends traveling from the transmitter to the receiver. Since the speed of RF propagation is very well known in both free space and air, it gives a direct estimation of the distance between the transmitter and the receiver once the travel time is estimated. When TOA systems are considered, the only important parameter that needs to be estimated correctly in a multipath propagation environment is the TOA of the LOS path or the DP. Other multipath components are not important for ranging and localization purposes except for the cases when the DP is not available. This condition will be investigated in detail in the section "channel modeling aspects". The basic equation needed to obtain the distance is given as

$$d = \tau_{DP}c \tag{2.10}$$

where d is the distance estimate, τ_{DP} is the TOA of the DP and c is the speed of light. Accurate TOA estimation needs perfect synchronization between the clocks of the
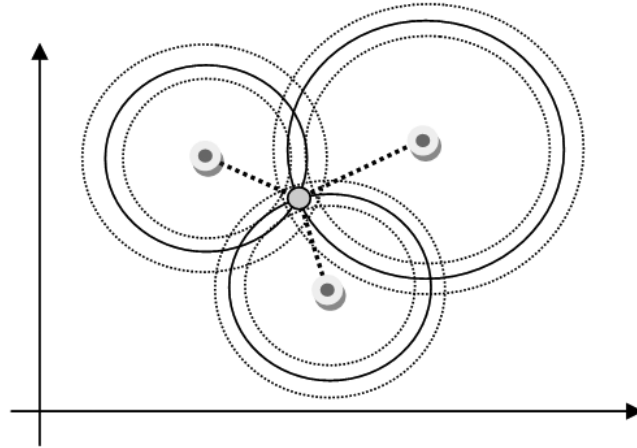
Figure 2.3: Trilateration of a node by three anchors (RSS and TOA)

transmitter and the receiver. Clock synchronization might be achieved by regular data exchange between the transmitter and the receiver or an additional anchor for correcting the clock bias. Although 3 anchors are necessary to obtain position, a 4th anchor will be needed for time correction. This method is readily applied for the GPS in which a 4th satellite is used to compensate for the receiver clock bias. The TOA location estimation is depicted in figure 2.3 where a perfect synchronization is assumed between the transmitters and the receiver. Same procedure also applies to the RSS method in which individual distance estimates are also used for position fixing. The dotted circles denote the uncertainty in range estimation hence leading to an area for the possible location of the receiver between the three estimation circles, rather than a single point.

2.1.3   Practical TOA Ranging and Localization

In order to successfully apply TOA methods to practical systems especially for indoor ranging and positioning we need to use higher bandwidth systems in order to resolve dense MPCs. One such solution is the use of UWB systems.

Due to recent advances in UWB signaling and hardware and its potential for accurate

ranging, TOA based ranging systems utilizing UWB signals have gained particular popularity [17, 53, 54]. On the other hand, the knowledge gained by the implementation and challenges of the now widely used GPS system has been instrumental in the advancement of these TOA systems. Hence borrowing the algorithmic developments from GPS and applying them to indoor environment paved the way for the deployment of UWB systems for localization applications. Next we will discuss some fundamental aspects of TOA estimation and ranging.

TOA Estimation   Several methods are available to estimate the TOA. The traditional methods of estimation are the IFT and ML estimations. The latter one is also called the cross-correlation method.

In the IFT method, observed frequency domain channel response is transformed into time-domain to obtain the time-response of the channel (figure 2.4). The delay value of the DP is then used to calculate the distance.
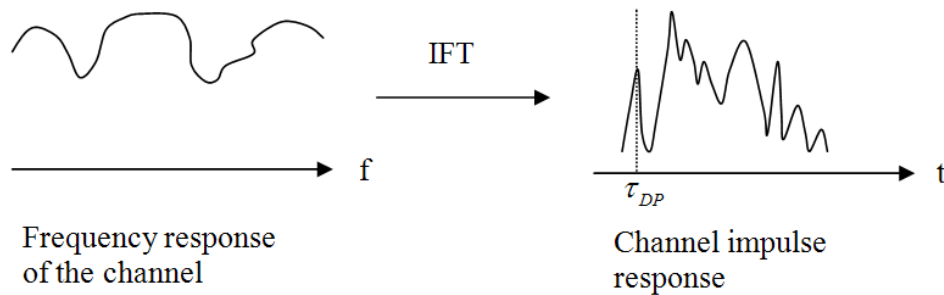
Figure 2.4: IFT operation for obtaining CIR

In the ML method, the following signal model is assumed for the estimation of TOA [55]

$$r(t) = s(t - \tau) + w(t) \tag{2.11}$$

19

Here $r(t)$ is the received signal, $s(t)$ is the transmitted signal, τ is the delay and $w(t)$ is noise modeled as AWGN. The signal at the receiver is basically a delayed version of the signal plus noise. ML dictates that maximum possible cross-correlation of the transmitted and the received signal occurs at the actual delay of the signal shown as [55, 56]

$$\frac{d}{d\tau}\left(\int_{T_0} r(t)s(t-\tau)dt\right)\bigg|_{\tau=\hat{D}_{ML}} = 0 \qquad (2.12)$$

To obtain the delay estimate, τ is varied over a range of delay values and the value of τ that gives the maximum of the cross-correlation (or equivalently makes the derivative of the cross-correlation equal to 0) becomes the distance estimate. A block diagram is also given in figure 2.5 to show the implementation of this method.
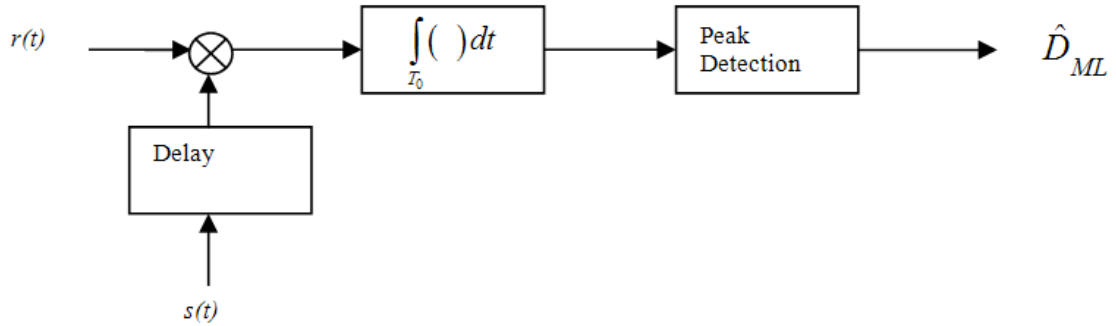
Figure 2.5: ML TOA estimation (reproduced from [55])

In the case of single path TOA estimation as applied to equation (2.11), CRLB is computed to be

$$\sigma_{\hat{D}}^2 \geq \frac{1}{8\pi^2 \text{ SNR } BT_0 f_0^2 + B^2/12} \qquad (2.13)$$

where $\sigma_{\hat{D}}^2$ is the variance of TOA estimate, $B = f_2 - f_1$, $f_0 = (f_2 + f_1)/2$, f_1 and f_2 are the 3dB low and high frequency points and f_0 is the center frequency. T_0 is the observation time. From equation (2.13), it is easy to see that the bound is inversely proportional to the SNR, the signal bandwidth and observation time.

20

Similar to the AOA case, super-resolution methods might be used to extract indistinguishable peaks from the channel response in time-domain. This method has been shown to be effective in both wideband and narrow band TOA estimation methods [57, 58] making these methods superior to traditional ML and cross-correlation methods.

Peak Detection Strategies for TOA based Systems

In this part, we present the two most commonly used methods for obtaining ranging measurements, which have also been outlined by [59]. In the following, τ_{sel} denotes the estimated TOA.

Detection of the First Peak This method relies on the detection of the first available peak in the CIR. As long as the first path power is above the detection threshold of the system, the method gives the best possible results for ranging. However, accurate detection depends on high SNR which is not always possible. The path decision can be expressed as

$$\tau_{sel} = \tau_i | i = \operatorname*{argmin}_{p} \tau_p \tag{2.14}$$

where τ_p is the TOA for the pth path.

Detection of the Strongest Peak In this method, the path with the strongest power is detected and its TOA is considered as the ranging estimate between the transmitter and the receiver. Detecting the strongest peak is easily implementable when compared with the first method; however ranging accuracy is not always acceptable since the strongest path may not always be the DP. Most practical receivers implementing this method are S-rake receivers [60]. Path decision in this case is

$$\tau_{sel} = \tau_i | i = \operatorname*{argmax}_{p} P_p \tag{2.15}$$

21

where P_p is the power of the pth path.

TDOA

TDOA, also known as hyperbolic positioning, is a method whereby the receiver calculates the differences in the TOAs from different RPs. By using this method the clock biases between the transmitters and receivers are automatically removed, since only the differences between the TOAs from two transmitters are only considered. The estimation using TDOA is shown in figure 2.6.
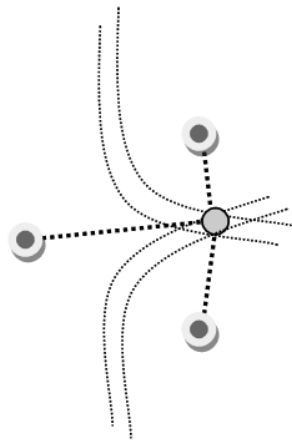
Figure 2.6: Hyperbolic positioning of a node by three anchors (TDOA)

RSS, TOA/TDOA and AOA can be regarded as geometric estimation methods for which we do not have a priori information about environment. Next we discuss the mapping techniques with which a certain signal database is produced for position estimation.

Mapping techniques

Mapping or fingerprinting techniques are also widely studied for their robustness in terms of performance and some advantages in comparison to geometric methods. The fingerprinting methods employ a two-step approach. The first step involves the construction

22

of the signal map for a desired environment (also called the offline phase), the second step is the actual positioning step (online phase). These techniques inherently capture all environment related propagation effects like multipath, shadowing, scattering etc. and hence might be used for applications where geometric methods fall short of expectations. However due to extensive measurement and mapping involved in this approach, it might not be preferred for large areas where it may not be feasible. Additionally the structural changes in the environment might necessitate remapping for the affected regions of the database [10, 15, 61]. The two most commonly used mapping methods are the RSS mapping and CIR mapping. In RSS mapping, a receiver terminal is taken to almost every feasible part of an area that is intended to be mapped and signal power from multiple anchors are recorded into the database. Once mapping is done, actual positioning is obtained by comparing the RSS in online phase to one of the mapped points. The algorithms employed for this purpose are mostly k-NN or statistical location estimation algorithms [8, 62, 63]. Another application is the mapping of CIR for desired locations. The unique characteristics of the CIR, such as RMS delay spread, average power etc. might then be used for comparison [10, 11]. The authors in [10] also discusses the use of neural networks for position estimation.

Table 2.1 gives an overall comparison of different positioning methods and summarizes the advantages and disadvantages of these approaches.

Tracking and Dynamic Monitoring

Most of the time, the nodes to be located are mobile and hence it becomes essential to determine the location of these mobile nodes periodically. This real-time periodic location update is also called "tracking". Tracking keeps a history of the location information and hence is considered as a dynamic methodology for the localization problem. As opposed to blind positioning, which is based either on geometric or fingerprinting method

Table 2.1: Comparison of different positioning methods

Geometric Methods	Advantages	Disadvantages
RSS	- Simple to implement (most wireless devices report power) - Not sensitive to timing and RF bandwidth	- Not accurate - Requires models specific to application case and environment
AOA	- Only requires 2 anchors for localization	- DP blockage and multipath affects accuracy - Requires use of antenna arrays/smart antennas - Accuracy is dependent on RF bandwidth
TOA/TDOA	- Accurate ranging/localization can be obtained - Can be scaled to a multitude of applications	- Accuracy is dependent on RF bandwidth - DP blockage might cause large errors
Mapping Methods	- Captures all channel related parameters hence resilient to DP blockage	-Requires extensive database construction/training

and which basically requires locating the node without any prior position information, tracking makes use of location history to estimate the future positions. This might be obtained by various methods. The most popular of these approaches is to employ a Kalman Filter [64], which is a recursive filter that estimates the state of a system in the presence of noisy measurements. However, for most systems that do not exhibit linear behavior, Kalman filtering is not an effective solution. For these non-linear systems other types of filtering such as EKF [65] and UKF [66] are preferred. EKF is particularly useful for nonlinear but differentiable systems. It is a first order approximation for the nonlinear filtering problem. UKF, on the other hand is applicable to highly nonlinear systems and produces more accurate results than EKF. Another advantage of UKF over EKF is that UKF does not require the computation of Jacobians that are needed for EKF. Hence it is more practical from an implementation point of view.

Another method is to use dead reckoning [67, 68] which estimates the future position based on current speed, bearing and elapsed time. Inertial navigation systems are based on this principle. Even though these systems might obtain estimates for incomplete mea-

surements, error propagation is a major concern for prolonged duration of information absence. Hence these tracking methods should be complemented with other true positioning approaches for a more complete positioning system design.

Since the focus of this thesis is precise positioning in the absence of DP we put more emphasis on TOA based systems. Next section discusses the challenges involved with these systems.

2.2 Channel Modeling Aspects

2.2.1 Challenges for the TOA-Based Systems

One major challenge facing the high precision TOA systems is the obstruction of the DP in the channel profile. Since the DP is the true indicator of the range between the transmitter and the receiver, its obstruction by various means such as metallic or thick concrete walls will lead to substantial ranging errors. This particular obstruction of the DP leads to a specific channel impairment that has been named as the undetected direct path (UDP) condition [12, 69]. To understand the effects of DP obstruction, it is convenient to consider the commonly used mathematical expression for channel impulse response at this point. This model takes into account the MPCs that arrive at the receiver via different propagation mechanisms such as reflection, transmission or scattering and is given as:

$$h(t, \tau) = \sum_{i=1}^{L} \beta_i \delta(t - \tau_i) e^{j\phi_i} \qquad (2.16)$$

where h denotes the CIR, L is the number of MPCs, β_i is the gain(amplitude), τ_i is the TOA and ϕ_i is the phase of the ith arriving path respectively. The DP might be characterized as the path having gain β_1, TOA τ_1 and phase ϕ_1. In this case the range between the receiver and the transmitter will be

$$d = \tau_1 c \tag{2.17}$$

However, we should also point out that equation (2.16) is the basic channel model based on Turin's model [70]. Later in the thesis, we will expand this model to incorporate number of paths, as well as AOA and spatial movement of the receiver.

When the DP is blocked or cannot be detected, the indirect paths will be detected giving rise to substantial ranging errors. Figure 2.7 and figure 2.8 show real world example channel profiles for both DDP and UDP obtained using a 1GHz bandwidth UWB signal. In the DDP case there is only 50cm of ranging error that can be attributed to the limited bandwidth (multipath error) of the signal, whereas the UDP case (by inserting a metallic shield in between the transmitter and receiver) introduces more than 2m of ranging error for the same setup.
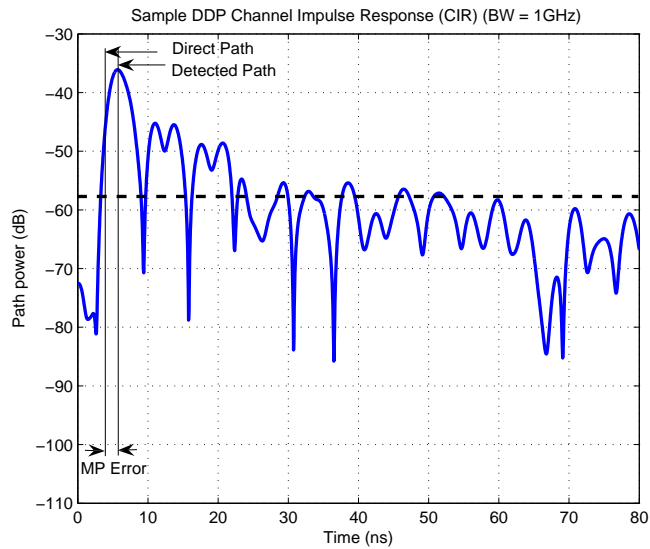
Figure 2.7: Sample DDP channel profile

26
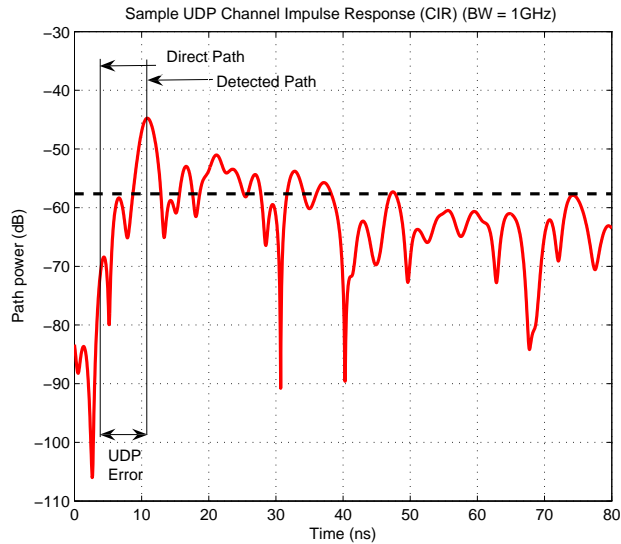
Figure 2.8: Sample UDP channel profile

2.3 Two sample study: MSE Profiling and Node Density

In order to show the effect of UDP on basic positioning systems we have also carried out two studies in a typical setup. The first study explores the MSE profiling of wireless channel and the second study tries to evaluate the effect of RP density on localization performance in a typical indoor positioning setup (such as a WSN). Both of these studies have been carried under the effect of UDP channels.

2.3.1 MSE Profiling

Due to the site-specific nature of indoor radio propagation, the very occurrence of UDP conditions is random and is best described statistically [71]. That being the case, the accuracy of the location estimate will also need to be characterized in the same manner. The accuracy of the location estimate can be viewed as a measure of the QoS provided by the geolocation system. Different location-based applications will have different require-ments for accuracy. In a military or public-safety application (such as keeping track of the

locations of fire-fighters or soldiers inside a building), high accuracy is desired. In contrast, lower accuracy might be acceptable for a commercial application (such as inventory control in a warehouse). In such cases, it is essential to be able to answer questions like: "What is the probability of being able to obtain an MSE of $1 \ m^2$ from an algorithm x in any building configuration?" or "What algorithm should be used to obtain an MSE of $0.1 \ cm^2$ in any building configuration?". Answers to such questions will heavily influence the design, operation and performance of indoor geolocation systems. In this study, we propose the use of the *MSE Profile* to answer these kinds of questions and illustrate its use with examples.

Related Work on Performance Metric

Foy [72] used the covariance matrix of the position estimation error as a performance metric for the evaluation of Taylor-Series algorithm for geolocation. Torrieri [73] formally defined and used the circular error probability (CEP), which is a measure of the uncertainty in the location estimate $\hat{x}$, relative to its mean, $E\{\hat{x}\}$. The calculation of the CEP is, in general, quite complicated. This issue can be alleviated by making suitable approximations. However, from a QoS perspective, the most we can say after calculating the CEP is that the estimate is likely to be within $\hat{x} + CEP$ with probability $1/2$. The CEP, therefore, will only be of limited use in answering the types of questions given in the previous section.

The work of Deng and Fan [74] and others working in the *E-911* field bears the closest resemblance to our work in the sense that it considers the CDF of the MSE in order to assess the performance of outdoor cellular positioning systems in relation to E-911 requirements outlined by the FCC. However, this cannot be directly applied to our work, as we specifically consider the effect of varying UDP conditions on UWB indoor geolocation system performance. Therefore, to the best of our knowledge, our approach to

performance analysis of such systems is unique.

UDP Conditions and MSE Profile

UDP conditions generally occur in cases where there are multiple walls and/or metallic objects between the transmitter and the receiver. As a result, the DP can experience severe fading [12, 75]. It has also been observed that UDP conditions tend to occur along coverage boundaries or areas with coverage deficiencies [76]. As mentioned above, UDP occurs only on occasion and when it does, it is the dominant source of error for distance measurements. However, the DDP error is always present.

Based on extensive UWB measurements, a DME model is introduced in [71]. The model is given by:

$$
\hat{d}_i = \begin{cases} d_i + \xi_{DDP,w} log(1 + d_i) & \text{DDP case} \\ \\ d_i + \xi_{DDP,w} log(1 + d_i) + \xi_{UDP,w} & \text{UDP case} \end{cases} \tag{2.18}
$$

where $\hat{d}_i$ is the observed distance measurement from the i-th RP, and $\xi_{DDP,w}$ and $\xi_{UDP,w}$ are random variables that characterize the DDP and UDP-based DME respectively. The distributions of $\xi_{DDP,w}$ and $\xi_{UDP,w}$ have been observed to be Gaussian and dependent on bandwidth, i.e, $\xi_{DDP,w} = \mathcal{N}(m_{DDP,w}, \sigma_{DDP,w}^2)$ and $\xi_{UDP,w} = \mathcal{N}(m_{UDP,w}, \sigma_{UDP,w}^2)$ where the means (denoted by $m_{DDP,w}$ for ξ_{DDP} and $m_{UDP,w}$ for ξ_{UDP}) and standard deviations (denoted by $\sigma_{DDP,w}$ for $\xi_{DDP,w}$ and $\sigma_{UDP,w}$ for $\xi_{UDP,w}$) are a function of the system bandwidth, w, used to make the TOA-based distance measurements (hence the subscript w). The parameters for the distributions, as a function of the bandwidth w, are listed in Table 2.2.

Additionally, it has been determined through measurements that the probability of UDP occurrence $P_{UDP,w}$ increases as the bandwidth is increased [71]. Observations in-

Table 2.2: Parameters for DDP and UDP-based DME

$w(MHz)$	500	1000	2000	3000
$m_{DDP,w}$ (m)	0.21	0.09	0.02	0.004
$\sigma_{DDP,w}$ (cm)	26.9	13.6	5.2	4.5
$m_{UDP,w}$ (m)	1.62	0.96	0.76	0.88
$\sigma_{UDP,w}$ (cm)	80.87	60.45	71.53	152.21
$P_{UDP\_far,w}$	0.33	0.62	0.74	0.77
$P_{UDP\_close,w}$	0.06	0.06	0.07	0.12

dicate that $P_{UDP,w}$ values also depend on the actual distance between the transmitter and the receiver. Specifically,

$$
P_{UDP,w} = \begin{cases} P_{UDP\_close,w} & d \leq 10 \text{ m} \\ \\ P_{UDP\_far,w} & \text{otherwise} \end{cases} \tag{2.19}
$$

The error modeling introduced here is detailed in [71]. This model can be compared to [77] and has a fundamentally different approach. In [77], the authors developed the model based on Ray-Tracing results and categorized the conditions of the channel as LOS/OLOS, assuming that in the OLOS case, we always have the UDP case. However, the introduced DME model is based on UWB measurement data and classification of the channel as DDP and UDP, as this approach reflects the behavior of the indoor channel in a more realistic manner.

Figure 2.9 shows the general system scenario, where a regular grid arrangement of RPs are assumed to be available. RPs are radio transceivers whose locations are known more or less precisely with respect to some global coordinate system and which perform TOA-based distance measurements to locate a sensor. The use of the regular grid arrangement for the RPs is common in indoor wireless networks, as this approach often provides adequate coverage [78].

Given the variability of the indoor propagation conditions, it is possible that the dis-
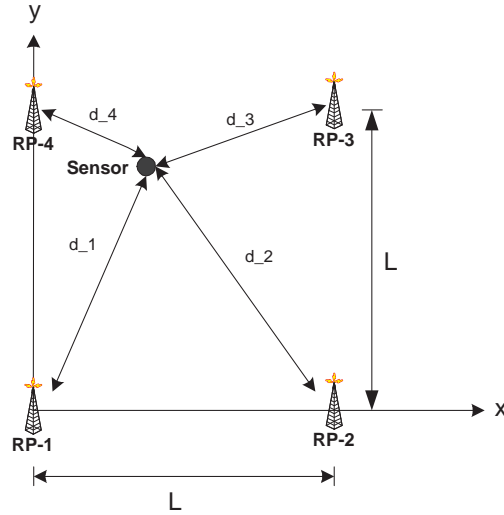
Figure 2.9: General system scenario

tance measurements performed by some of the RPs will be subject to DDP errors, while some will be subject to UDP-based errors. The DDP/UDP errors can be observed in various combinations. For example, the distance measurements performed by RP-1 in figure 2.9 may be subject to UDP-based DME, while the measurements performed by the other RPs may be subject to DDP-based DME; we can denote this combination as *UDDD*. Other combinations can be considered in a similar manner.

Since the occurrence of UDP conditions is random, the performance metric used for the location estimate (such as the MSE) will also vary stochastically and depends on the particular combination observed. For the four-RP case shown in Figure 2.9, it is clear that we will have the following distinct combinations: *UUUU*, *UUUD*, *UUDD*, *UDDD*, and *DDDD*. Each of these combinations can be used to characterize a different type of building environment. The occurrence of each of these combinations will give rise to a certain MSE value in the location estimate. This MSE value will also depend on the specific algorithm used. There may be more than one way to obtain each DDP/UDP combination. If UDP conditions occur with probability P_{udp}, then the overall probability

of occurrence of the *i*-th combination, P_i can be generally expressed as:

$$P_i = \begin{pmatrix} N \\ N_{udp,i} \end{pmatrix} P_{udp}^{N_{udp,i}} (1 - P_{udp})^{N - N_{udp,i}} \tag{2.20}$$

where N is the total number of RPs (in this case four), and $N_{udp,i}$ is the number of RPs where UDP-based DME is observed. Combining the probabilities, P_i, with the associated MSE values for each combination we can obtain a discrete CDF of the MSE. We call this discrete CDF the *MSE Profile*.

Algorithms

As an illustration of the use of the MSE Profile, we investigate the performance of two algorithms using simulations: the Closest-Neighbor with TOA Grid (CN-TOAG) [79,80], and the Davidon LS algorithm [81].

CN-TOAG Algorithm   In essence, the CN-TOAG algorithm [79, 80] estimates the location of the sensor S, by minimizing the following objective function:

$$f(x,y) = \sqrt{\sum_{k=1}^{N} \left(d_k - \sqrt{(x - X_k)^2 + (y - Y_k)^2} \right)^2} \tag{2.21}$$

where (X_k, Y_k) is the location of the *k*-th RP, d_k is the observed distance measurement from the *k*-th RP and (x, y) is the unknown location of the sensor to be estimated. The estimated location is the one that minimizes equation (2.21). In order to find the minimum, one needs to solve the following partial differential equation:

$$\nabla f(x,y) = \mathbf{0} \tag{2.22}$$

Due to the complexity of $f(x, y)$ in (2.21), it is not feasible to solve (2.22) analytically.

Therefore, the CN-TOAG algorithm tries to solve it numerically using the concept of a TOA grid [80]. The size of the grid, as given by the spacing between grid points, h, is a major determinant of performance for this algorithm. Specifically, values of h below a certain value can result in better performance than the LS algorithm [79].

Davidon Least-Squares Algorithm   The particular instance of the LS algorithm that has been used for our evaluations is the one by Davidon [81], which attempts to minimize the objective function:

$$
\begin{aligned}
f(\mathbf{x}) &= f(x, y) \\
&= \sum_{k=1}^{N} \left(d_k - \sqrt{(x - X_k)^2 + (y - Y_k)^2} \right)^2
\end{aligned}
\tag{2.23}
$$

in an iterative manner using the following relation:

$$
\mathbf{x}_{k+1} = \mathbf{x}_k - \mathbf{H}_k \mathbf{g}(\mathbf{x}_k)
\tag{2.24}
$$

where $\mathbf{H}_k$ represents an approximation to the inverse of the Hessian of $f(\mathbf{x})$, $\mathbf{G}(\mathbf{x})$, which is defined as:

$$
\mathbf{G}(\mathbf{x}) = \begin{pmatrix} \frac{\partial^2 f}{\partial x^2} & \frac{\partial^2 f}{\partial x \partial y} \\ \frac{\partial^2 f}{\partial y \partial x} & \frac{\partial^2 f}{\partial y^2} \end{pmatrix}
\tag{2.25}
$$

and $\mathbf{g}(\mathbf{x})$ is the gradient of $f(\mathbf{x})$, defined as:

$$
\mathbf{g}(\mathbf{x}) = \nabla f(\mathbf{x})
\tag{2.26}
$$

The following relation defines when the computations will be terminated:

33

$$\rho_k = (\mathbf{g}(\mathbf{x}_{k+1}))^T \, \mathbf{H}_k \, (\mathbf{g}(\mathbf{x}_{k+1})) \qquad (2.27)$$

so that the iterations will stop when $\rho_k \leq \epsilon$, where ϵ is a small tolerance value.

Performance Evaluation & Discussion

Simulation Platform We consider the system scenario in Figure 2.9 with $L = 20$ m for each algorithm. A total of 1000 uniformly distributed random sensor locations are simulated for different bandwidth values. In line with the FCC's formal definition of UWB signal bandwidth as being equal to or more than 500 MHz [82], we will present our results for bandwidths of 500, 1000, 2000, and 3000 MHz. For each bandwidth value we also simulate different combinations of UDP and DDP-based DMEs for each RP, specifically *UUUU*, *UUUD*, *UUDD*, *UDDD*, *DDDD*. Once a sensor is randomly placed in the simulation area, each RP calculates TOA-based distances to it. The calculated distances are then corrupted with UDP and DDP-based DMEs in accordance with equation (2.18). The positioning algorithm is then applied to estimate the sensor location. Based on 1000 random trials, the MSE is calculated for each bandwidth value and the corresponding combinations of UDP and DDP-based DMEs. The probability of each combination is also calculated. For example, take the combination *UUUU* for a bandwidth of 3000 MHz, where two of the RPs are assumed to be far from the sensor, and the other two are assumed to be close. Using the values for $P_{udp,close}$, and $P_{udp,far}$, we can obtain the probability of the combination as 0.0085.

As noted in [80], the performance of the CN-TOAG algorithm is dependent on the size of the TOA grid, as determined by the the bin size, h, which for the purposes of this study, was varied between 1.25 m down to 0.3125 m for a total of three different values.

Results The results are shown in figures 2.10, 2.11, 2.12, and 2.13. Figures 2.10 and 2.11 show the MSE Profiles for the LS and CN-TOAG algorithms respectively. From these plots, we observe that as the bandwidth increases from 500 MHz to 2000 MHz, the range of MSE Profile values gets smaller. This correlates with the findings of [76], where it has been observed that the overall DME goes down over this specific range of bandwidths. Above 2000 MHz, however, the MSE Profile becomes wider as a result of increased probability of UDP conditions [76], which increases the overall DME. This, in turn, translates into an increase in the position estimation error for both algorithms.

Using the MSE Profile, we can gain insight into the MSE behavior of a given algorithm under varying amounts of UDP (i.e. different building configurations) by calculating the mean and the variance of the MSE for a given bandwidth value. The results of these calculations are shown as a function of bandwidth in Figures 2.12 and 2.13. These results clearly indicate that CN-TOAG can outperform LS as long as $h \leq 0.3125$ m. In addition, there appears to be an optimal bandwidth for both algorithms where the average MSE is minimum. Our results indicate that this bandwidth value is 1000 MHz.
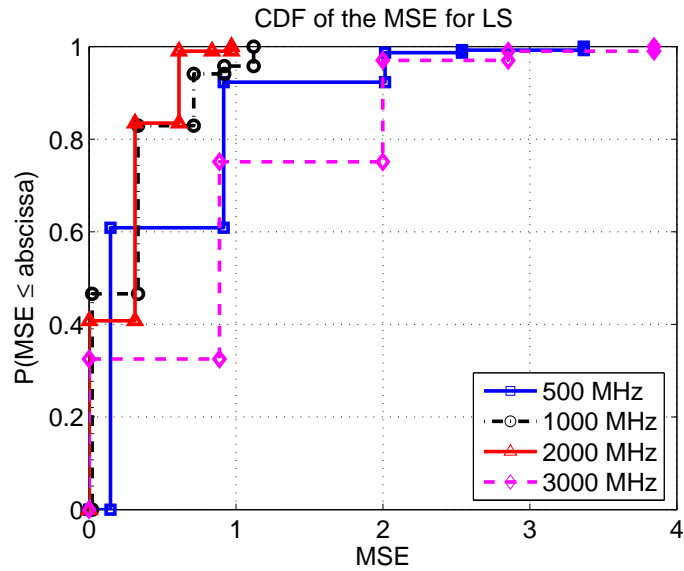
Figure 2.10: MSE profile for the LS algorithm
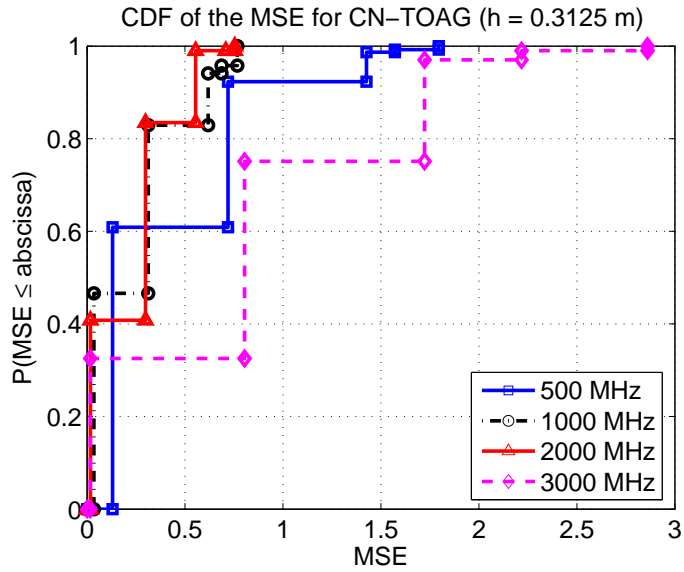
Figure 2.11: MSE profile for the CN-TOAG algorithm
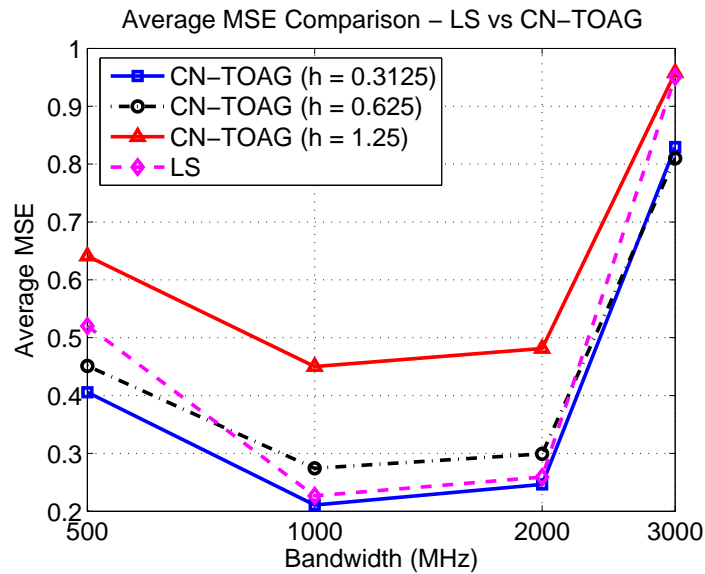
Figure 2.12: Average MSE comparison: LS vs CN-TOAG

2.3.2 Node Density

The second study addresses the effect of RP density on a typical positioning system under the aforementioned impairments of wireless indoor channel.

Apart from the inherent stochastic variations of the channel (which can induce DME),
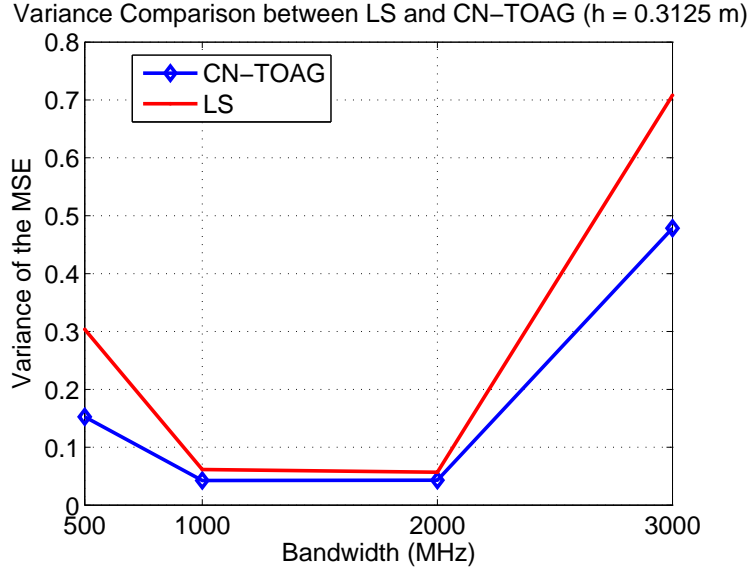
Figure 2.13: Variance comparison: LS vs CN-TOAG

the indoor environment itself also does not necessarily stay static. Indoor areas can be remodeled, made larger, or portions of them can be rebuilt with different building materials. This will change the RP density and by extension, the estimation accuracy that we can obtain from the network used for positioning. The RP density, denoted by ρ, can be viewed as a measure of the number of RPs per unit area, and is defined as

$$\rho = N/A \qquad (2.28)$$

where N is the number of RPs covering a given indoor area, and A is the size of the area, generally given in m^2.

It has been noted in a prior work [83] that given a *fixed* number of RPs, the performance of certain positioning algorithms tends to degrade as the size of the area to be covered is increased (i.e the RP density is decreased). This observation makes intuitive sense since the DP will be attenuated more as the distance between the RP and the sensor is increased. This will give rise to more DME which, in turn, will lead to degraded location estimation performance.

Although the effects of RP density on location estimation accuracy has been known, the exact nature of the functional relationship between these two quantities has not, to the best of our knowledge, been formulated to date. This raises a valid question: Why is it important to characterize this relationship? The answer fundamentally lies in the fact that different indoor positioning applications have different requirements for estimation accuracy. For example, in a commercial application (such as inventory tracking in a warehouse), low accuracy might be acceptable. However, in a public-safety or military application (such as keeping track of the locations of fire-fighters or soldiers within a building), much higher accuracy would be needed. This implies that the RP densities required for these two application domains would be different. Knowledge of the functional relationship between RP density and estimation accuracy enables a system designer to figure out how many RPs are required to meet a given accuracy target, thereby results in a cost-effective network deployment.

The manner in which RP density affects positioning accuracy depends principally on two factors: the particular algorithm used for the location estimation, and the DME model. The basic contribution of this study is to explore these kinds of relationships for different positioning algorithms, both to get an insight into their performance, and also to provide a useful tool for designers of indoor positioning networks.

In addition to addressing the above-mentioned issues, this study also extends the study reported in [83] in two important ways. First, the performance evaluations we undertake are based on DME models obtained from empirical UWB measurements in a typical indoor area, rather than models derived from ray-tracing simulations. Second, since the DME also depends on bandwidth [71], we also explore the impact of bandwidth on the performance of a given algorithm.

Related Work

The relationship between RP density and positioning accuracy has been studied, mainly for ad-hoc sensor networks. Savarese, Rabaey and Beutel have studied positioning in distributed ad-hoc sensor networks through cooperative ranging [84]. The paper by Chintalapudi et al studies the effects of density of RPs on ad-hoc positioning algorithms employing both distance and bearing measurements [85].

While these works have identified the relationship between positioning accuracy and RP density, they have not explicitly presented that relationship mathematically. Also, the DME models used in these studies are generally very simple. In this study, we seek to explore the functional dependency of the positioning accuracy (as expressed by the MSE) on RP density in the presence of DME models based on empirical measurements within actual indoor environments. Similar to first study we also use the DME model as described in equation (2.18).

Algorithms

We investigate the effects of RP density on the performance of two algorithms as described earlier in the previous study. These algorithms are CN-TOAG and Davidon LS algorithms.

Performance Analysis & Discussion

Simulation Platform   We consider the general system scenario given in figure 2.9 where a regular grid arrangement of RPs is assumed to be available. We also note that this system scenario is a fundamental building block for certain indoor ad-hoc sensor networks, and could be a considered a realistic deployment scenario for such scenarios [86]. The important parameter that determines performance is not the absolute number of RPs, but the ratio of the number of RPs to the area, as given by equation (2.28).

39

Here, we consider varying sizes of L for each algorithm. By varying the room size while keeping the number of RPs fixed at each of the four corners, we evaluate the performance of positioning algorithms as a function of RP density in the scenario and also show the effect of system bandwidth on overall performance. Synchronization mismatch between the transmitter and receiver is assumed to be small. For each algorithm, a total of 5000 uniformly distributed random sensor locations are simulated for different bandwidth values and for varying room dimensions. We will present our results for bandwidths of 500, 1000, 2000, and 3000 MHz.

Once a sensor is randomly dropped in the area, the actual distance measurements, d_i, from each RP at the corners are individually corrupted with DME, as given in (2.18). The corrupted distance measurements are then fed into the positioning algorithm to get the position estimate.

Results The results are shown in figures 2.14, 2.15, and 2.16. From the figures 2.14 and 2.15 we can immediately see that as the node density is increased, the MSE decreases. This is an expected result, since a finer installation of the RPs will reduce the probability of the occurrence of UDP conditions and hence will result in better positioning accuracy. Another important observation is that as the bandwidth of the system is increased, the estimation accuracy is also increased with the exception of 3 GHz. Increasing the system bandwidth provides a better time resolution, thereby ensuring accurate estimation of the TOA of the DP. However, increasing the bandwidth beyond a certain point (2000 MHz in this case) also gives rise to increased probability of UDP conditions due to the faster attenuation of higher bandwidth signals.

In Figure 2.16, we compare the performance of LS and CN-TOAG as a function of RP density using a system bandwidth of 2000 MHz. This bandwidth was arbitrarily selected, since it appears to be the bandwidth where both algorithms perform best. The results

clearly indicate that CN-TOAG has better performance, particularly for higher values of ρ. Since CN-TOAG is based on the concept of a TOA grid [79], increasing ρ (i.e. decreasing the area) for a fixed bin size h brings the grid points closer together. This, in turn, places a much tighter bound on the positioning error for CN-TOAG.

By examining the results of the simulation, we can derive a mathematical relation between RP density and MSE by applying a third order polynomial fit to the results. Our choice of the third order polynomial was simply influenced by the fact such a fit showed better agreement with simulation results than, say, a second-order fit. We have chosen to derive these relations on the basis of Monte-Carlo simulations, rather than analytically, in order to be able to compare and contrast the performance of the LS and CN-TOAG algorithms. It is certainly possible to derive these relations analytically for the LS algorithm, but not necessarily for CN-TOAG due to the complexity of the objective function of equation (2.21). These relations can be a valuable tool in determining the RP density for a required positioning accuracy. The 3rd order polynomial is given as:

$$MSE = a_3\rho^3 + a_2\rho^2 + a_1\rho + a_0 \qquad (2.29)$$

where a_i ($i \in \{0, 1, 2, 3\}$) denote the polynomial coefficients. Tables 2.3 and 2.4 show the coefficient values for the two algorithms. These values are dependent on the DME model used; however, we note that the DME model parameters are still representative of typical indoor environments.

A simple numerical example illustrates how these relations could be used. Suppose we have a 900 m^2 indoor area where we would like to implement a positioning system using CN-TOAG at a bandwidth of 1 GHz, and we would like the MSE to be no more than 1.5 m^2. Referring to Figure 2.15, we see that the corresponding value of ρ should be no less than 0.004. Using our knowledge of the size of the area, the value of ρ, and equation (2.28), we see that we need to have a minimum of 4 RPs in order to ensure satisfactory

performance.
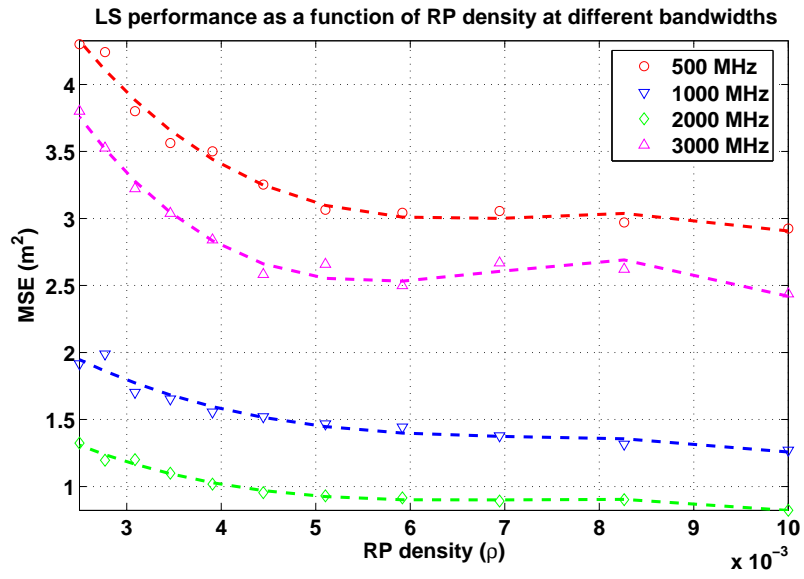
Figure 2.14: Performance of LS algorithm
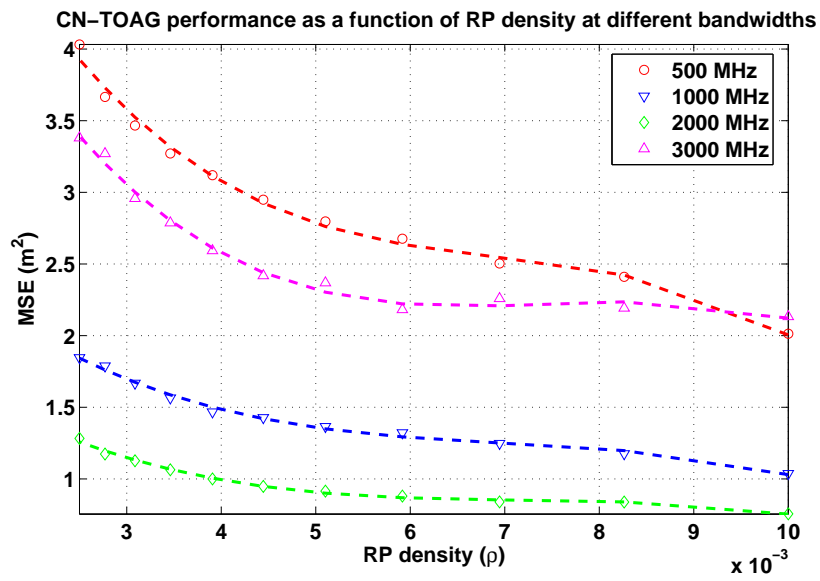
Figure 2.15: Performance of CN-TOAG algorithm
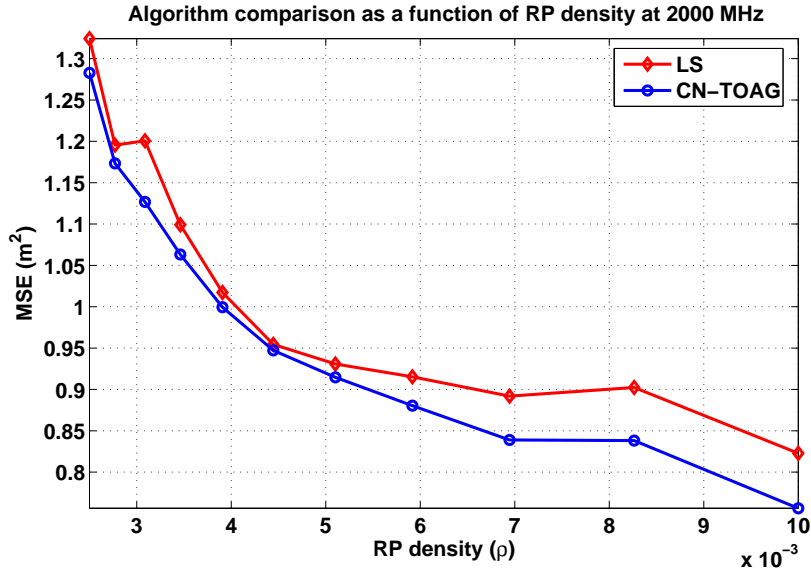
Figure 2.16: Performance comparison of LS and CN-TOAG for 2000 MHz

Table 2.3: Coefficients of the 3rd degree polynomial fit for LS Algorithm

w (MHz)	a_3	a_2	a_1	a_0
500	-1.20E+07	2.69E+05	-1.98E+03	7.7776
1000	-4.53E+06	1.00E+05	-749.52	3.2647
2000	-4.36E+06	93645	-662.95	2.4484
3000	-1.72E+07	3.60E+05	-2427.4	7.8446

2.4   Conclusions

In this chapter we gave an overview of both system engineering and channel modeling aspects of geolocation with a focus on TOA based ranging and localization. We proposed the use of the MSE Profile to gauge the performance of any indoor geolocation algorithm under a variety of building conditions. We showed that the MSE Profile can be used for performance benchmarking of different TOA-based indoor geolocation algorithms. For our purposes we used CN-TOAG and LS. We have also investigated the performance of these indoor positioning algorithms as a function of RP density and system bandwidth. We presented mathematical relations between RP density and achievable MSE and showed how they can be used to ensure the required performance with a given

Table 2.4: Coefficients of the 3rd degree polynomial fit for CN-TOAG Algorithm

w (MHz)	a_3	a_2	a_1	a_0
500	-1.15E+07	2.42E+05	-1771	7.0203
1000	-4.61E+06	97736	-725.22	3.1171
2000	-3.51E+06	76142	-557.93	2.2317
3000	-1.04E+07	2.34E+05	-1728.7	6.4152

indoor positioning network scenario.

Chapter 3

UDP Identification

Since UDP poses an important challenge especially for TOA based positioning systems, identification of UDP conditions is an important research area. This chapter proposes a new method for UDP identification and draws substantially from results presented previously in: [23].

Previous measurements and simulations for identification and modeling of the ranging error associated with each of these conditions have been carried out in [18, 87]. Here we propose an identification method of the UDP conditions and furthermore, based on the statistics of the ranging error associated with each class of receiver location, we mitigate the ranging problem.

The ideal CIR is usually referred to as the infinite-bandwidth channel profile since with infinite bandwidth the receiver could theoretically acquire every detectable path. In practice, however, the channel bandwidth is limited. Filtering the CIR with a limited bandwidth filter results in paths with pulse shapes. It can be shown that the sufficient bandwidth for accurate indoor localization based on the TOA metric is around 200 MHz [20] for the receiver to be able to resolve the multipath and mitigate the ranging error associated with MPC.

Applying a peak detection algorithm to the filtered channel results in detecting FDP and its respective TOA. The TOA of FDP, τ_{FDP}, is then used to approximate the distance of the antenna pair

$$d_{FDP} = \tau_{FDP} \times c \qquad (3.1)$$

where d_{FDP} is the estimate of the distance of the antenna pair and τ_{FDP} represents the estimate of the τ_{DP}. The erroneous detection of the DP component results in ranging error, ε, which can then be defined as

$$\varepsilon = d_{FDP} - d_{DP} \qquad (3.2)$$

In the absence of multipath and presence of LOS conditions, the estimate of τ_{FDP} is very close to the true value, τ_{DP}, therefore, error is insignificant. However, in practice there are three main sources of ranging errors in indoor localization systems. The first source of error is multipath error which is the shift of FDP from DP due to a combination of bandwidth limitation and presence of rich multipath in indoor environments. The ranging error in the presence of multipath is inversely proportional to the order of the bandwidth of the measurement system. Indeed in the presence of multipath and LOS conditions accurate UWB TOA estimates of the distance are feasible due to their high time-domain resolution [20] which allows the TOA-based localization systems to efficiently and properly function under such conditions. However, in the absence of LOS conditions it is possible for UWB systems to observe large errors depending on the availability of DP. It is worth mentioning that the absence of LOS condition does not necessarily imply that ranging error is bound to be large as discussed below.

Previous research classifies the receiver locations of a sample indoor environment into four main categories of DDP, natural-UDP (NUDP), shadowed-UDP (SUDP) and no
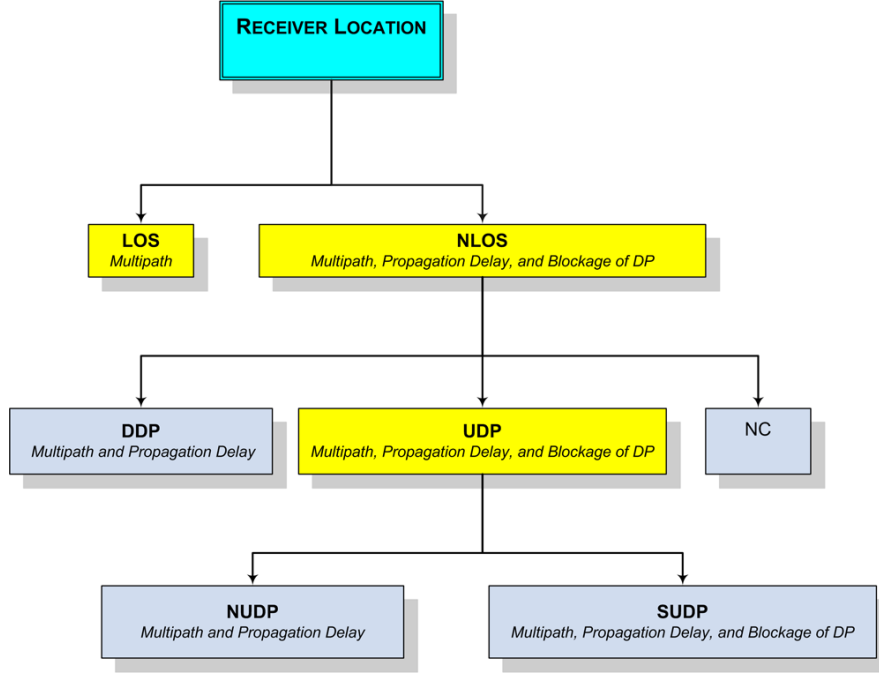
Figure 3.1: Hierarchical illustration of the channel classification

coverage (NC) [20, 88, 89], which are best described in figure 3.1. In general, DDP and NUDP classes exhibit small ranging errors which makes their range estimate suitable to be used for localization purposes. On the other hand, SUDP class exhibits unexpectedly large ranging error; therefore its respective range estimate, if used for localization purposes, degrades the performance of the system drastically. Range estimate is assumed to be unavailable for NC class. Here, we should point out that this classification further breaks down the UDP condition into two different categories and we still retain bipolar channel characteristics (DDP/UDP) for positioning applications.

Depending on the availability of DP, we face two hypotheses:

$$
\begin{cases}
H_0 : DDP \mid d_{FDP} \approx d_{DP}, \varepsilon \approx 0 \\
H_1 : UDP \mid d_{FDP} \gg d_{DP}, \varepsilon \gg 0
\end{cases}
\tag{3.3}
$$

where H_0 denotes the DDP hypothesis, which indicates that the channel profile can effec-

tively be used for localization, and H_1 denotes the UDP hypothesis, which indicates that the channel profile is not appropriate for being used for localization purposes. d_{DP}, d_{FDP} are the DP and FDP distances and ε is defined in equation (3.2).

Here we propose a methodology to distinguish between the DDP and UDP conditions by investigating the statistics of the specific metric of the channel profile. For the purpose of simulation we formed a grid of receiver locations on the third floor of the AK building at WPI. We, then, generated the respective CIR of each receiver location for different transmitter locations, for a total of 40000 CIRs. In order to simulate the real-time channel profile of the CIR, a finite bandwidth raised-cosine filter is used to extract the channel profile. Post processing peak detection algorithm is used to extract the desired metrics, range estimate, τ_{FDP}, and subsequently we can estimate d_{DP}.

There are two types of metrics being extracted from channel profile which can be utilized in identification of UDP conditions. The first class of metrics, is the time delay characteristics of the channel profile, while the second class deals with power characteristics of the channel profile. We can also utilize a hybrid metric, consisting of time and power, in order to classify the receiver location.

3.1 Time Metrics

The time characteristics of channel profiles have been used in the literature for a variety of applications in communication field [90]–[92]. RMS delay spread and mean excess delay are being used to determine the data-rate of the communication systems in indoor and outdoor environment. Here, we utilize the time characteristic to identify UDP condition.

3.1.1   Mean Excess Delay

Delay information encrypted in the channel profile is our first time metric to investigate. Amongst all of the delay metrics the mean excess delay of the channel profile is the easiest to find and perhaps the most effective metric, relatively, to efficiently identify the UDP conditions. Mean excess delay is defined as the

$$\tau_m = \frac{\sum_{i=1}^{L_{dp}} \hat{\tau}_i |\alpha_i|^2}{\sum_{i=1}^{L_{dp}} |\alpha_i|^2} \tag{3.4}$$

where $\hat{\tau}_i$ and α_i represent the TOA and complex amplitude of the ith detected path, respectively, and L_{dp} represents the number of detected peaks.

Conceptually, it can be observed that profiles with higher mean excess delay are more likely to be UDP conditions as it is illustrated in figure 3.2 in which the τ_m values are converted to distances. The probability plots of the distribution of DDP and UDP clearly indicate that they can be best modeled with normal distribution and their separation indicates that their normal distribution parameters are distinct.

In order to quantitatively determine the goodness-of-fit of the data to the normal distribution we apply the K-S and χ^2 hypothesis tests. The results of the normal distribution parameters, K-S test and χ^2 test are summarized in table 3.1.

Table 3.1: The mean and standard deviation of the normal distribution for the τ_m

Channel Profile	μ_τ	σ_τ	$K - S_\tau$	χ^2_τ
DDP	17.65	7.90	94.02%	55.61%
UDP	28.54	8.95	98.31%	59.72%

It can be observed that normal distribution supports the assumption of normality for both DDP and UDP classes. It is worth mentioning that the other measures of time delay characteristics of channel profile are found not to be as effective.
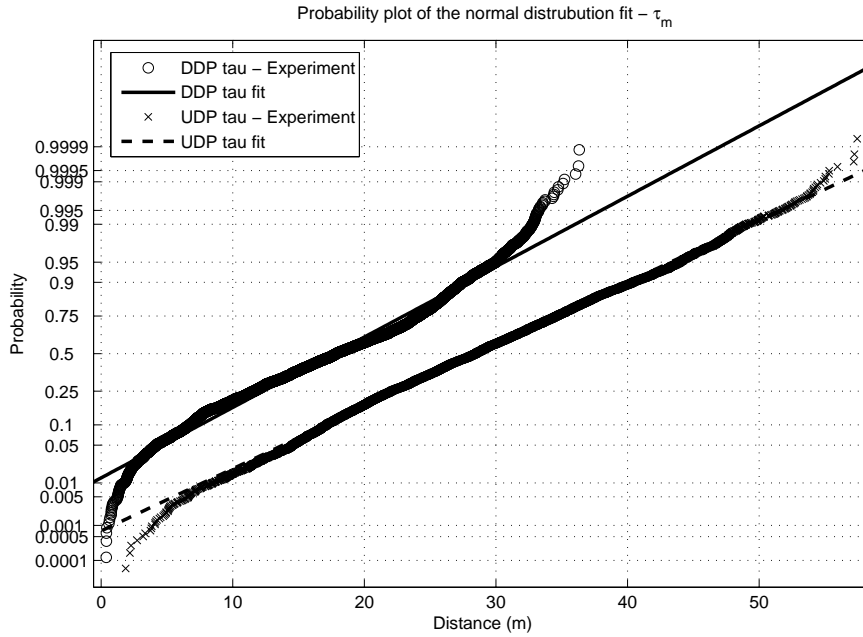
Figure 3.2: Normality of τ_m for DDP and UDP profiles

3.2 Power Metrics

The other class of metrics that can be extracted from the channel profile are power characteristics. There is hidden information regarding the DDP/UDP classification in the respective power characteristics. Amongst the useful power metrics, total power and FDP power are the most popular ones.

3.2.1 Total Power

RSS is a simple metric that can be measured easily and it is measured and reported by most wireless devices. For example, the MAC layer of IEEE 802.11 WLAN standard provides RSS information from all active APs in a quasi-periodic beacon signal that can be used as a metric for localization [93]
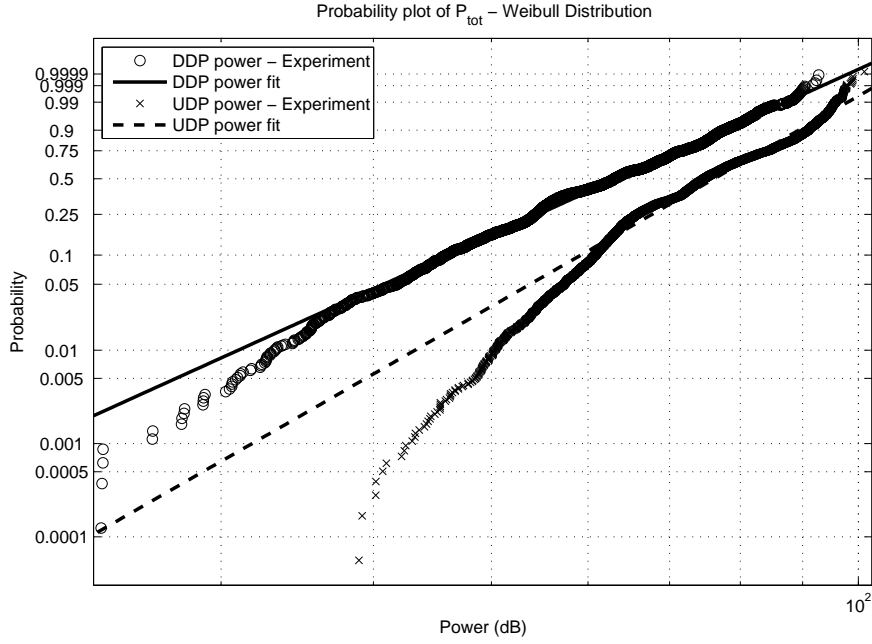
Figure 3.3: Weibull distribution modeling of total power

$$P_{tot} = P_r = 10 \log_{10}(\sum_{i=1}^{L_p} |\alpha_i|^2) \qquad (3.5)$$

For identification, we used $-P_{tot}$ which is referred to as power loss. It can be observed that profiles with higher power loss are more likely to be UDP conditions. This is best illustrated in figure 3.3 in which their respective probability plots with their Weibull fits are shown. The separation of the curves illustrates the difference of the P_{tot} behavior for different DDP/UDP conditions.

Again, in order to quantitatively determine the goodness-of-fit of the Weibull distribution to the data we apply the K-S and χ^2 hypothesis tests. The results of the Weibull distribution parameters, K-S test and χ^2 test are summarized in table 3.2.

It can be observed that Weibull distribution passes the K-S and χ^2 hypothesis tests.

Table 3.2: The a and b parameters of the Weibull distribution for the P_{tot}

Channel Profile	a_P	b_P	$K - S_P$	χ^2_P
DDP	67.38	5.92	95.11%	55.97%
UDP	79.94	7.49	94.78%	46.51%

3.3 Hybrid Time/Power metric

Although, the power metrics can be used individually to identify the class of receiver locations, one can form a hybrid metric to achieve better results in identification of the UDP conditions. Here, we propose to use a hybrid metric consisting of TOA of DP component and its respective power as the metric to identify the UDP conditions. Mathematically we have

$$\xi_{hyb} = -P_{FDP} \times \tau_{FDP} \tag{3.6}$$

where ξ_{hyb} represents the metric being extracted. It can be shown that the desired metric can be best modeled with Weibull distribution. Figure 3.4 represents the separation of the fits and proves that, indeed, the proposed metric can efficiently be used in UDP condition identification.

The results of K-S and χ^2 tests for goodness-of-fit show close agreement for the assumption of the Weibull distribution. The results of the Weibull distribution parameters, K-S test and χ^2 test are summarized in table 3.3.

Table 3.3: The a and b parameters of the Weibull distribution for the ξ_{hyb}

Channel Profile	a_m	b_m	$K - S_m$	χ^2_m
DDP	1056.89	1.50	94.58%	56.69%
UDP	2236.32	2.08	97.46%	55.19%
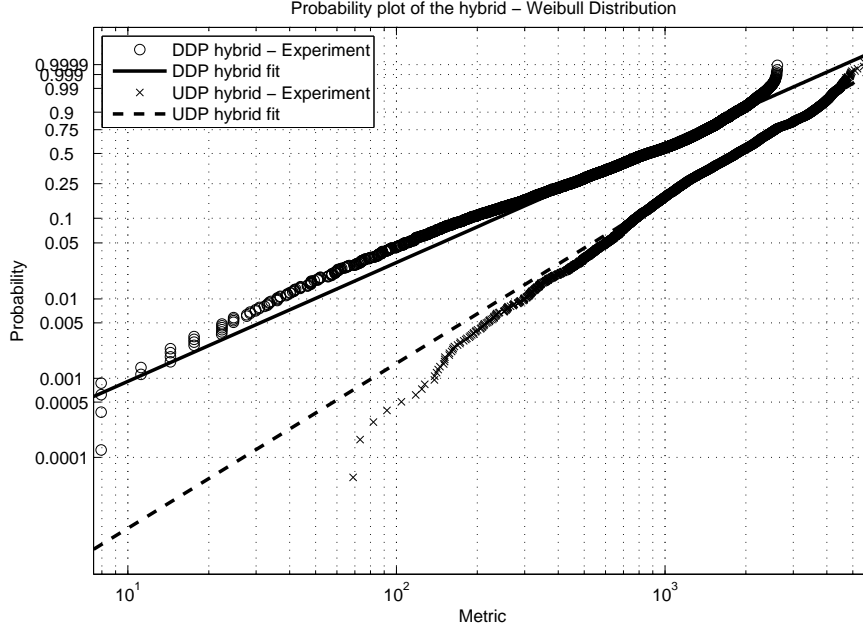
Figure 3.4: Weibull distribution modeling of hybrid metric

3.4 Binary Hypothesis Testing for UDP Identification

Knowledge of the statistics of τ_m, P_{tot}, and ξ_{hyb} enables us to identify the UDP conditions. In order to do so binary likelihood ratio tests can be performed to select the most probable hypothesis. For this purpose, we picked a random profile and extracted its respective metrics. The likelihood function of observed mean excess delay, τ_{m_i}, for DDP condition can then be described as

$$L(H_0|\tau_{m_i}) = p(\tau_{m_i}|H_0) = p(\tau_d)|_{\tau_d = \tau_{m_i}} \tag{3.7}$$

Similarly, the likelihood function of observed mean excess delay, τ_{m_i}, for UDP condition can then be described as

$$L(H_1|\tau_{m_i}) = p(\tau_{m_i}|H_1) = p(\tau_u)|_{\tau_u = \tau_{m_i}} \tag{3.8}$$

The likelihood ratio function of τ_m can then be determined as

$$\Lambda(\tau_{m_i}) = \frac{\sup\{L(H_0|\tau_{m_i})\}}{\sup\{L(H_1|\tau_{m_i})\}} \tag{3.9}$$

The defined likelihood ratio functions are the simplified Bayesian alternative to the traditional hypothesis testing. The outcome of the likelihood ratio functions can be compared to a certain threshold, i.e. unity for binary hypothesis testing, to make a decision.

$$\Lambda(\tau_{m_i}) \underset{H_1}{\overset{H_0}{\gtrless}} \eta_m \tag{3.10}$$

Similarly, we can define the likelihood functions for P_{tot} and ξ_{hyb} as

$$\Lambda(r_i) = \frac{\sup\{L(H_0|r_i)\}}{\sup\{L(H_1|r_i)\}} \tag{3.11}$$

$$\Lambda(\xi_i) = \frac{\sup\{L(H_0|\xi_i)\}}{\sup\{L(H_1|\xi_i)\}} \tag{3.12}$$

which leads us to the corresponding hypothesis tests as

$$\Lambda(r_i) \underset{H_1}{\overset{H_0}{\gtrless}} \eta_r \tag{3.13}$$

$$\Lambda(\xi_i) \underset{H_1}{\overset{H_0}{\gtrless}} \eta_\xi \tag{3.14}$$

Each of the above likelihood ratio tests can individually be applied for UDP identification of an observed channel profile. The outcome of the likelihood ratio test being greater than unity indicates that the receiver location is more likely to be a DDP condition and can appropriately be used in localization algorithm while the outcome less than unity indicates that the profile is, indeed, more likely to belong to the UDP class of receive loca-

tion; hence, the estimated τ_{FDP} has to be mitigated before being used in the localization algorithm.

For more effectively using the likelihood functions, we can combine the functions and form a joint likelihood function. Assumption of the independence of the likelihood functions along with combining them leads to a suboptimal likelihood function defined as

$$\delta(\tau_{hyb}, P_{tot}, \xi_m) = L(H_0|\tau_m, P_{tot}, \xi_{hyb}) =$$

$$(3.15)$$

$$L(H_0|\tau_m) \times L(H_0|P_{tot}) \times L(H_0|\xi_{hyb})$$

which can be compared to a given threshold for decision making, i.e. $L(H_0|\tau_m, P_{tot}, \xi_{hyb}) \underset{H_1}{\overset{H_0}{\gtrless}}$ 1. The results of the accuracy of the likelihood hypothesis tests, individually and as a joint distribution, are summarized in table 3.4.

Table 3.4: Accuracy of the likelihood hypothesis test

Likelihood Ratio	$Correct Decision$
τ_m	70.85%
P_{tot}	67.06%
ξ_{hyb}	69.73%
δ	89.29%

It can be observed that the accuracy of using individual metrics for identification of UDP conditions is about 70% while combining the metrics for UDP identification can achieve 90% of accuracy.

3.5 Conclusions

In this section, we have introduced a methodology to identify the UDP condition. We have proposed the use of power and time metrics for the received channel profile to obtain the likelihood functions for binary hypothesis testing. Comparing the outcome of the

hypothesis tests to a certain threshold determines if a receiver is in DDP or UDP condition. Once the condition is identified, the ranging error associated with it can be mitigated using certain methods one of which will be discussed in the next chapter.

Chapter 4

Precise Ranging and Localization in the Absence of Direct Path

In this chapter we will introduce precise ranging in the absence of DP using a concept called path persistency. Path persistency is part of the spatial channel model that will be introduced in detail in chapter 7.

High precision ranging involves a two-stage approach:

1. UDP identification

2. UDP mitigation

We discussed the UDP identification stage in the previous chapter. The mitigation stage builds on top of the information gained through UDP identification and tries to get precise ranging using certain methods.

Error mitigation in NLOS (UDP) conditions has been previously addressed in literature. Besides identification and modeling efforts, methods have also been proposed to mitigate the error based on statistical characterization of previously obtained data [69,94].

Here we will present a proof of concept by using a method called temporal TDOA to

show how a persisting path can be used to obtain precise ranging under UDP conditions. AOA assistance in mitigating UDP related errors will also be introduced. This chapter draws substantially from results presented previously in: [24, 25].

The sudden and random occurrence of UDP conditions may resemble sudden hits of signal fading in radio communications. Therefore, a seemingly reasonable approach to mitigating the problem is to employ well-known diversity techniques. To improve the performance of a radio modem in fading we can replicate the signal in multiple frequency channels to provide frequency diversity, we can apply a variety of coding techniques, or we can simply repeat the signal multiple times to provide time-diversity, or we can use multiple antennas to provide space-diversity. Since these techniques have been very effective, widely utilized, and analytically sophisticated, a rich literature has gradually evolved around them in the past fifty years. The latest innovative research in this field has evolved into the introduction of OFDM modulation, MIMO systems, and space-time coding techniques [14]. If we ignore the complexity of the behavior of the indoor radio propagation and the fact that the models developed for indoor propagation characteristics for telecommunication applications are not useful for indoor geolocation, as first described in [12], using diversity techniques may appear promising. In fact the lack of understanding of the complexities of indoor radio propagation has been the main source of failure for precise indoor geolocation projects over the past decade. In principle, when the DP is shadowed, none of the traditional diversity techniques are effective for precise indoor geolocation.

As an example, consider the traditional frequency diversity technique used in frequency selective multipath fading on indoor radio channels. In telecommunication applications the basic principle is that rather than transmitting all the information using one wideband channel, we can send several streams of lower rate data over multiple narrowband sub-channels. If one of the sub-channels is hit by frequency selective fading we can still use other sub-channels to achieve reliable communications. This basic principle

is very effective in telecommunication applications and it is applied in OFDM, which is the technology of choice for wideband data communications in WLANs, WPANs, and WiMAX. If we apply the same basic concept to indoor geolocation in the absence of DP, rather than using the TOA of FDP from a single wideband channel, we can use the TOAs of the FDP obtained from multiple sub-channels to reduce the DME. However, in the absence of DP when the TOA estimate in one channel is not reliable it is also unreliable for other sub-channels. Therefore, frequency diversity techniques are not capable of providing significant improvements to the performance in UDP conditions.

After nearly a decade of research and analysis on the effects of multipath on the accuracy of the indoor localization systems [12], our understanding of this important and complicated problem today is that the traditional radio communication techniques such as frequency diversity, time diversity, or space diversity using MIMO techniques are not effective in mitigating large ranging errors resulting from the absence of the DP. Two promising approaches to precise indoor localization in the absence of DP are localization exploiting non-direct paths, and cooperative localization. Although these approaches to algorithm development are intuitively sound, the degree of their effectiveness and their implementation details in a realistic indoor environment are subjects for current research. Next we will focus on ranging and localization using non-direct paths. Cooperative localization is beyond the scope of this thesis and hence will not be discussed.

4.1 Localization Exploiting Non-Direct Paths

Figure 4.1-a illustrates the basic principle underlying the relationship between the TOA of the DP and a path reflected from a wall, for a simple two path scenario. As the mobile receiver moves along the x-axis, the change in the distance in that direction is related to the length of the DP by $dxcos(\alpha) = dl_{DP}$. As the geometry of the figure 4.1-a shows, for

59

the reflected path we also have $dxcos(\beta) = dl_{P_n}$. Therefore, we can calculate the change in the length of the direct path from the change in the reflected path, using

$$dl_{DP} = dl_{P_n}\frac{cos\alpha}{cos\beta} \text{ or } d_{TOA_{DP}} = d_{TOA_{P_n}}\frac{cos\alpha}{cos\beta} \tag{4.1}$$

In other words, knowing the angle, β, between the arriving path and direction of movement and the angle, α, between the direction of movement and the DP, we can estimate the changes in the TOA of the DP from changes in the TOA of the reflected path. This basic principle can be extended to paths reflected from many objects and to the three dimensional case as well. This general treatment is available in [95]–[97].

In indoor geolocation applications, we can think of applying this principle to locating a mobile in UDP areas in the absence of DP. Knowing the previous location of the transmitter and the direction of movements we can always calculate α even in the absence of the DP. If we can find a way to measure β, using values of α and β in equation (4.1) we can track the location as the mobile receiver moves along in a UDP environment.

In order to use a path other than the DP for tracking the location, we should be able to identify that path among all other paths, and the number of reflections for that path should remain the same in the region of interest. In the simple two path model shown in figure 4.1-a, the second path consistently reflects from one wall as we move along the region and hence we can identify that path easily because it is the only path other than the DP. Since both conditions hold for the second path, the behavior of the TOA of that path, shown in 4.1-b, is smooth and we can use it for tracing the DP. In realistic indoor scenarios, in the absence of direct path, we have numerous other paths to use and the simplest paths to track are the FDP and the SP.

Figure 4.3 shows the behavior of the distances calculated from the TOA of FDP and the SP for a system with 200MHz bandwidth, and a comparison with the actual distance between the Tx-1 and the receiver when the receiver moves across the loop in our example

scenario shown in figure 4.2. Both SP and the FDP have inconsistent behavior in the UDP region of interest. This inconsistent behavior is caused by changes in the path index of these paths. In other words, if we associate a path number or index to a path associated with a specific reflection scenario from given walls, as we move along in a region, the path index or reflection scenario for the FDP or the SP changes. Each of these changes causes a jump in the behavior of the TOA of the path, thus impairing the smoothness needed for our estimation process.
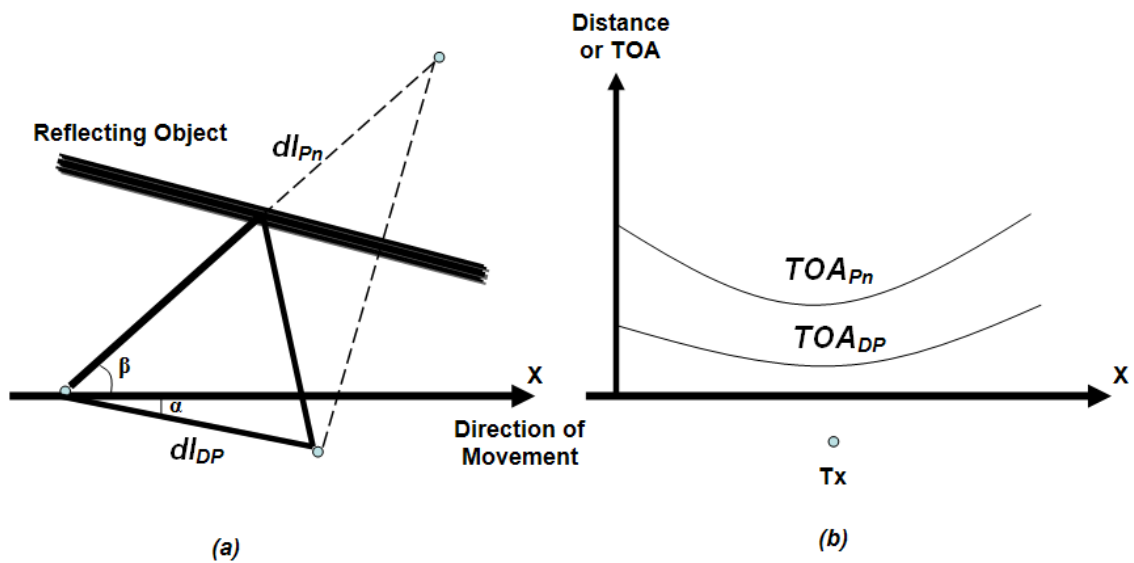
Figure 4.1: (a) Basic two-path reflection environment (b) Relation between the TOA of paths

With regard to channel behavior, we need to look into the principles underlying this behavior to learn how to remedy the situation. The basic problem is path-indexing changes, and the rate of path indexing exchange is a function of number of paths in the impulse response. The number of paths can be reduced by restricting the AOA of the received signal using a sectored antenna. Using sectored antennas to restrict the AOA provides two benefits: (1) it reduces the number of multipath components and hence reduces the path index crossing rate, facilitating improved tracking of specific paths in the channel profile;
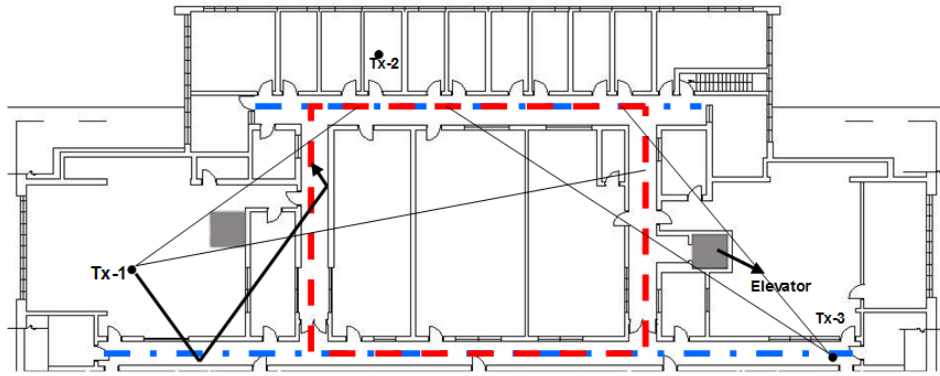
Figure 4.2: Dynamic scenario on the 3rd floor of AK Laboratory at WPI
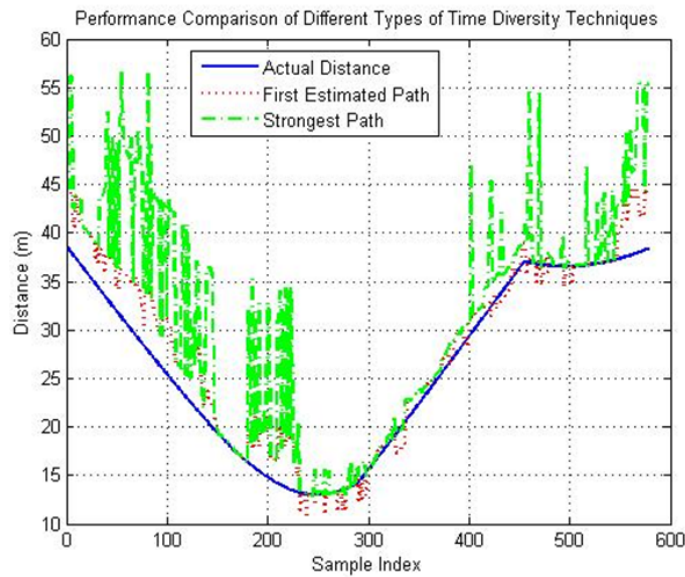
Figure 4.3: Behavior of the distances calculated from the FDP and SP vs. actual distance

(2) it allows a means for estimating the angle of the arriving path needed for equation (4.1). To further clarify the benefits of this technique, we resort again to our loop-route scenario to explain the behavior of the SP in the channel impulse response in a receiver using sectored antenna with a variety of aperture angles.

To begin we examine a sample location on the loop-route and we use the RT software to generate the impulse response of the channel for different aperture angles to observe how the number of multipath components in a UDP region relates to the aperture angle.

62

Consider the location indicated by an arrow in the left side of our loop-route shown in figure 4.2. The DP between Tx-1 and this location is blocked by the metallic chamber and the SP is a path arriving after two reflections. The ray tracing generated impulse response of the channel at this location has 590 arriving paths with no restrictions on AOA. With a 45-degree aperture, we have 91 paths and with 5 degrees the number of paths decreases to 12. As the aperture angle becomes narrower, number of paths reduces significantly allowing a better tracking of a desirable path.

Figure 4.4 shows the ideal behavior of different paths without bandwidth considerations as a receiver moves along the left segment of the rectangular route. The blue line shows the actual distance and the blue line with star marker shows the behavior of the FDP, which in this case is also the strongest path. The receiver starts in a DDP condition, then moves to a UDP region, and then returns to another DDP area. In the DDP regions the DP, FDP and the SP are the same and the range estimate is accurate and consistent (steady). In the UDP region, the FDP, which is also the SP, remains steady for short periods but due to the path index changes of the FDP it can not maintain its steadiness and it experiences about ten transitions of the path index or reflection scenario for the FDP. This high rate of transitions is due to the large number of MPCs and we can reduce these components by using sectored antennas to limit the AOA of the paths.

Figure 4.4 also shows the behavior of the SP in three neighboring 5 degree sectors along the UDP region of the left side corridor in figure 4.2. These are three of the 72 ideal 5 degree sectors assumed in this example. The SP of the entire profile, shown with two reflections in figure 4.2, is first in sector 61, and then it moves to sectors 62 and 63. As the SP moves among these sectors it has a steady behavior with no change in path index, which we can use for the detection of the TOA of the DP.

The discussion above shows the potential for the implementation of ranging using non-direct paths with an ideal sectored antenna with 5 degrees aperture angle for each

63
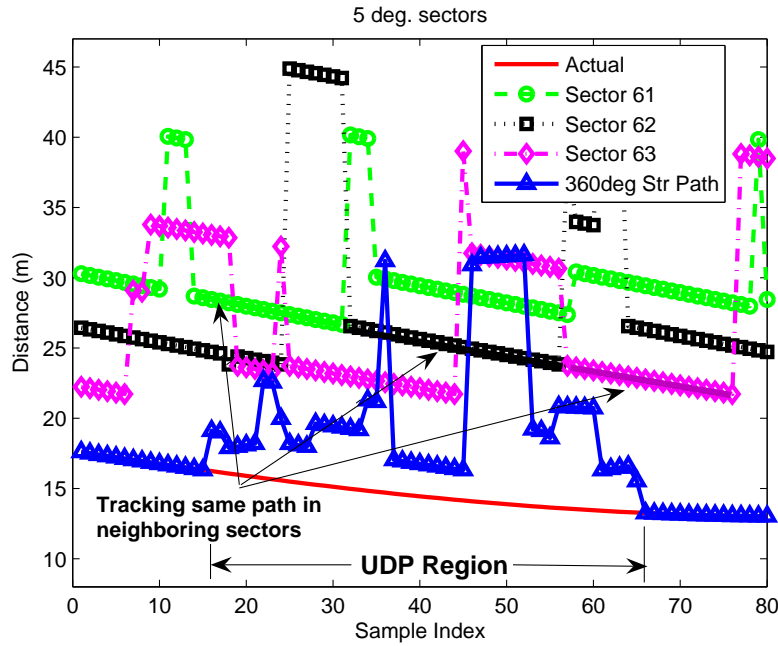
Figure 4.4: Effectiveness of AOA in the UDP region

sector and a simple algorithm which traces the strongest path as it moves from one sector to the next neighboring sector. Development of more practical algorithms to implement this concept with finite bandwidth and realistic antennas will require significant additional research.

4.2 Path Persistency

In this section, we will introduce the concept of persistency of a path (or equivalently lifetime of a path) and how persisting paths can be used in an indoor localization/tracking system for remedying the UDP condition by employing sectorized/smart antennas [98]. The study will be a continuation of the concept of exploiting non-DP paths introduced in [20] and outlined above. Another study exploiting multipath has been introduced in [96]. The intuition for using multipath is that even in the absence of DP there will be multipath components that might show stable and persistent behavior and hence can be related to

the DP to aid in more precise localization as will be explained in the next section. To the best of our knowledge, this aspect of indoor localization/tracking has not been studied before.

Before describing the concept of persistency we will once again give a characterization of wireless channel. The characterization of indoor wireless medium can be given by its channel impulse response (CIR):

$$h(\tau, t) = \sum_{i=1}^{L} \beta_i \delta(t - \tau_i) e^{\phi_i} \tag{4.2}$$

where β_i and ϕ_i are the complex magnitude and phase of the path arriving at τ_i, respectively. The received signal can be represented as:

$$r(t) = \sum_{i=1}^{L} \beta_i p(t - \tau_i) e^{\phi_i} \tag{4.3}$$

where p is the pulse being transmitted by the transmitter. Ideally we assume that $p(t)$ is a Dirac delta function, $\delta(t)$, which has infinite bandwidth, thus we will have $r(t) = h(\tau, t)$. If we consider a bandlimited signal, $p(t)$ will be the sinc function.

As a receiver moves along a certain trace with a steady speed v, the paths will exhibit variations in their amplitudes, TOAs and AOAs. The rate and amount of these changes are highly dependent on the reflection/transmission interactions of the paths. These three entities can be considered as detectable (traceable) features of a path. By detectability or traceability, we emphasize being able to obtain measurements of these features. Persistency is basically the evolution of a particular path in which its traceable features exhibit differential changes in accordance with its differential motion. Persistency results from the fact that a certain path preserves its reflection/transmission pattern. As an example, a wall running continuously parallel to the motion path of the receiver yields a persistent path. Figure 4.5 shows the path persistency (equivalently lifetime of a path) conceptually.

65
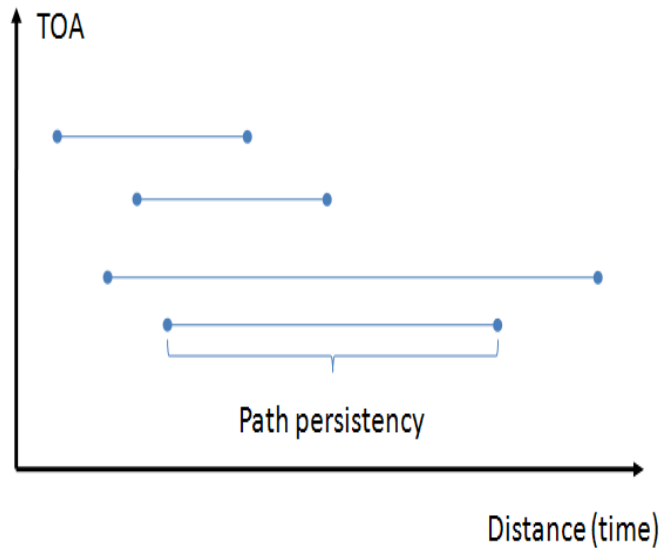
Figure 4.5: Concept of path persistency

The analysis of persistency would provide us with the tools necessary to overcome the difficulties introduced by the UDP condition. If we can track the paths that exhibit persistent behavior even when the DP is not present, then we can use this additional information to properly adjust the ranging measurements for true distance.

4.3 Geometric Basis of the Concept

In order to explain how multipath components can be used to aid in the ranging and thus precise localization in a dynamic scenario, we conceptualize the problem as a simple geometric analysis of arriving paths. We further assume that we only have two arriving paths, one of which is the direct path between the transmitter and the receiver and the other one is a path that is reflected from a continuous wall that runs parallel to the direction of the movement of the receiver. Figure 4.6 shows the configuration of the postulated scenario. We consider a metallic obstacle at certain coordinates which blocks the direct path for a portion of the receiver's motion path. The path that gets reflected from the wall is always

detected at the receiver. As the receiver moves with a certain velocity in the indicated direction, these two paths will exhibit differential changes in their amplitudes, TOAs, and their arrival angles which can be regarded as the traceable features of that path. Assuming the receiver has an omnidirectional antenna which basically picks the strongest path for ranging, as soon as the direct path is blocked, it will begin picking up the reflected path and consequently there will be a major difference in the TOA, amplitude and arrival angle. This, in turn, suggests the reception of a completely different path having a different reflection/transmission pattern. If we were to gather ranging data based solely on omnidirectional strongest path selection, we would observe a substantial amount of ranging error as the receiver moves along the shadowed portion of its pathway. However, if we can detect paths based on their arrival angle (i.e by using sectorized/smart antennas) we can keep track of these paths separately, and thus once the DP is blocked we will still have the reflected path. The TOA for this reflected path will be offset by the TOA of the DP by a certain amount that can in fact be obtained by temporal TDOA between consecutive receiver locations. Therefore, by acquiring this reflected path and subtracting this offset from its TOA, we can find the TOA of the DP, which is blocked, with high accuracy. As long as there is a consistent region along the path of movement (a continuous wall in our case), this method can be applied to aid in high bandwidth TOA ranging in a dynamic scenario where the direct path is non-existent for certain portions of the receiver's pathway.

4.4 Temporal TDOA

In this section, we introduce a method which basically employs TDOA in a new context. As opposed to traditional TDOA from multiple transmitters, we consider TDOA of a certain path as the receiver moves along its pathway. Here TDOA will represent the

67
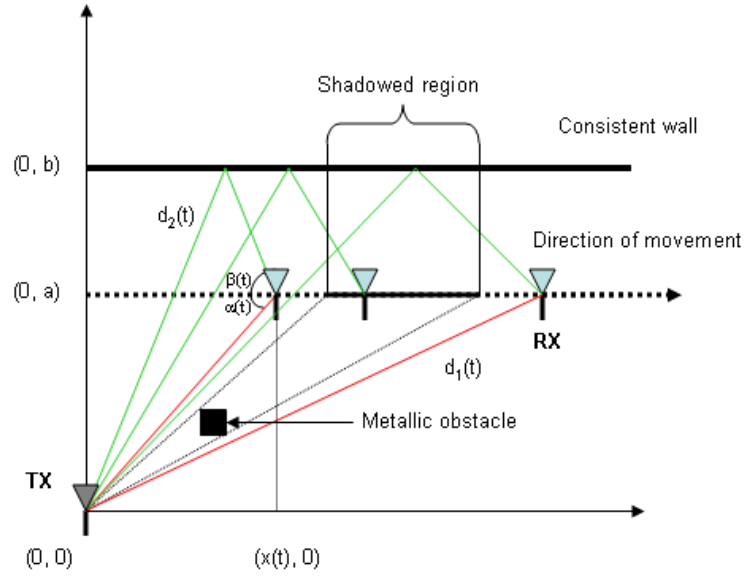
Figure 4.6: Geometric explanation for path persistency

difference of TOA of a certain path between two adjacent sampling locations separated by δt or since the receiver is assumed to be moving at constant velocity v, they will be separated by $v\delta t$. Hence we will be using TDOA in a temporal sense.

Assuming we have DP ranging on points uniformly spaced along this pathway, we can keep track of the difference between the TOAs of this particular path at these predefined points. In fact, we assume a differential distance between these points so that the change in the TOA or TDOA also exhibits a differential change as long as the this path persists. From this point on, we will be using the term TDOA with the meaning just outlined. Once TDOA is tracked along the receiver's motion, a sudden positive or negative change would indicate the fact that another path starts to become detectable. In order for this method to be useful, it is also important to be able to track paths based on their AOA [99]. In this sense, we propose a smart antenna based multisector tracking system that can utilize both AOA and TDOA information to make use of multipath components other than the DP. A preliminary analysis of this approach has been introduced in [20]. A previous study also exploited multipath components to obtain accurate results, but the internal geometry of

68

the buildings needed to be known or estimated using complex algorithms [96].

Referring to figure 4.6 we can write

$$
\begin{aligned}
d_1(t) &= \sqrt{x(t)^2 + a^2} \\
d_2(t) &= \sqrt{x(t)^2 + (2b - a)^2} \\
\alpha(t) &= arctan(\tfrac{a}{x(t)}) \\
\beta(t) &= arctan(\tfrac{2b-a}{x(t)})
\end{aligned}
\qquad (4.4)
$$

where $d_1(t)$, $d_2(t)$, $\alpha(t)$,$\beta(t)$ are the path lengths and arrival angles of the DP and the reflected path respectively.

In order to relate the changes in path lengths and the arrival angles we will consider figure 4.7 and show the calculations on DP only. Same calculations will also apply to the reflected path. In this figure, we assume receiver is at $x(t - \delta t)$ at time $t - \delta t$ and its distance from the transmitter is $d(t - \delta t)$. It moves a differential distance δx in time δt to the position $x(t)$. Since we consider a differential movement along the given path we can assume that previous and current paths are almost parallel. Thus we can write

$$
d(t) = d(t - \delta t) + \delta x cos(\alpha(t)) \qquad (4.5)
$$

From equation (4.5) we can easily write the temporal TDOA for the two paths as:

$$
\begin{aligned}
d_1(t) - d_1(t - \delta t) &= \delta x cos(\alpha(t)) \\
d_2(t) - d_2(t - \delta t) &= \delta x cos(\beta(t))
\end{aligned}
\qquad (4.6)
$$

which is the discrete representation. If divide both sides of 4.6 by δt we obtain the continuous time equivalent as:
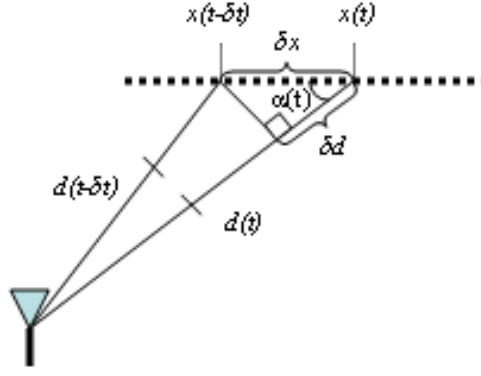
Figure 4.7: Calculation of TDOA for consecutive locations

$$
\begin{aligned}
\frac{d}{dt} d_1(t) &= v\cos(\alpha(t)) \\
\frac{d}{dt} d_2(t) &= v\cos(\beta(t))
\end{aligned}
\tag{4.7}
$$

where v is the speed of the receiver. Furthermore from 4.7, the differential change in the length of DP is related to the differential change in the length of the reflected path as follows:

$$
\frac{d}{dt} d_1(t) = \frac{d}{dt} d_2(t) \frac{\cos(\alpha(t))}{\cos(\beta(t))}
\tag{4.8}
$$

In the following section we develop a practical approach to precise ranging using temporal TDOA and multipath tracking.

4.4.1 Temporal TDOA and AOA for Precise Ranging

Substantial research effort has focused on methods to identify the cases of UDP and mitigate the errors occurring in these areas. Although identification of UDP conditions is the first and an important aspect of error mitigation, methods and algorithms to actually mitigate the error also play a vital role in the overall performance of the system. In this part, we focus on the mitigation stage.

As explained in the previous section, once the DP is lost, it might be possible to track a persistent secondary path and still obtain precise ranging by using the relations previously outlined. With the assumption that the tracking for the receiver starts in the DDP region, the receiver keeps track of the multipath information using its smart/sectored antenna subsystem, specifically keeping track of traceable path features: TOA and AOA. The RSS information can be also tracked, however, due to its unreliability caused mainly by shadow and mutlipath fading for path tracking, it is omitted in our study. The vectors of TOA and AOA being tracked in each sector can be represented as a pair:

$$F = (\overline{\tau}_i, \overline{\theta}_i) \tag{4.9}$$

where F is the multipath information matrix, $\overline{\tau}_i$ and $\overline{\theta}_i$ denote the vectors of TOA and AOA for each sector $i \in [1..K]$ respectively, and $\overline{\tau}_i = [\tau_{i,1}, \tau_{i,2}, ...\tau_{i,m}], \overline{\theta}_i = [\theta_{i,1}, \theta_{i,2}, ...\theta_{i,m}]$ denote the m paths that can be tracked in each sector separately. The number of these paths, m, depends on the angular and time resolution (bandwidth) of the system being utilized. When a certain path being tracked persists its traceable features will exhibit a differential change, i.e

$$
\begin{aligned}
\tau_{i,k+1} - \tau_{i,k} &= \delta T \\
\theta_{i,k+1} - \theta_{i,k} &= \delta\theta
\end{aligned}
\tag{4.10}
$$

Here δT is the TDOA expressed as (referring back to figure 4.7)

$$\frac{\delta d}{c} = \frac{\delta x cos(\alpha(t))}{c} \tag{4.11}$$

where c is the speed of light.

Whenever there is a substantial change in the TDOA between consecutive points, this will most likely be caused by the detection of a completely different path. When

this occurs, the system will make use of multipath information that still shows persistent behavior and the precise ranging will be obtained by compensating TOA of the persistent multipath by the offset that has been observed and also applying AOA correction as in equation (4.8).

4.4.2 Proof of Concept via Simulations

In order to show how TDOA and AOA can be used to obtain precise ranging a two-step simulation platform has been developed. The first part uses a CWINS developed RT software that generates the CIR of a given floorplan in a building. The data that is output is the amplitude, TOA, AOA information for each specific path. RT assumes infinite bandwidth operation, which is practically impossible but sets a baseline for the performance analysis of indoor positioning methodologies.

Figure 4.8 shows the sample scenario which demonstrates the existence of a UDP condition but which can be complemented by the presence of persistent multipath component. After the RT results are obtained, the outputs have been processed by MATLAB in the second step to actually implement the multipath tracking using temporal TDOA. The operation of the algorithm can be summarized as:

1. The receiver keeps track of the DP and secondary path (multipath) information in the form given in equation (4.9).

2. Whenever the DP signal is lost, estimated TOA information at the kth time step is updated as:

$$\hat{TOA}(k) = TOA_{mp}(k) - \delta T + AC \tag{4.12}$$

where

$$\delta T = [TOA_{mp}(k) - TOA_{DP}(k-1)] \tag{4.13}$$
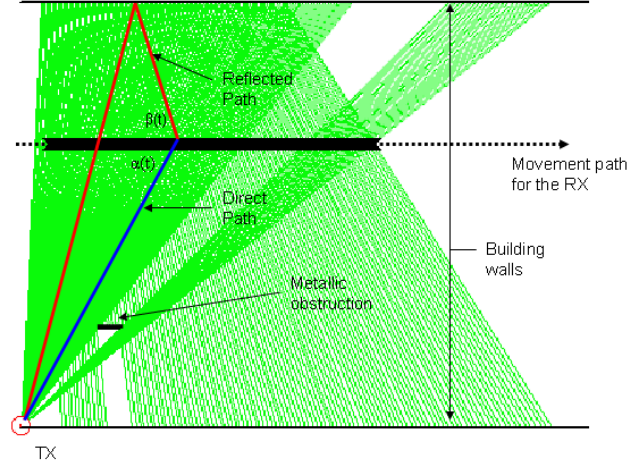
Figure 4.8: Sample scenario for demonstrating the effectiveness of multipath tracking

and

$$AC = [TOA_{mp}(k) - TOA_{mp}(k-1)]\frac{cos(\alpha(t))}{cos(\beta(t))} \tag{4.14}$$

Here $T\hat{O}A(k)$ is the estimated TOA, $TOA_{mp}(k)$ is the secondary path TOA at time step k and $TOA_{DP}(k-1)$ is the DP TOA at time step $k-1$ where it was last observed. AC stands for angular correction and is calculated as in equation (4.14).

To assess the performance of the proposed scheme, we employ the RMSE of the receiver's ranging data for both omnidirectional strongest path detection and the proposed multisector multipath strongest path tracking. The RMSE is defined as:

$$\sqrt{\frac{1}{N}\sum_{i=1}^{N}(\hat{R} - R)^2} \tag{4.15}$$

In figures 4.9 and 4.10 we can see how multipath correction may be used to substantially decrease ranging error together with the temporal TDOA data. Figure 4.11 shows the tracking of TDOA for each location considered in the simulation. In this figure, the first positive jump of about 17 m in TDOA denote the location where a switch from DDP to UDP occurs. At this point the amount of jump will be utilized in offset correction.

73

The negative jump in TDOA marks the location where the channel goes back to DDP condition.

Referring to figure 4.10, using only omni-directional strongest path selection, we obtained an RMSE of 7.3316 m. However when we apply the offset only multisector based tracking we observe a substantial amount of drop in the RMSE and we obtain 0.6387 m. Furthermore if we also apply angle correction RMSE drops down to 0.0634 m. The gain in ranging accuracy (in terms of RMSE) in this particular scenario is about 115.

However the use of this method is dependent on the internal structure of the building in which the tracking is needed. The number of the walls, wall material, average wall length as well as the distance of the transmitter to the walls and the receiver all affect the fact that different multipath components will be available for varying amounts of time. Since persistency is important, to use the proposed method in the most effective way possible, statistical characterization of buildings in terms of building parameters (number of walls, wall lengths, wall material etc.) gain importance. Buildings with simple internal structures and with less clutter will provide better tracking under UDP conditions, than buildings with a large number of walls and metallic objects. Effect of building architecture on path persistency in the next chapter.

4.5 Hybrid TOA/AOA Multipath Tracking for UDP Error Mitigation

The previous section demonstrated how TOA and AOA information can be used to obtain precise ranging information for a persistent path. In this section we introduce an actual path tracking algorithm that tries to counter the effects of UDP by using joint TOA and AOA information.
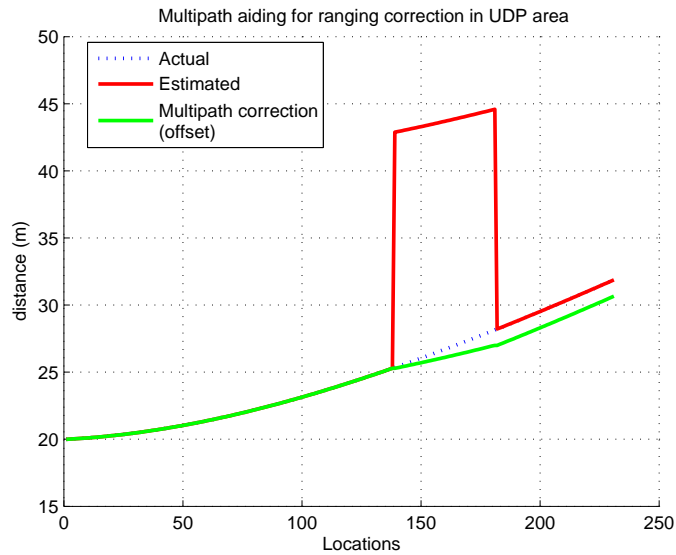
Figure 4.9: Ranging correction with offset compensation only
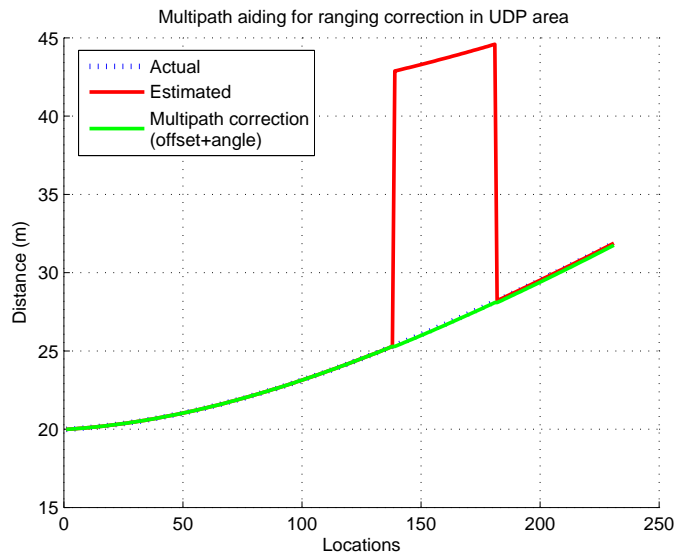
Figure 4.10: Ranging correction with combined angle and offset compensation

4.5.1 Algorithm Description

Whenever DP is lost a certain path is selected according to SP or FP rule and the algorithm tries to follow this particular path by selecting the consecutive paths that have the path metrics (TOA+AOA) closest to the metrics obtained from the previous sampling
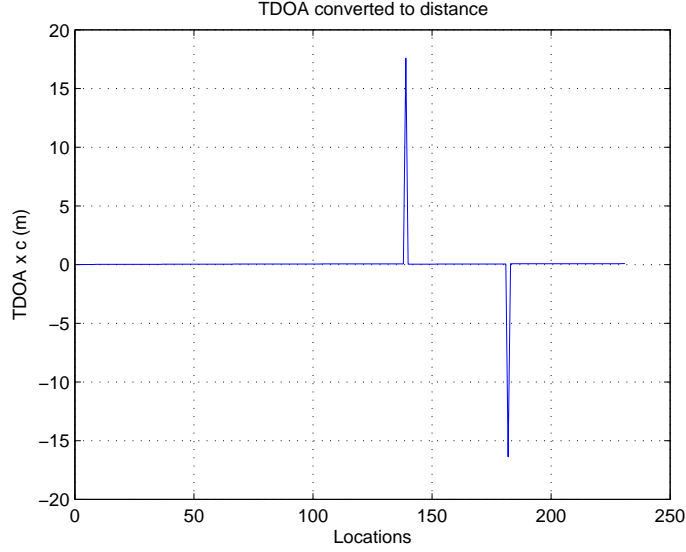
Figure 4.11: Temporal TDOA vs receiver locations

point. Since sudden jumps will be observed when a path switching occurs, the amount of jump will be compensated by offset correction. The algorithm will also employ AOA adjustment as presented in equation 4.8. The motivation behind this algorithm is that when DP is lost, there might be persistent paths whose characteristics do not change substantially along the UDP region. Since a certain persisting path will preserve its reflection/transmission pattern, it will experience only differential amounts of change in both its TOA and AOA. The path selection at the kth location is a LS solution that can be expressed as

$$\tau_{sel,k} = \{\tau_{i,k} | i = \operatorname*{argmin}_{p} \sqrt{M1_{p,k}^2 + M2_{p,k}^2}\} \tag{4.16}$$

where

$$M1_{p,k} = \tau_{p,k} - \tau_{sel,k-1} \tag{4.17}$$

$$M2_{p,k} = \theta_{p,k} - \theta_{sel,k-1} \tag{4.18}$$

76

$\tau_{sel,k-1}$ is the TOA, and $\theta_{sel,k-1}$ is the AOA of the selected path at the $(k-1)$th sampling location respectively. Here, $\tau_{p,k}$ denotes the TOA of the pth path at kth sampling instant and $p \in [1..L]$ is the index of the path in the CIR.

4.5.2 Simulation Platform and Results

Simulations have been performed with a RT software package. These simulation results are then processed by MATLAB to obtain ranging information. Throughout the simulations infinite bandwidth for the pulses has been assumed. The floorplan of the 3rd floor of the AK Laboratories at WPI and the test route for the receiver are shown in figure 4.12. On this floorplan there is one anechoic metallic chamber that blocks the DP for a certain part of the route and hence creates UDP conditions. The transmitter is placed at pixel coordinates (400,170). The receiver start location is taken to be a DDP position which means the receiver position is known exactly when the simulation starts. Throughout the receiver route, there are various segments that are DDP and UDP. Our assumption throughout the simulation is that whenever a DDP condition occurs this information is made available at the receiver such that FDP is taken into consideration since it provides the most accurate ranging. We will not be addressing the identification problem of DDP/UDP conditions (as noted earlier) since we assume this information is readily available. Figure 4.13 gives the distance estimation for the algorithms considered, namely FDP, SP and our proposed algorithm. The shaded regions denote the UDP areas. Referring to figure 4.12, there are 2 UDP regions. The last UDP region in figure 4.13 is actually a continuation of the first region. This figure is referenced to the point at the lower left corner of the receiver loop which is located at pixel coordinates (149, 87). Receiver start location corresponds to point 290 which is a DDP point. From this figure, we can easily see that SP gives us a considerable amount of variation in ranging estimates in the UDP areas, which greatly increases overall error. FDP gives us better and more stable results, however we can still

77
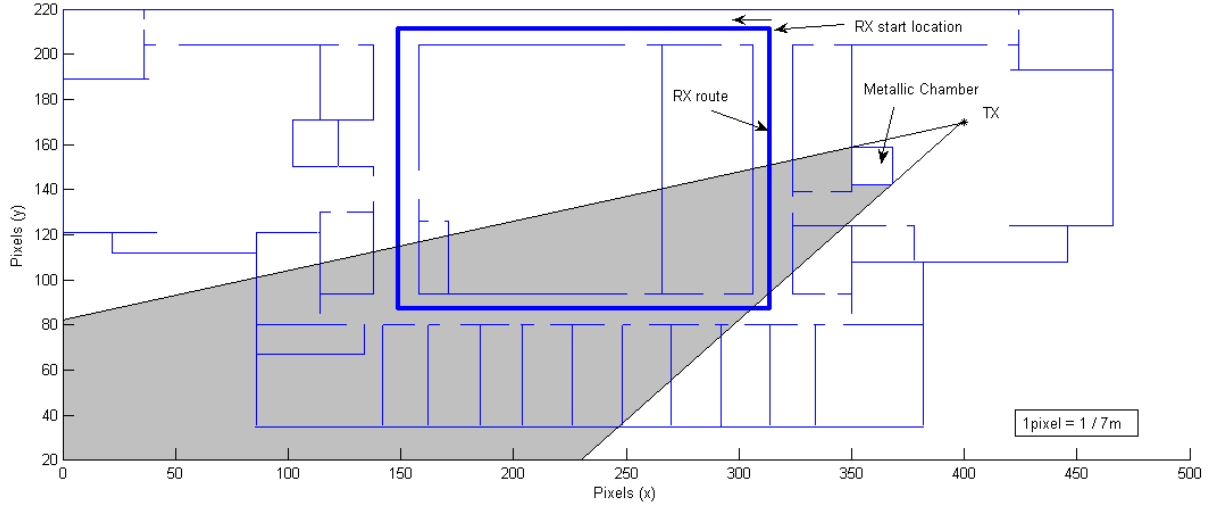
Figure 4.12: Floorplan of AK 3rd floor at WPI and the simulation setup

see variations of the estimates and the offset in the UDP region. Our proposed algorithm, which takes into account the offset correction and angle adjustment from equation 4.8, greatly improves the ranging accuracy in the UDP region and hence mitigates the error with good performance. Figure 4.14 presents the CDF of the errors obtained using each of the algorithms. From figure 4.14, we can clearly see overall performance achievement with the proposed algorithm. Almost 90% of the locations have errors less than 1.7 m, with the overall error not exceeding 3 m.

One important measure for the comparison of how well the ranging/positioning algorithms is the RMSE.

The RMSEs obtained from the SP, FDP and our proposed algorithm in the UDP areas can be seen in table 4.1.

Table 4.1: RMSE comparison among ranging methods

Algorithms	RMSE (m)
SP	11.69
FDP	4.82
Prop. Alg.	1.23

78
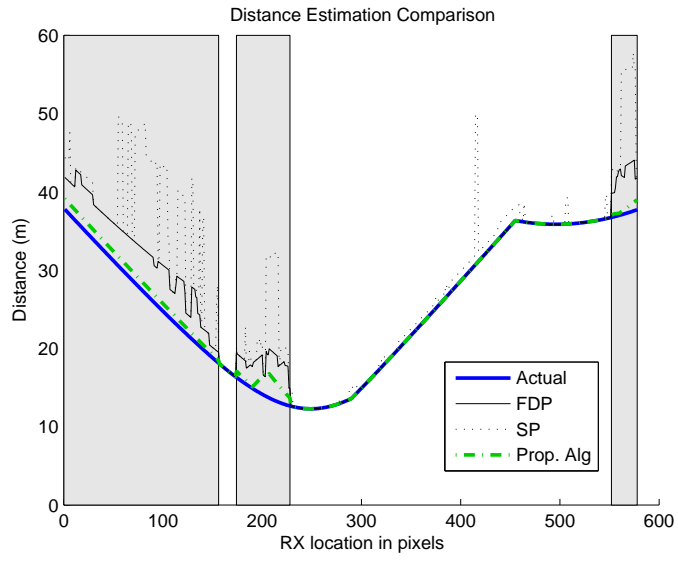
Figure 4.13: Distance estimation comparison
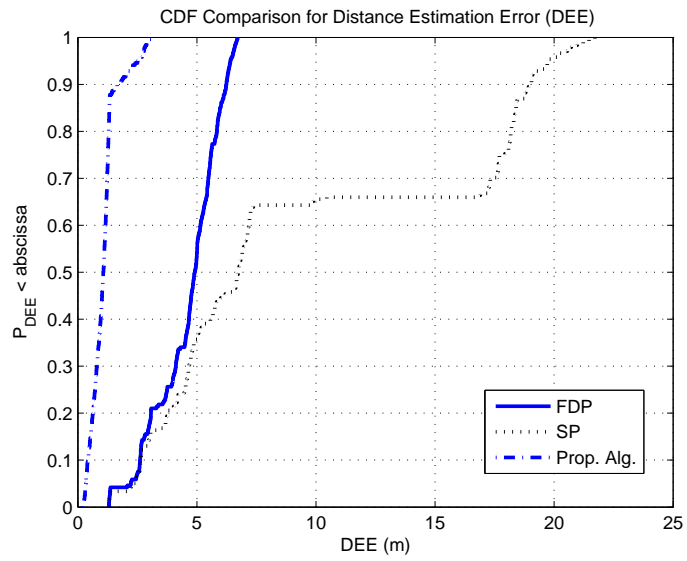
Figure 4.14: CDF comparison

79

4.6 Conclusions

In this section, we introduced the concept of path persistency and how it can be used to obtain precise ranging in the absence of DP. One such method is the temporal TDOA and multipath tracking based high precision ranging. We have also presented a new method for TOA-based systems to mitigate the ranging error. The proposed method relies on the fact that there might be persisting non-direct paths present even in the UDP conditions, which can be used to aid in precise ranging. The previous AOA and TOA information of these persisting paths may be utilized in mitigating the large errors associated with UDP regions. An RMSE of about 1.23 m is achieved with the RT simulation of AK 3rd floor at WPI, utilizing the proposed method, whereas, the FDP and SP give us RMSEs of 4.82 and 11.69 m respectively.

Chapter 5

Effects of Building Architecture on Persistency

This chapter discusses the effect of building architecture on path persistency based on sample scenarios and it draws partly from results presented previously in: [26].

Path persistency is primarily affected by the architecture of the building. The existence of long continuous walls such as corridors will certainly help in getting a longer path persistency if the receiver is following the wall.

In order to relate path persistency to building architecture, we will be showing the dependency on wall lengths quantitatively.

5.1 Dependence of Path Persistency on Floorplan Complexity

The use of the method mentioned in the previous chapter is dependent on the internal structure of the building in which tracking is needed. The number of the walls, wall material, average wall length as well as distance of the transmitter to the walls and the

receiver all affect the fact that different MPCs will be available for a varying amounts of time. Since persistency is important to use the proposed method in the most effective way possible, statistical characterization of buildings in terms of building parameters (number of walls, wall lengths, wall material etc.) gain importance. Buildings with simple internal structures and with less clutter will provide better tracking under UDP conditions than buildings with a large number of walls and metallic objects. Hence the number of persistent regions (NPR) on a receiver's pathway will be our first metric in the characterization of buildings. Other two metrics related to persistency are the average segment length (average path lifetime (APL)) and average path displacement (APD). APL is the mean length of all different persistent regions on the receiver's motion path and is an indicator for the average lifetime of a certain path. It shows for how long a path will be persistent in units of distance. It can be written as:

$$APL = \frac{\sum_{i=1}^{NPR} l_i}{NPR} \tag{5.1}$$

where l_i is the lifetime of each persistent path in m. Here we can easily see that low number of persistency regions indicate higher APL meaning paths are more persistent.

The other metric is the APD that shows how much TOA difference there is between different persistency regions on the average. It can be represented as:

$$APD = \frac{\sum_{k=1}^{NTD} dp_i}{NTD} \tag{5.2}$$

where dp_i is the amount of displacement in m when a switch occurs from one persistent path to another and NTD is the number of total displacements.

As a measure of complexity, we consider total number of walls and the mean length of all the walls for a given floorplan. Complex building architectures will have a large

number of walls thus creating a dense multipath environment for the RF propagation. If we assume the floorplan area stays approximately the same, this will result in a shorter mean wall length. Thus reducing the number of walls will result in higher mean wall lengths. This identification might be important to assess the performance of a certain localization system since persistency will directly be related to these parameters. Here we propose a floorplan complexity function $f = f(N, M)$ as

$$f(N, M) = \frac{M}{N} \tag{5.3}$$

where N is the number of walls and M is the mean wall length of a certain floorplan. For the purpose of this study, we consider floorplans with the same total area with different levels of complexity and N and M will be inversely proportional hence the ratio will provide us with a single numeric value that is representative of how complex a floorplan is. The higher this value, the less complex the floorplan is.
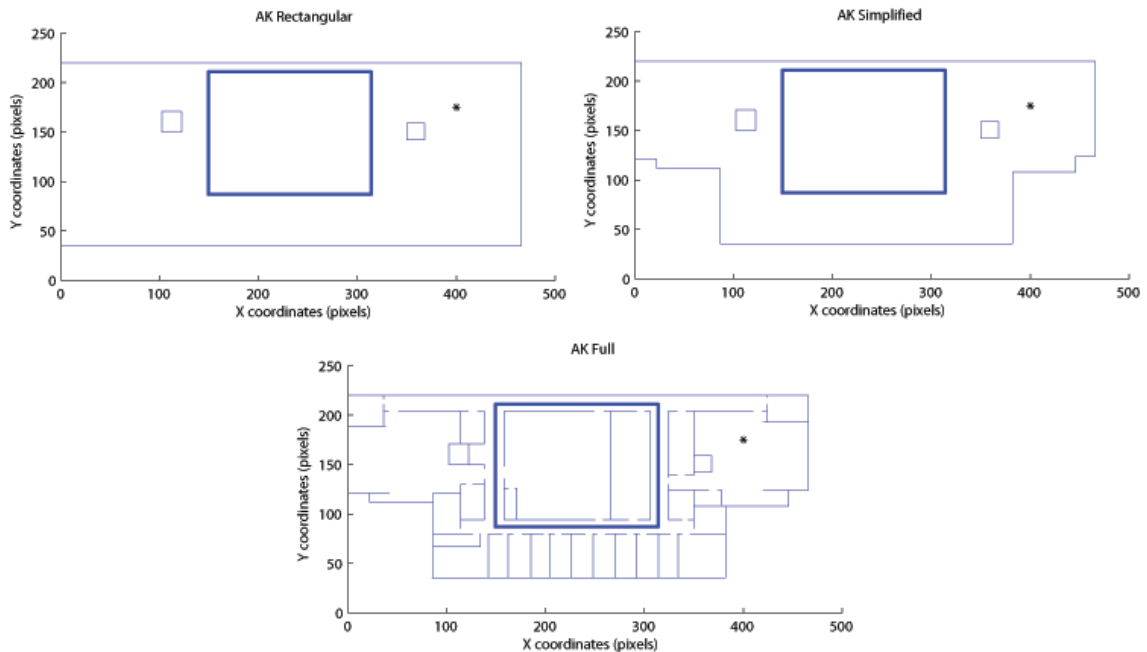
Figure 5.1: 3rd floor floorplan of AK Laboratories with varying levels of complexity

We now present a comparative analysis of persistency for varying levels of floorplan complexity and how certain building parameters affect persistency. In this simulation, SP detection has been performed. Three different layouts of AK Laboratories at WPI with varying levels of complexity have been considered for the simulation. Figure 5.1 shows these layouts. Here AK Rectangular refers to the layout in which the outer walls of the AK 3rd floor is assumed to form a simple rectangle without any interior walls. AK Simplified is the layout with the true outline of the exterior walls but still without the interior walls. AK Full is the full layout of the floor. The closed loop seen in the middle in each of the floorplans is the test loop for the receiver. The two small boxes represent the metallic anechoic test chamber and the elevator shaft respectively. They cause UDP condition on the test loop for certain regions. The asterisk at pixel coordinates (400,170) represents the transmitter. In these floorplans the scaling is such that every 7 pixels represent 1 m. On the test loop each sample measurement is taken every pixel corresponding to about 13 cm.

Table 5.1: Persistency analysis of varying levels of floorplan complexity

Building Type	Number of Walls (N)	Average Wall Length (M) (m)	Number of Persistency Regions (NPR)	Average Path Lifetime (APL) (m)	Average Path Displacement (APD) (m)	$f(N, M)$
AK Rectangular	12	17.31	5	16.37	9.22	1.4425
AK Simplified	20	10.37	7	11.65	9.97	0.5185
AK Full	97	5.46	65	1.09	5.32	0.0563

Figure 5.2 shows the ranging estimate from the transmitter for three different versions of the AK 3rd floor floorplan. The gray rectangular areas represent the UDP regions as blocked by the metallic chamber. From this figure we can see that AK Rectangular and AK Simplified, since very similar in complexity, give smooth (persistent) ranging estimates. When full details are included in the floorplan, ranging estimation becomes rather random especially in the UDP regions due to presence of many MPCs in a confined area. Hence, as the receiver moves on the loop, strongest path changes rapidly meaning
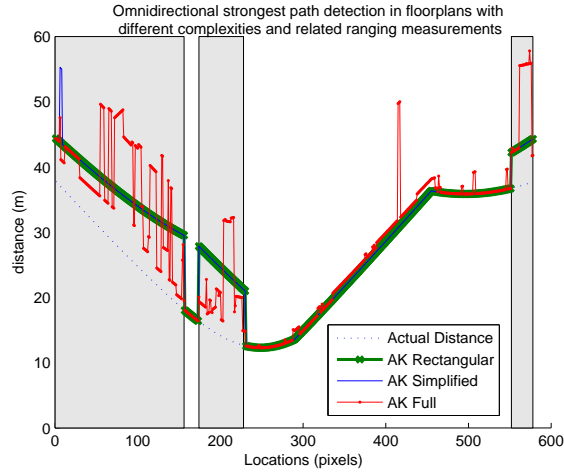
Figure 5.2: Omnidirectional strongest path detection in floorplans with different complexities and related ranging measurements

paths do not persist as much.

For the results of architecture effect on persistency we refer to table 5.1. The table lists floorplan characteristics and the obtained persistency metrics such as NPR, APL and APD as a function of $f(N, M)$. Here we can easily observe that the AK Full floorplan with all the walls, give us 65 different persistency regions, whereas AK simplified gives 7 and AK rectangular 5. As the complexity decreases we get a lower number of persistency regions and higher APL which basically means we have a higher percentage of exploiting persistent paths on a given receiver trace. Figure 5.3 presents cumulative distribution of path lifetimes for the floorplans. This figure is representative of how floorplan complexity greatly affects the persistency behavior of the paths, i.e average path life time decreases significantly with increasing floorplan complexity. The relation of $f(N, M)$ to ranging accuracy can be given as the system's multisector tracking granularity and its computational resources. If paths persist for a longer time it will be easier to track this path with a given angular granularity and with the help of offset/AOA correction precise ranging will be achieved. If the paths do not persist as much, then the system will not be able to differentiate those different paths in a given sector and the relation of these paths to DP

will not be accurately obtained hence leading to inferior ranging estimates.
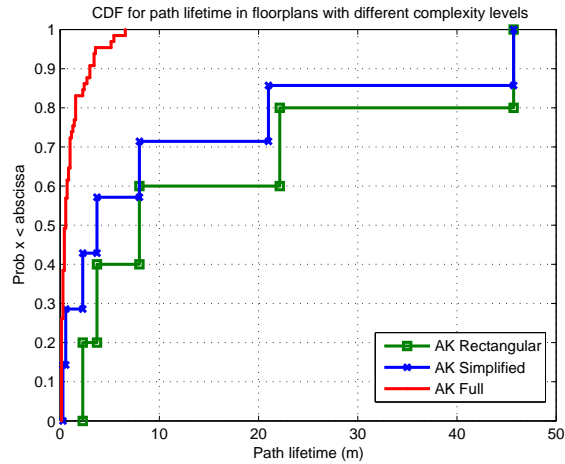
Figure 5.3: CDF for path lifetime for different floorplan complexities

5.2 Relation between Path Persistency and Internal Walls of a Building

In the previous section we showed how the complexity of a floorplan affects path persistency. In this section we will give a geometric explanation for the dependence of path persistency on the length of internal walls of a floorplan.

We will assume there are two walls, a transmitter and a receiver as shown in figure A.1. The receiver moves along the indicated path. We further assume the transmitter location, wall locations and receiver's motion path are predefined as constants.

Here we will only consider two different reflections, a first order reflection from the horizontal wall and a 2nd order reflection from the vertical wall. This concept will be applicable to multiple reflections from multiple walls.

Assuming receiver's line of motion is adequately long a certain path's existence due to a certain wall (corresponding to its persistency) will be directly proportional to the length

of the corresponding wall. The derivation of this dependency is presented in appendix A.

In order to compare the derivation with simulations we developed a simulation platform which is explained in the next section.

5.2.1 Simulations

We created 5 different sets of 50 random square floorplans. Each set represents a different floorplan area. The first set is 10m by 10m (representing very small residential/commercial settings), the second set is 20m by 20m (representing small residential/commerical settings), the third set is 50m by 50m (representing medium residential/commercial settings), the fourth set is 100m by 100m (representing large residential/commerical settings) and the fifth set is 200m by 200m (representing very large residential/commerical settings). The methodology we used in order to create the floorplans is called the slicing tree floorplan algorithm which is extensively used in VLSI floorplaning [100]–[103] and with applications to architecture and building design [104, 105]. This method ideally matches our purposes since most random floorplans obtained by using this method will be representative of real world settings with high efficiency as most buildings are comprised of rectilinear layouts. One such example is given in figure 5.4 as 20m by 20m and 50m by 50m samples. The details of the slicing tree algorithm can be found in appendix B.

After obtaining 250 different floorplans from the simulation platform we took the histogram of all wall lengths and we observed that the distribution can be best represented by a log-logistic random variable in comparison to Exponential and Weibull distributions which were candidate distributions for this type of data. Figure 5.5 shows the cumulative hazard function for the chosen distributions and we see that log-logistic has a better overall fit than the Exponential and Weibull fits. The cumulative hazard function is particularly useful in survival analysis studies and will be presented in more detail in chapter

(a) 20m by 20m   (b) 50m by 50m
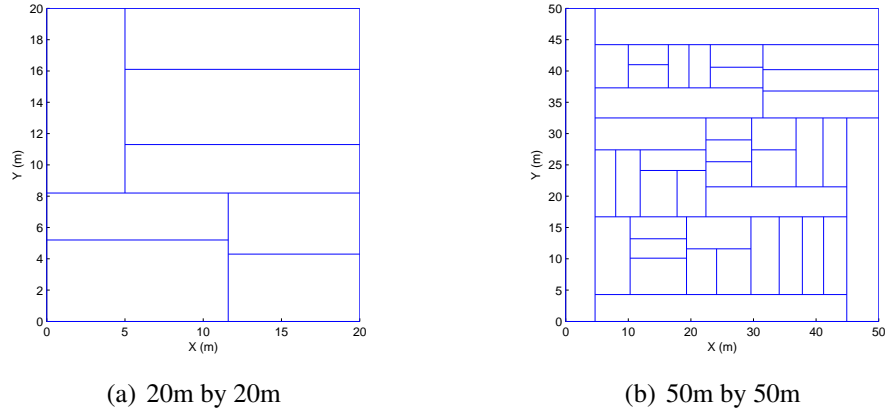
Figure 5.4: Two sample generated floorplans for 20m by 20m and 50m by 50m buildings

7.
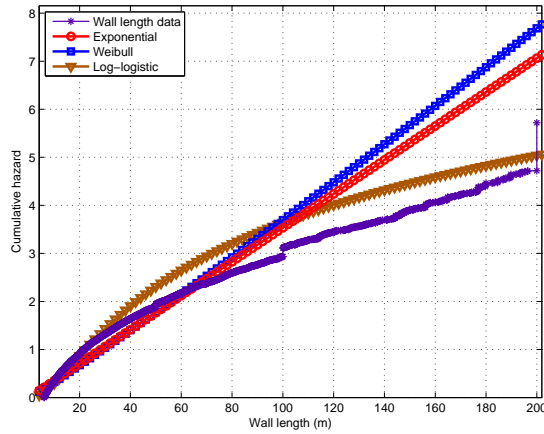
Figure 5.5: Cumulative hazard function for wall length distributions

As we will show in chapter 7, the path persistency is also best modeled using a log-logistic distribution. The fact that the path persistency and wall lengths follow the same distribution (up to scale factor that is dependent on the placement of the wall, transmitter and receiver line of motion) is a strong indication of the validity of our approach in deriving the dependence of path persistency on wall lengths.

5.3 Conclusions

In this chapter we presented a study that analyzed the effect of building architecture on path persistency. We observed that as the floorplan (building) gets more complex (having more walls) the persistency of MPCs drop as expected. Hence accurate indoor ranging will be more challenging in these structures. We also presented the dependence of path persistency on the distribution of internal wall lengths of a floorplan and showed that path persistency follows the same family of distribution as that of wall length.

Chapter 6

Sensitivity Analysis for Multipath Diversity

In this chapter, we present the results of empirical measurements for the sensitivity analysis of MPCs. We practically analyzed the effect of bandwidth, peak detection threshold and UDP occurrence on the number of MPCs and their persistency in a typical office environment using two different measurement scenarios: namely loop and corridor scenarios. This chapter draws substantially from results presented previously in: [27, 28].

The study in this chapter has also been presented as part of the MS thesis by Mr. Yunxing Ye with whom I collaborated during my studies on spatial diversity.

Note: In this chapter LOS and DDP are used interchangeably. Similarly NLOS and OLOS are used interchangeably.

6.1 Spatial Measurements

Some previous measurement campaigns that were carried out in the context of indoor radio channel modeling [106]–[108] did not consider the spatial behavior of the channel.

The primary aim of these studies was to statistically characterize the indoor channel and hence for both practical and coverage reasons measurement points were at least 1 m apart from each other. For the purpose of our research, we developed a new measurement system which is suitable for spatial (dynamic) channel measurements. Spatial channel sounding is much more challenging than traditional static measurements, since it requires consecutive measurements during the movement of the receiver, and the step size between two consecutive measurements should be kept the same for all the measurement locations, which requires accurate control of the receiver's motion. For this purpose we utilized a remotely controlled robot that acted as the receiver in motion. Moreover, since the step size in spatial measurement is much smaller than in static measurements, a manual spatial measurement campaign can be extremely time consuming and requires a huge measurement database. For example, our first measurement scenario is the loop around the CWINS Lab. With the measurement step size of 5cm, we took measurements at 931 different locations to traverse the 46.55 meter distance around the loop.

The measurement scenarios which we will discuss in detail in this chapter are an effort to study the spatial behavior of the multipath channel and the influence of bandwidth, threshold for path detection and UDP occurrence on multipath parameters pertinent to indoor geolocation. The measurement campaign is composed of two experimental steps: Step 1 is designed to study the effect of bandwidth, threshold for path detection, and UDP occurrence on multipath parameters. The transmitter location was fixed and the receiver was moved around a loop which contains different propagation conditions. Step 2 is to study the distance effect on multipath parameters and compare the influence of micro-metal and macro-metal obstructions on multipath parameters.

6.2 Measurement Scenarios

The campaign of measurements was conducted on the third floor of AK Laboratories at WPI. The AK building was built in 1906 and underwent two major remodelings and additions in 1934 and 1981. Therefore, in some areas within the building, there is more than one exterior-type wall. The exterior walls of this building are heavy brick, the interior walls are made of aluminum studs and sheet rock, the floors are made with metallic beams, the doors and windows are metallic, and many other metallic objects are spread over various laboratory areas. The excessive number of metallic objects and heavy and multiple external walls makes this building a very harsh environment for radio propagation. As a result, this environment is suitable for the indoor geolocation experiment since the DP will be attenuated seriously in most locations.

6.2.1 Loop Measurement Scenario

The main purpose of the first set of measurements is to study the effect of bandwidth, path detection threshold and UDP occurrence on multipath parameters. We used the loop around AK 320 (CWINS lab) as the measurement site. Our loop scenario contained mixed conditions including DDP, SUDP and NUDP.

Figure 6.1 shows the measurement site plan and the measured points. The transmitter antenna was fixed at a position inside the CWINS laboratory as shown in figure 6.1, close to a metallic beam on the upper side. The receiver antenna was secured on a bar carried by the robot. This loop was designed to include different receiver location classes. We controlled the robot to move 5 cm at a time, each time stopping to take two measurements (snapshots). The total distance of the loop was 46.55 m which corresponds to 931 different receiver locations and $931 \times 2 = 1862$ bandwidth swept measurements by the VNA. The solid green line in the loop denotes the DDP conditions in which there is no blockage

92

between the transmitter and the receiver or only one wall with window between them. The dashed line denotes the SUDP conditions in which the DP between the transmitter and receiver is undetectable due to metallic obstruction. The blue line denotes the NUDP conditions in which several walls along with long distance between transmitter and receiver cause the DP to drop below the path detection threshold, making it undetectable.

In other words, prior to conducting the measurement, it was desirable to see what happens to the multipath parameters as the receiver moves between DDP, SUDP and NUDP conditions. In radio propagation, it is well known that metallic objects reflect most of the propagating wave and weaken the transmitted signal. Hence, it would be interesting to see whether or not the metallic chamber, metallic beam, and metallic objects would produce UDP conditions or not.
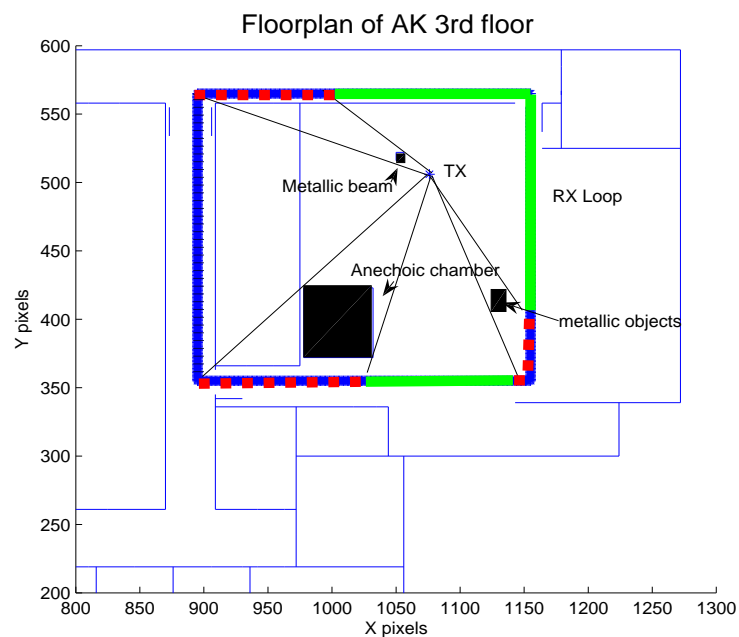
Figure 6.1: Loop scenario on 3rd floor of AK laboratory

6.2.2 Corridor Measurement Scenario

The main purpose of the second set of measurements is to relate the effect of distance on multipath parameters and provide comparison for the later scenarios with similar receiver route but different transmitter locations producing different propagation conditions between the receiver and the transmitter. We used the corridor on the third floor of AK laboratory as the route of the receiver. The transmitter was fixed on a point in the corridor, and the receiver moved smoothly away from the transmitter with a measurement step size 0.1 m as shown in figure 6.2.

As part of the second set of measurements we defined 3 different subscenarios each corresponding to DDP, OLOS and UDP cases to study the effect of UDP as well as the receiver-transmitter separation.

DDP Scenario

We started taking our measurements starting at 1 m up to an experimentally found distance of 30 m. This high range can be explained by the DDP case (no blockage between the transmitter and receiver), as well as a possible waveguiding effect introduced by the corridor.

OLOS Scenario

The purpose of the these measurements is to study the effect of micro-metal objects blockage on multipath parameters and compare this result with that of the LOS (DDP) measurements. We should note here that OLOS scenario is actually a combination of DDP/UDP conditions when the attenuation of the DP is usually more. It can also be regarded as a transitional case between DDP and UDP. We used the same receiver route but moved the transmitter inside the CWINS lab to a location that is the mirror image of the transmitter location used for the DDP scenario behind the wall. The distance range of this scenario
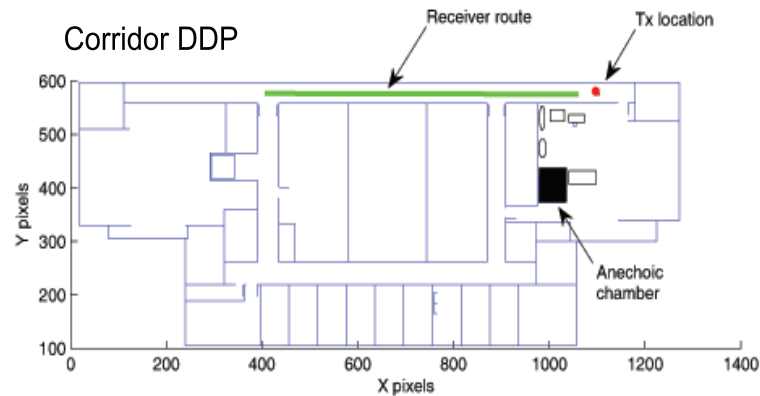
Figure 6.2: Corridor scenario 1 - DDP

has been found to be 16 m, corresponding to 161 different measurement locations. Because of the attenuation caused by micro-metal objects and wall, the UWB signal lost its coverage beyond a distance of 16 m.

UDP Scenario

The purpose of the measurements in this scenario is to analyze the effect on macro-metal object blockage (here referring to the anechoic chamber) on multipath parameters and compare this result with the results of the LOS (DDP) and OLOS measurements. Since we intended to have the anechoic chamber blockage all the time for this scenario, the route of the receiver is slightly different from the LOS and the OLOS scenario. However, we again moved the receiver from the proximity of the transmitter to locations further apart from the transmitter. The signal coverage in UDP condition has been found to be
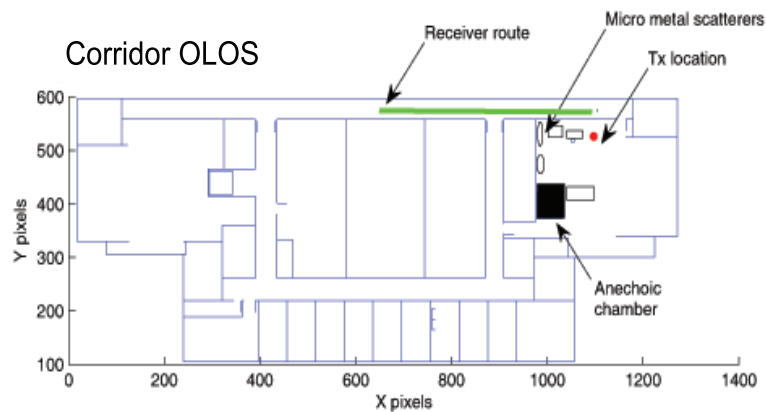
Figure 6.3: Corridor scenario 2 - OLOS

only around 8 m.

6.3   Measurement Setup and Post Processing Technology

With frequency domain sounders, the RF signal is generated and received using a VNA, which makes the measurement setup quite simple. The sounding signal is a set of narrow-band sinusoids that are swept across the band of interest. The maximum sweep time is limited by the channel coherence time. If the sweep time is longer than than the channel coherence time, the channel may change during the sweep. Therefore, in order to prevent the channel from fast variation, we conducted measurements when there were fewer people or other scatterers in the area.

The performance of the frequency domain sounding is also limited by the maximum
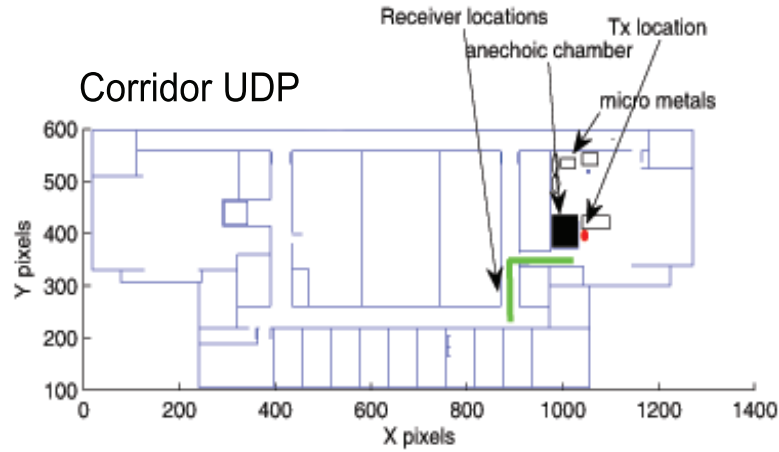
Figure 6.4: Corridor scenario 3 - UDP

channel delay. The upper bound for the detectable delay τ_{max} can be defined by the number of frequency points used per sweep and the bandwidth B (frequency span to be swept), as given by:

$$\tau_{max} = (N_{smp} - 1)/B \qquad (6.1)$$

where N_{smp} is the number of sampled frequency points. The main component of our measurement system is a 40GHz HP-8363B network analyzer. Figure 6.5shows the measurement system and its components.

The measurement system is composed of the network analyzer, two UWB disc-cone antennas with a bandwidth spanning from 3-8 GHz, a power amplifier at the transmitter end, an LNA at the receiver end, and the "ER1" robot system (6.6). The network analyzer is controlled by a laptop computer running MATLAB through wireless network,
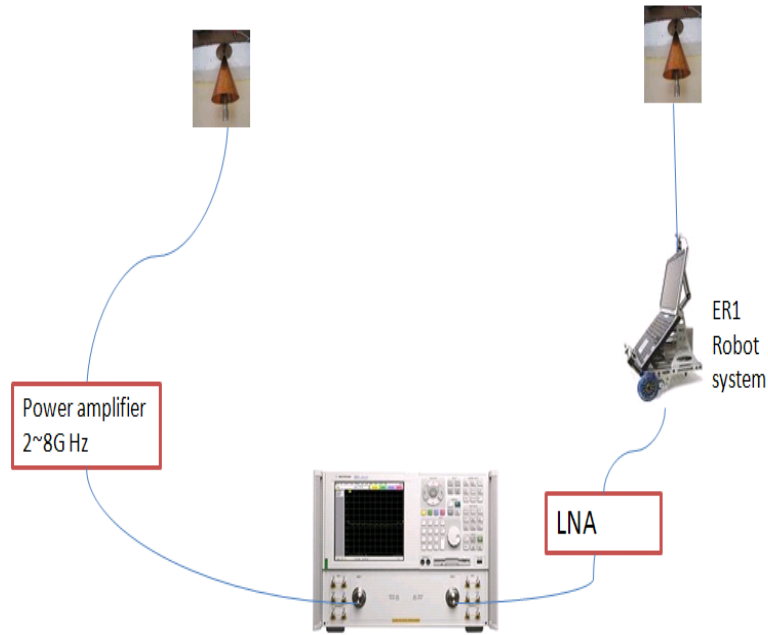
Figure 6.5: Frequency domain spatial measurement system

and Agilent Intuilink connectivity software is used to select the desired parameters of the measurement scenario. The laptop initializes the network analyzer preceding each measurement, where start and stop sweeping frequencies are selected along with the number of desired samples and the data is collected at the completion of each measurement. The transmitted signal passes through a 30dB amplifier before going to the transmitter. The receiver attenuates and pre-amplifies the incoming signal with an LNA before passing it to the network analyzer. For the analysis, The VNA was used to sweep the frequency spectrum of 3-8GHz with 1.5625MHz sampling interval, yielding 3200 frequency domain measurement samples at each location. The UWB antennas were connected to the VNA by low-loss, high quality doubly shielded cables.

Both the transmitter and receiver are fixed at a height of 1.3m during the measurements. The overall measurement system has a noise level of -90dB. A power amplifier at the transmitter side and an LNA at the receiver side are used to supply the experimental

system with enough power to get a range of about 30 m in the DDP scenario.

(a) Architecture of ER1 robot system   (b) User interface
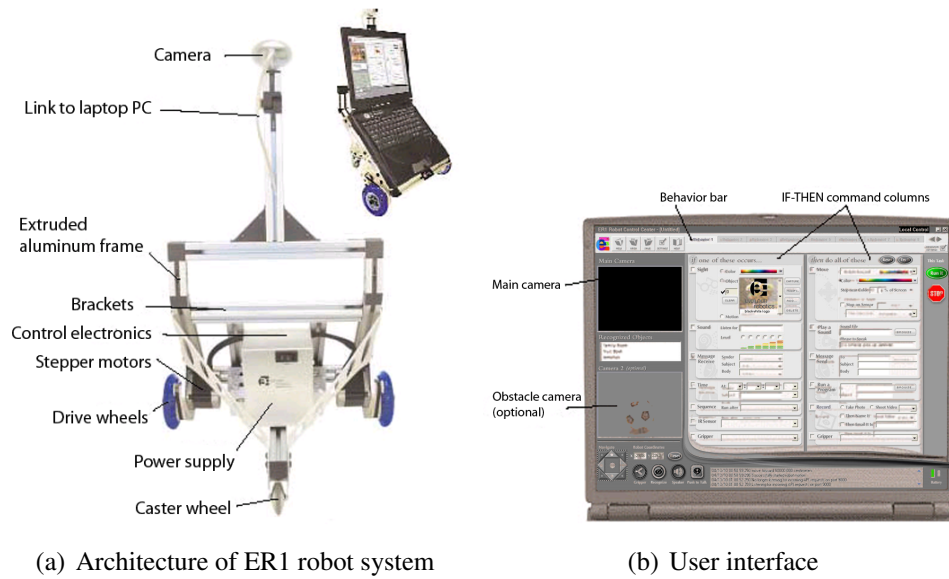
Figure 6.6: ER1 robot system

Before taking the measurements, we calibrated our system by what is called a S21 through response calibration which involves connecting the transmitter and receiver cables back-to-back without the antennas. This removes the delay and attenuation of the cables as well as the amplifiers. The second step of system calibration is connecting the antennas and performing a 1-meter LOS free space calibration. This removes the delay and gain caused by the antennas. As a result, the CIR after calibration would be a single path occurring at 0ns.

The spatial measurements were conducted by commanding the "ER1" robot system to carry our receiver antenna during the measurement campaign [109]. We used software to control the robot moving with a step size of 5 cm (for the loop scenario), 10 cm (for the corridor scenarios), then stopped it to take two measurements. The "ER1" robot system has three wheels, two of which were connected to the stepper motors for precise robot positioning and one dummy wheel used for rotation. There is also a camera on top of the

robot system, hence we made sure that the robot was moving along a straight path during the measurements. The speed and step size of movement can also be precisely controlled from the user end.

The measured frequency response data was windowed with a Hanning window [110] in order to reduce the noise sidelobes. Although some other window functions such as Kaiser window provides higher dynamic range, the Hanning window is selected for its much faster decaying sidelobes which significantly reduces the interfering effect of strong MPCs in peak detection. For the analysis we have chosen to parse 5GHz down to 50MHz bandwidth chunks out of the measured frequency domain data with a center frequency of 5.5 GHz. After obtaining frequency domain measurements, we used an inverse chirp Z transform to obtain CIR [107]. Specifically, 50MHz of bandwidth provides time-domain resolution in the order of $\triangle t_{50MHz} = 20ns \implies 6m(accuracy)$, while 5GHz provides $\triangle t_{5GHz} = 0.2ns \implies 0.06m(accuracy)$. The desired parameters such as amplitudes and delay of each path are detected from the time-domain channel profile using a peak detection algorithm.

Figure 6.7 shows a sample frequency domain measurement and its corresponding time-domain profile. Here we note the frequency selective fading in the frequency domain and the time-domain profile illustrating MPCs arriving at different delays.

6.4 Preliminary Results

In this section, we present some measurement results in order to illustrate the different channel behavior in different scenarios.

Figure 6.8 shows spatial MPC TOA behavior as the receiver moves on the loop. Here we observe that there are more MPCs at UDP locations than the number of MPCs at DDP locations for the loop scenario. One explanation would be that the power of the strongest

100
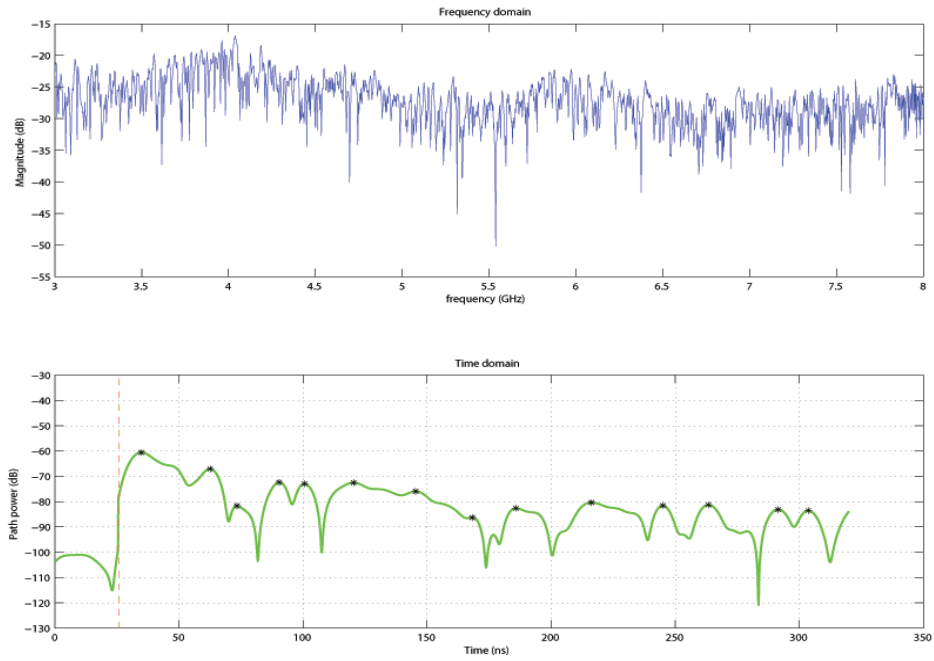
Figure 6.7: Sample frequency domain and time domain channel profile
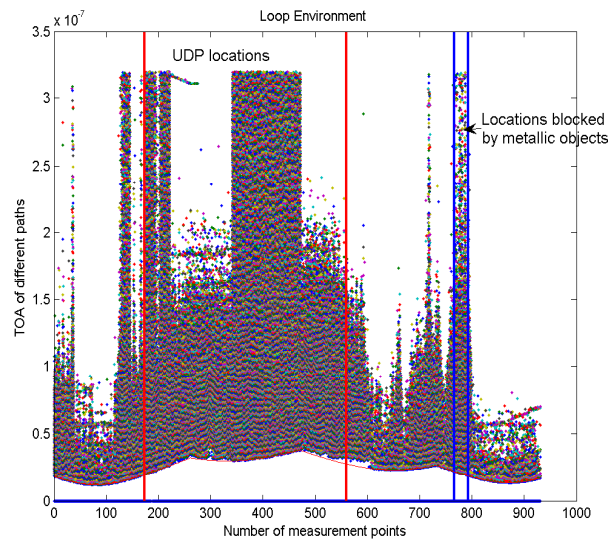
Figure 6.8: TOA of different paths for the loop scenario

path in UDP conditions is weaker compared to that in DDP conditions, bringing more MPCs above the path detection threshold.

Figure 6.9 shows spatial MPC TOA behavior for the corridor DDP scenario. This

101
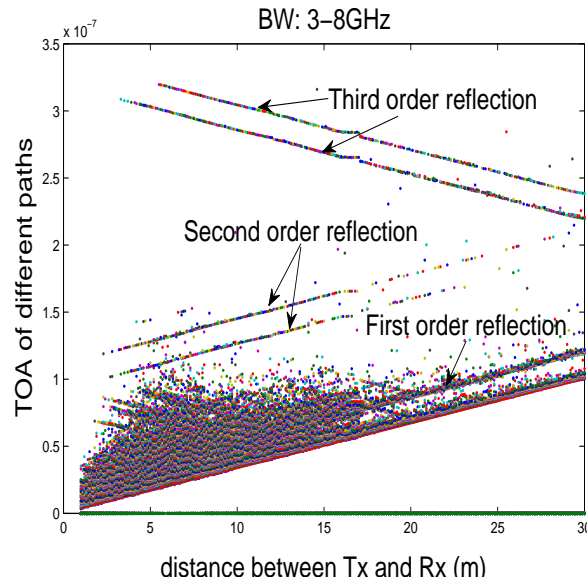
Figure 6.9: TOA of different paths for the DDP scenario

figure shows that for the LOS condition, the TOA of the strongest LOS component increases as the robot moves away from the transmitter. Also observable in the graph are the higher order reflections. These reflections are caused by the back and forth reflections at the two ends of the corridor, which can be shown by comparing their path TOAs to the actual geometric reflected path length. The TOA-distance profile shown in figure 6.9 further substantiate the following observations:

1. When the transmitter is close to the receiver, the number of MPCs is small due to the strong LOS component and the path detection threshold (which means we only consider those paths within α dB of the strongest paths as eligible paths). Most MPCs are below the threshold at the beginning. As the receiver moves away from the transmitter, more paths will be resolved due to the reduction of the gain of the strongest path. After a certain break point, the number of MPCs will start to decrease since as distance increases more and more paths will be buried below noise floor.

2. For the OLOS condition, due to at least one wall separation, even when the transmitter and receiver are at the closest distance, the strongest path between them is much weaker compared to that in LOS condition. Hence, all the resolvable paths above the noise floor will be counted as eligible paths. The cutoff effect of path detection threshold is weaker. As the receiver moves away, the number of MPCs will keep decreasing due to more paths becoming weaker and falling below the noise floor. In the end, resolvable paths disappear when the receiver moves beyond the coverage range of the transmitter. In our case, this limitation for OLOS is around 16 m.

3. When there is the metallic chamber between the transmitter and the receiver, the coverage of the UWB signal is further reduced to around 8 m, which is expected because of the very short wavelength and low transmission power of the UWB signal.
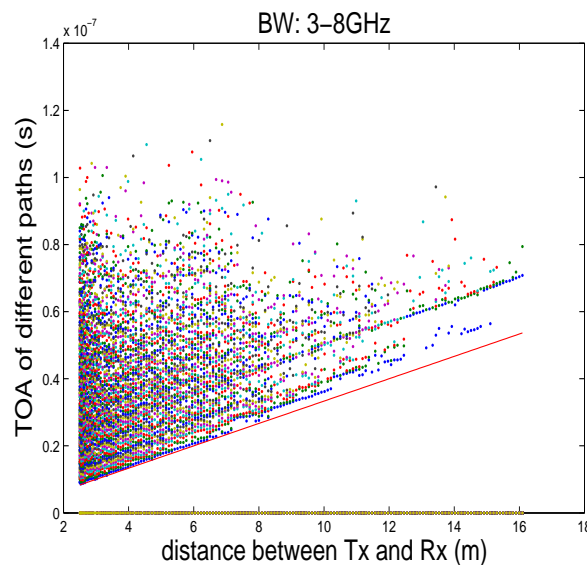
Figure 6.10: TOA of different paths for the OLOS scenario

Figures 6.10 and 6.11 show the spatial MPC TOA behavior for the corridor OLOS

103
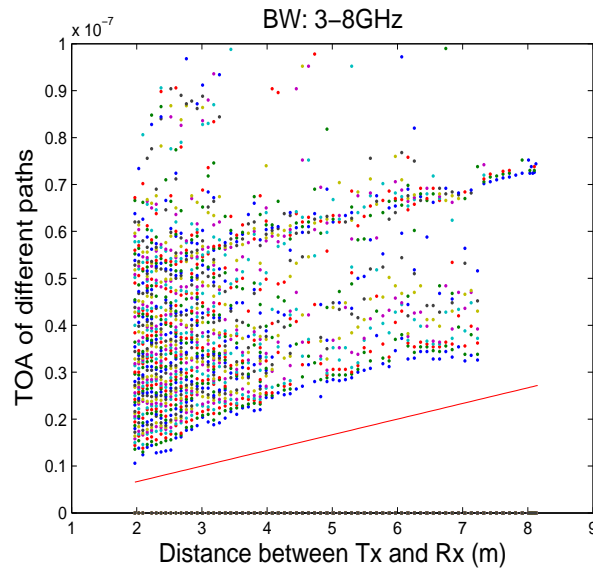
Figure 6.11: TOA of different paths for the UDP scenario

and UDP scenarios. One immediate conclusion we can get from these figures is that the number of MPCs is greatly reduced due to UDP conditions. Also we note in figure 6.11 that there is a significant discrepancy between the actual distance and the distance obtained from the FP.

Thus we can once again iterate that UDP occurrence has a strong effect on multipath parameters and ranging performance.

6.5 Sensitivity Analysis for Multipath Diversity

For the sensitivity analysis of multipath parameters pertinent to indirect path based ranging technique, we will first look into the number of MPCs. Empirical models will be built for different scenarios to reveal the effect of distance, bandwidth, and dynamic range threshold on number of MPCs. After this, we will analyze the sensitivity of two parameters named average path lifetime (APL) and average path displacement (APD) as discussed in the previous chapter. The effect of bandwidth, path detection threshold and

UDP occurrence on path persistency is studied in this section.

Because we want to use other MPCs to mitigate the distance measurement error in UDP conditions, we are interested in the number of available MPCs. The number of resolvable MPCs is important for evaluating the performance of various types of diversity, modulation and equalization techniques (e.g., RAKE receiver) [111]. An MPC measured in a particular profile is defined to arrive at the receiver at a particular excess delay bin τ_k if the integrated power within a discrete excess delay interval β_k^2 is greater than the minimum detectable signal threshold of the receiver. No MPC exists if β_k^2 does not exceed the minimum detectable signal threshold at the excess delay bin τ_k.

Several researchers have analyzed the number of available multipath components in the sense of static channel modeling [111,112]. They looked into the behavior of the number of MPCs at certain locations with different transmitter receiver distances. Then they studied the distribution of the number of MPCs for telecommunication applications. However, due to measurement system limitation and target difference, they have not looked at the the spatial behavior of number of MPCs and the effect of bandwidth, path detection threshold, and UDP occurrence on the number of MPCs, which is also important for indoor geolocation. The analysis of the dynamic behavior of the number of MPCs in different multipath conditions would provide an insight into the resources that can be used to aid the localization in harsh environments.

The comprehensive measurement database introduced earlier is used for spatial multipath analysis. The main focus here is the dependency between the distance-related number of MPCs and the effect of bandwidth, path detection threshold, and UDP occurrence on the number of MPCs and path persistency.

6.6 Behavior of the Number of MPCs

The number of MPCs has been studied in [112, 113] for telecommunication applications. The authors mainly looked into the distribution of the number of MPCs at some selected locations. However, more research is needed for modeling the effect of distance, bandwidth and OLOS UDP occurrence on the number of MPCs for indoor geolocation applications. Since the number of MPCs is sensitive to the threshold value used in postprocessing, we also specify the threshold used for picking MPCs.

6.6.1 Distance Dependency of Number of Paths

As mentioned earlier, we have the following observations for the three different cases:

1. When the transmitter is close to the receiver, the number of MPCs is small due to the strong LOS component and the path detection threshold (which means we only consider those paths within α dB of the strongest paths as eligible paths). Most MPCs are below the threshold at the beginning. As the receiver moves away from the transmitter, more paths will be resolved due to the reduction of the strength of the strongest path. After a certain break point, the number or MPCs will start to decrease due to distance reducing the strengths of more paths and bringing them below the noise floor threshold. Our inference is validated by the measurement result which is shown in figure 6.12.

2. However, for OLOS condition (figure 6.13), due to at least one wall of separation, even when the transmitter and receiver are at the closest distance, the strongest path between them is much weaker compared to the one in the LOS condition. Hence, all the resolvable paths above the noise floor will be counted as eligible paths. The cutoff effect of path detection threshold is weaker. As the receiver moves away, the number of MPCs will keep decreasing due to more paths becoming weaker than the

noise floor. In the end, resolvable paths disappear when the receiver moves beyond the coverage of the transmitter. In our case, this limitation for OLOS is around 16 m.

3. For UDP condition depicted in figure 6.14, the number of MPCs decreases with distance between the transmitter and receiver similarly as the behavior in the OLOS scenario. However, since the anechoic chamber made of metallic material always exists between the transmitter and receiver, the The power of all the MPCs is further reduced compared with that in OLOS condition. Therefore, for the same distance between the transmitter and receiver, there are fewer MPCs above the noise floor. Meanwhile, the coverage of resolvable paths in UDP condition is only around 8 m.
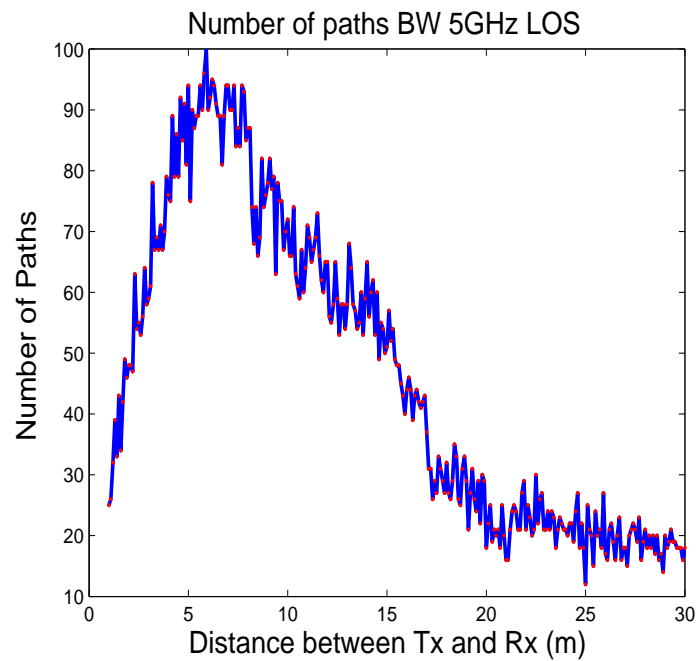

Figure 6.12: DDP scenario number of paths spatial behavior
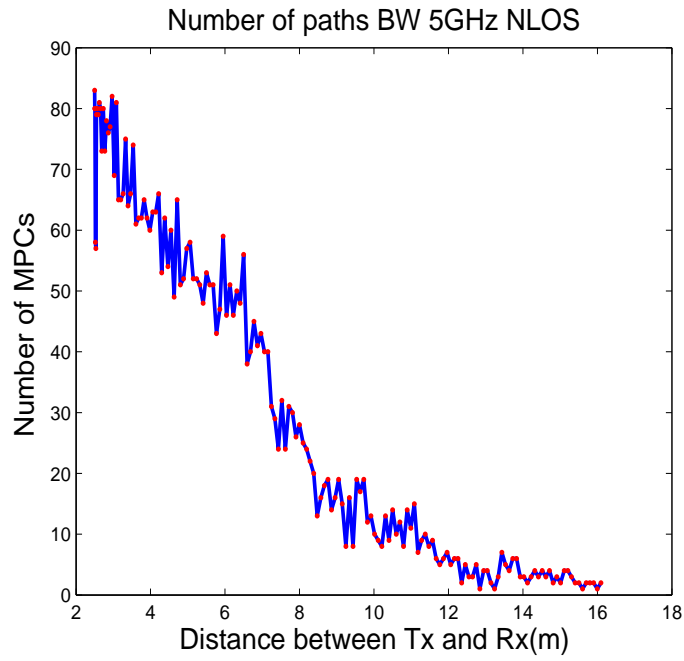
Figure 6.13: OLOS scenario number of paths spatial behavior
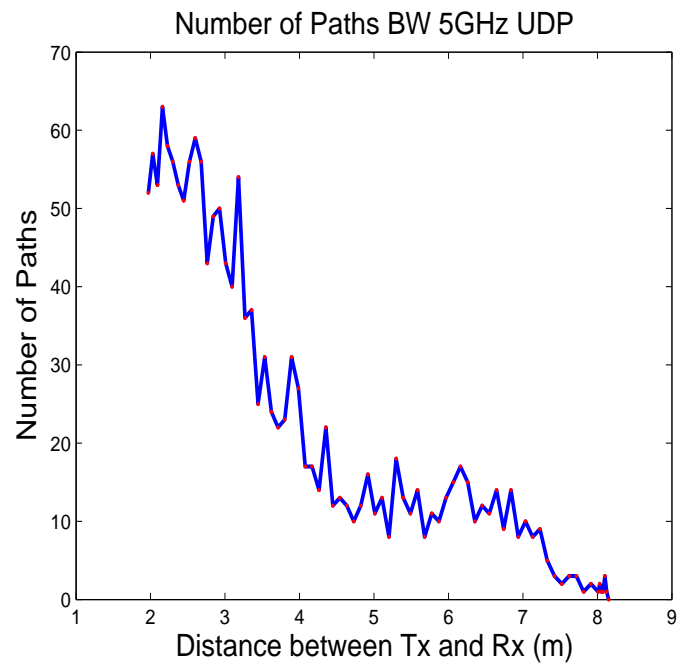
Figure 6.14: UDP scenario number of paths spatial behavior

6.6.2 Modeling Number of Paths based on Bandwidth and Distance

DDP (LOS) Scenario

By analyzing measurement data from the LOS scenario, we observed a Rayleigh-like dependency between the number of MPCs and distance. Hence, we first try to model the relationship between number of MPCs and distance as a Rayleigh-like function as :

$$N = A\frac{de^{(\frac{-d^2}{2\sigma^2})}}{\sigma^2} + \chi_{LOS}, \tag{6.2}$$

where d is the distance between the transmitter and receiver in m. and A, σ and χ_{LOS} are the parameters that need to be estimated. χ_{LOS} is a random variable that can be conveniently modeled with a normal distribution $\chi_{LOS} \sim N(0, \sigma_{\chi_{LOS}})$. Naturally, one expects an increase in the number of MPCs with an increase in bandwidth, an increase in path detection threshold, and a decrease in noise floor. For our specific environment and measurement system, we fixed the path detection threshold at 30dB and noise floor at -90dB. However, the results showed that the Rayleigh-like function is not a very good fit to the measured data when the distance between the transmitter and receiver is larger than 20 m, as in figure 6.15.

Hence, we propose to model the dependence of number of MPCs and distance in LOS condition as a two-piece exponential function. A distance break point exists and for our LOS scenario, the break point is around 6.5 m. The model based on non-linear least square regression is as:

$$\begin{cases} N = \left(2 - e^{0.1032(d-d_{bp})}\right) \cdot N_{max_{LOS}} + \chi_{LOS}, \ \text{d} \leq d_{bp} \\ \\ N = e^{-0.0956(d-d_{bp})} \cdot N_{max_{LOS}} + \chi_{LOS}, \ \text{d} > d_{bp} \end{cases} \tag{6.3}$$

where $N_{max_{LOS}}$ is the number of MPCs at the break point distance, which is related
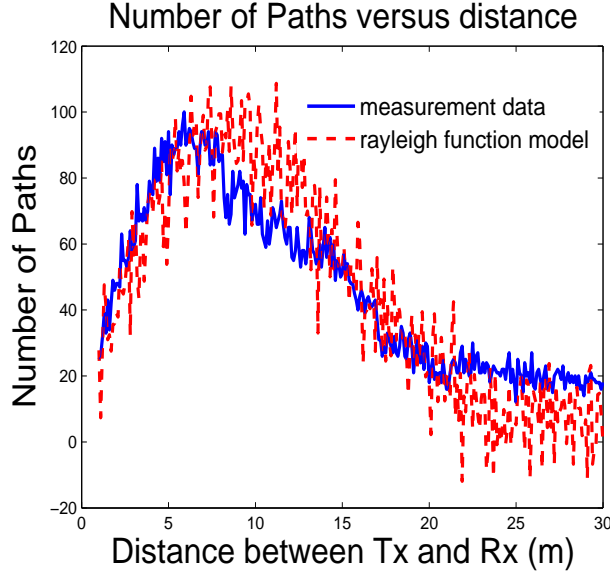
Figure 6.15: Rayleigh model

to the bandwidth (in MHz) f as: $N_{max_{LOS}} = f^{0.547}$, χ is a random variable with normal distribution $\chi_{LOS} \sim N(0, \sigma_{\chi_{LOS}})$, and $\sigma_{\chi_{LOS}}$ is related to bandwidth f as: $\sigma_{\chi_{LOS}} = f^{0.212}$. Figures 6.18 and 6.19 show the relation between $N_{max_{LOS}}$ and bandwidth and the CDF of measured and simulated number of MPCs using our two-piece model for LOS scenario respectively. Figure 6.20 compares the performance of each model in RMSE value at different bandwidth, which demonstrates the superiority of the two-piece model over Rayleigh-like function model at higher bandwidth.

NLOS(OLOS) Scenario

For the NLOS (OLOS) scenario, the relationship between the number of MPCs, distance and bandwidth can be modeled as

$$N = e^{-0.1309d} \cdot N_{max_{NLOS}} + \chi_{NLOS}, \tag{6.4}$$

where $N_{max_{NLOS}}$ is the number of MPCs when the receiver is at the closest distance to the transmitter, which is related to the bandwidth f as $N_{max_{NLOS}} = f^{0.5273}$, and χ_{NLOS}

110
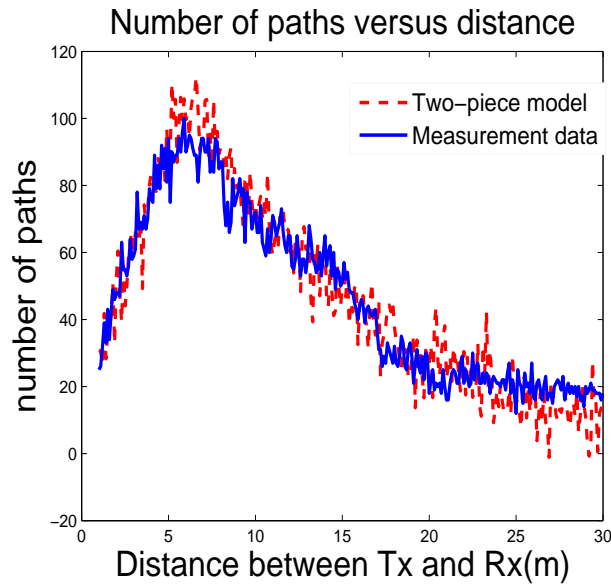
Figure 6.16: Two piece model
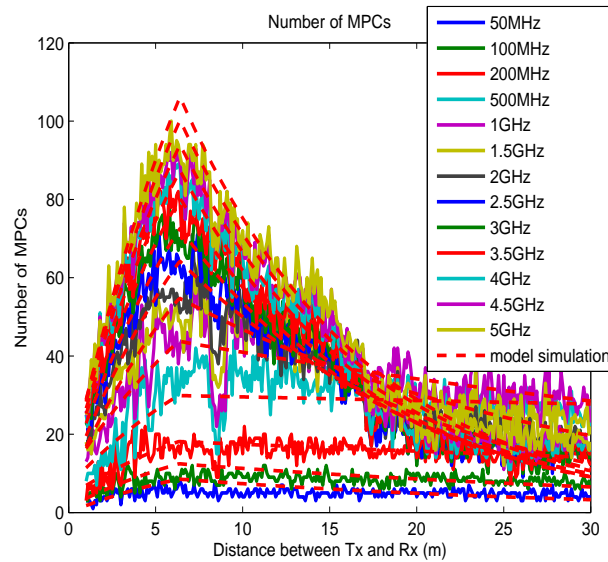
Figure 6.17: Two piece model performance for different bandwidths without χ variable

is a random variable with normal distribution $\chi_{NLOS} \sim N(0, \sigma_{\chi_{NLOS}})$, where $\sigma_{\chi_{NLOS}}$ is related to the bandwidth f as: $\sigma_{\chi_{NLOS}} = f^{0.2645}$. Figure 6.22 and 6.23 show the relationship between $N_{max_{NLOS}}$ and bandwidth, and the CDF of measured and simulated number of MPCs using our model for NLOS scenario. Comparing figures 6.19 and 6.23,
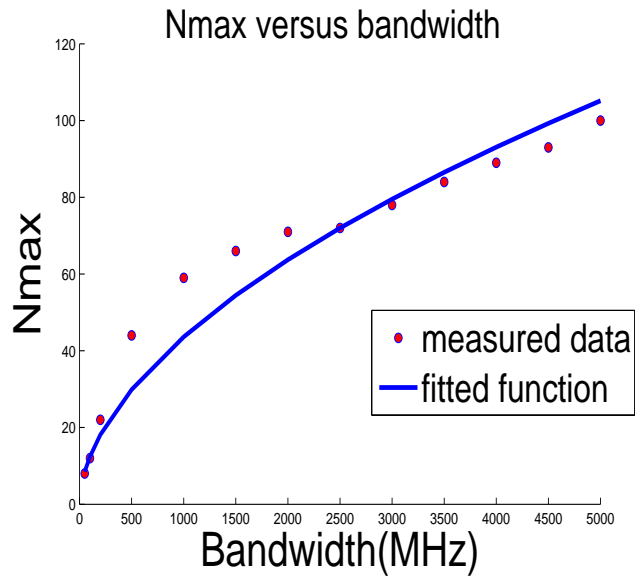
Figure 6.18: N_{max} versus bandwidth for DDP scenario
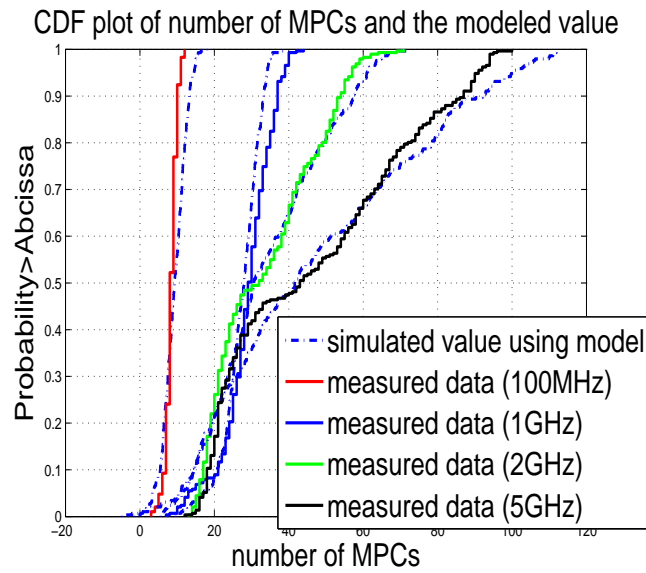
Figure 6.19: CDF of measured and simulated number of MPCs in LOS scenario

our model fits the number of MPCs for LOS conditions slightly better than that for NLOS condition. This is reasonable because NLOS condition is much more complex than LOS condition caused by the blockage of walls and micro-metalic objects.

RMSE for two models predicting the number of paths
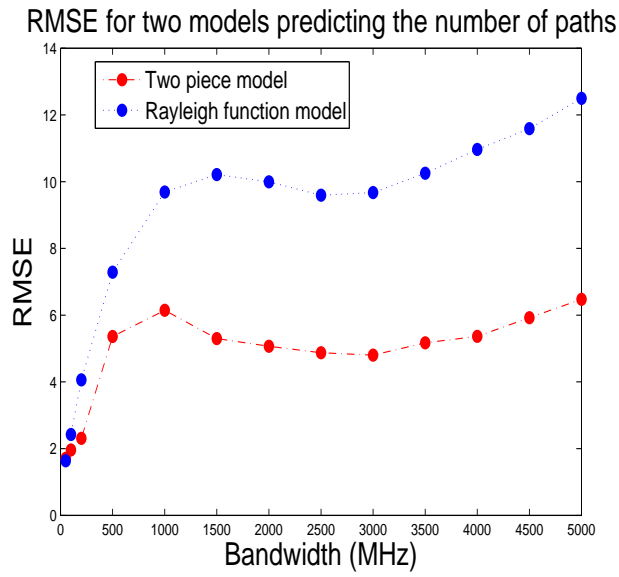
Figure 6.20: RMSE of calculated number of paths using two models at different bandwidths

Number of Paths versus distance (NLOS scenario)
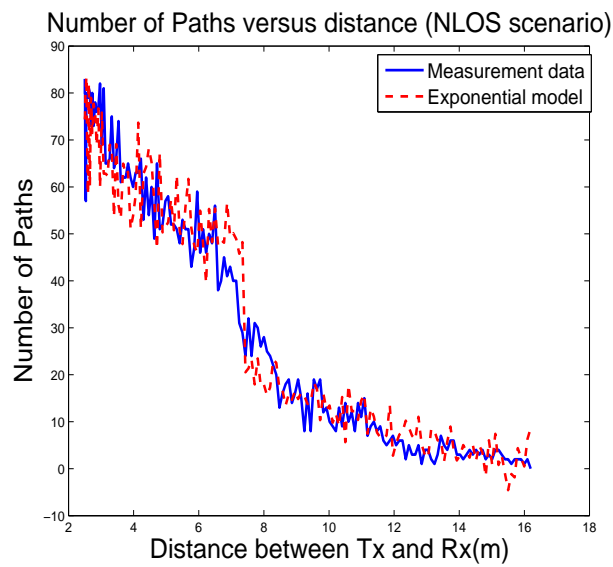
Figure 6.21: Exponential function model for number of paths for OLOS condition

UDP Scenario

For the UDP scenario the relationship between the number of MPCs, distance and bandwidth can be modeled as
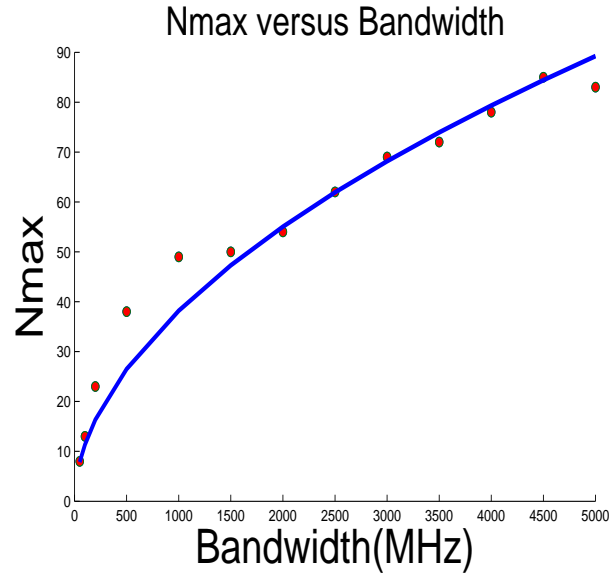
Figure 6.22: N_{max} versus bandwidth for OLOS environment
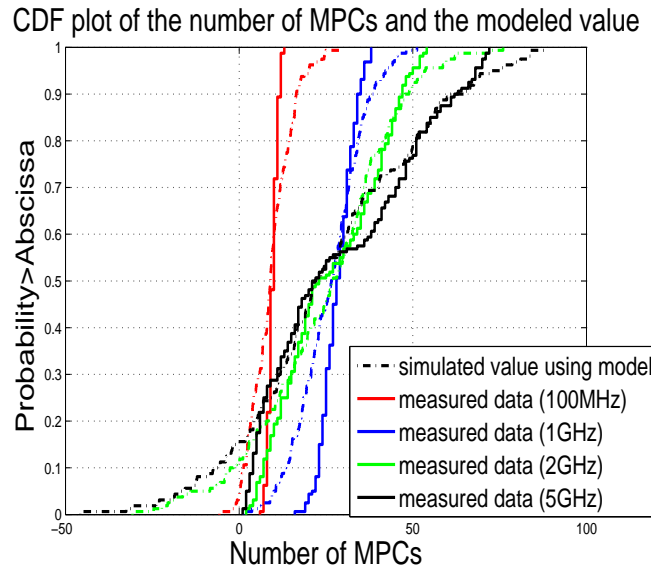
Figure 6.23: CDF of measured and simulated number of MPCs in OLOS scenarios

$$N = e^{-0.4714d} \cdot N_{max_{UDP}} + \chi_{UDP}, \qquad (6.5)$$

where $N_{max_{UDP}}$ is still a parameter related to the bandwidth f, which can be modeled as $N_{max_{UDP}} = f^{0.5844}$, and χ_{UDP} is a random variable with normal distribution $\chi_{UDP} \sim$

$N(0, \sigma_{\chi_{UDP}})$,where $\sigma_{\chi UDP}$ is related to the bandwidth f as:$\sigma_{\chi_{UDP}} = f^{0.1835}$. Figures 6.25 and 6.26and 6.27 show the relationship between $N_{max_{UDP}}$ and bandwidth, the results of model fitting for different bandwidth, and the CDF of measured and simulated number of MPCs using our model for the UDP scenario. The CDF results show our model for the number of MPCs matches well with the measured data in UDP scenario.
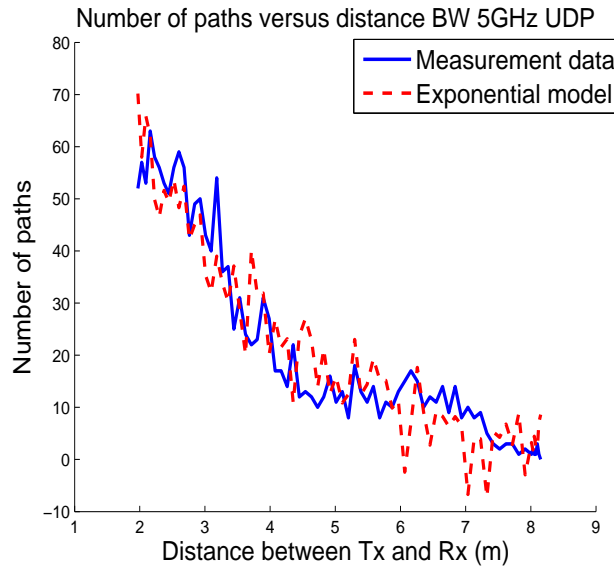
Figure 6.24: Exponential function model for number of paths for UDP condition

6.7 Behavior of Path Persistency

The concept of path lifetime or path persistency has been proposed in [24, 113] and has been explained in the previous chapters. It denotes the lifetime of a particular path in which its traceable features exhibit differential changes in accordance with the receiver's differential motion. Due to the limitation of our measurement system, we only look into the TOA of persistent paths.

To illustrate how we defined path persistency in terms of TOA, it is necessary to introduce two different resolution terms used in time domain:
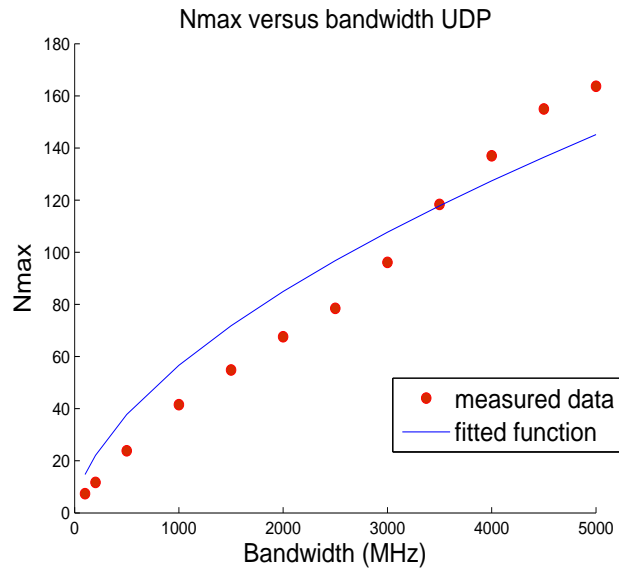
Figure 6.25: N_{max} versus bandwidth for UDP environment
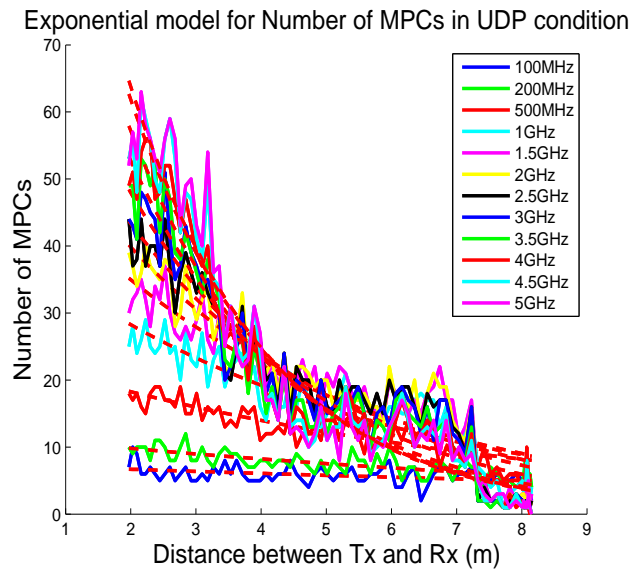
Figure 6.26: Exponential model performance for different bandwidths without χ variable in UDP scenario

- The response resolution

- The range resolution
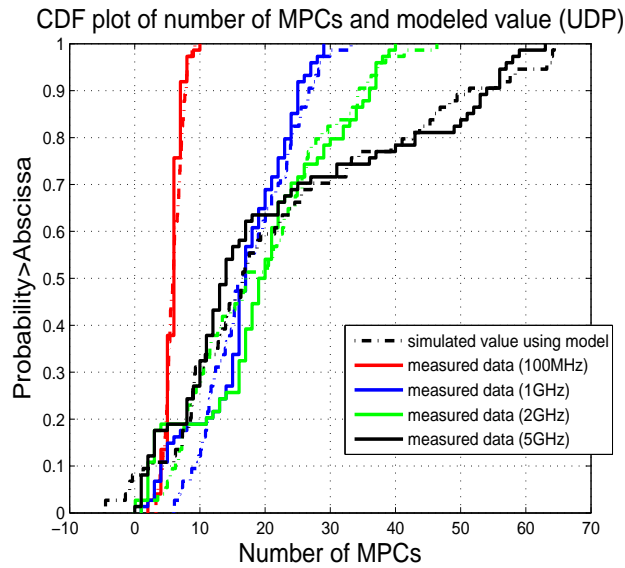
Figure 6.27: CDF of measured and simulated number of MPCs for UDP condition

Response resolution   Response resolution is defined as the ability to resolve two closely-spaced responses, or a measure of how close two responses can be to each other and still be distinguished from each other. It is inversely proportional to the measurement frequency span, and is also affected by the window function used in the transform.
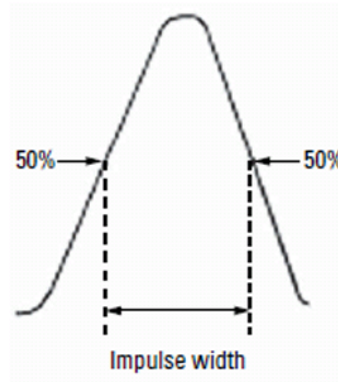
Figure 6.28: Response resolution

For example, using a normal window in the bandpass mode, we can calculate the response resolution for responses of equal amplitude as: Response resolution= 50% impulse width$\times$speed of light as indicated in figure 6.28.

117

Range resolution   Range resolution is defined as the ability to locate a single response in time. If only one response is present, range resolution is a measure of how closely we can pinpoint the peak of that response. The range resolution is equal to the digital resolution of the display, which is the time domain span divided by the number of points on the display. Range Resolution=T_{span}/(Points-1)
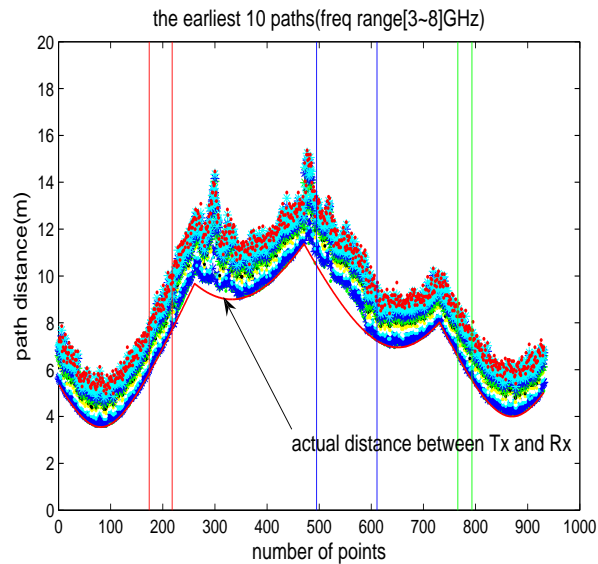
Figure 6.29: TOA of the earliest 10 paths during the measurement loop

Figure 6.29 shows the TOA of the earliest 10 paths during the movement of the receiver around the loop environment. We get the intuition that the paths' TOA exhibit differential changes in accordance with the motion of the receiver in the DDP conditions, which occur at the beginning and ending parts of the route. The solid line is the actual distance and the dotted lines are the earliest 10 paths' lengths calculated by TOA multiplied by the speed of light.

Our measurement step size is 0.1m, which means a maximum difference in TOA of $\delta_\tau = 0.1/C = 0.33ns$, ($C = 3 \times 10^8 m/s$) for a persistent path from one measurement location to the next. If the TOA difference of a particular path between several consecutive measurement points is within δ_τ, then the distance range of these measurement points is

118

defined as the path lifetime of this path. Here we should point out that δ_τ refers to spatial resolution. It does not refer to the response resolution, which is determined by signal bandwidth.

In this section, we investigated the effect of bandwidth, path detection threshold (α)and NLOS, UDP occurrence on path persistency of the SP and FDP, which are important for geolocation application based on measurement results. The parameters we focused on are the APL, and APD.

6.7.1 Parameters Affecting Path Persistency

For the loop scenario, which contains mixed channel profiles (DDP, OLOS and UDP), the path persistency results are summarized in Table 6.1 and figure 6.30.

Table 6.1: APL(m) and APD(m) for FDP and SP for different bandwidths and α=10,20,30dB for the Loop scenario

		Bandwidth				
		128MHz	320MHz	800MHz	2GHz	5GHz
	α	APL APD	APL APD	APL APD	APL APD	APL APD
FDP	10dB	0.02 1.74	0.07 0.72	0.15 0.36	0.15 0.53	0.20 0.33
	20dB	0.02 1.45	0.09 0.47	0.24 0.16	0.52 0.09	1.28 0.03
	30dB	0.02 1.50	0.09 0.46	0.27 0.14	1.61 0.02	7.71 0.003
SP	10~30dB	0.08 8.09	0.14 7.54	0.18 6.41	0.31 2.70	0.38 2.70

Based on the obtained results, we have the following observations:

1. For the same α, the APL of both FDP and SP increases with bandwidth. The relationship between the mean APL of FDP and bandwidth when $\alpha = 20dB$ can be modeled as:

$$APL = 0.0218BW + 0.0256 \qquad (6.6)$$

where BW is the bandwidth in units of 100MHz. The RMSE for this model is 0.046 m. Choosing 20dB has been found to be suitable for detecting paths, while
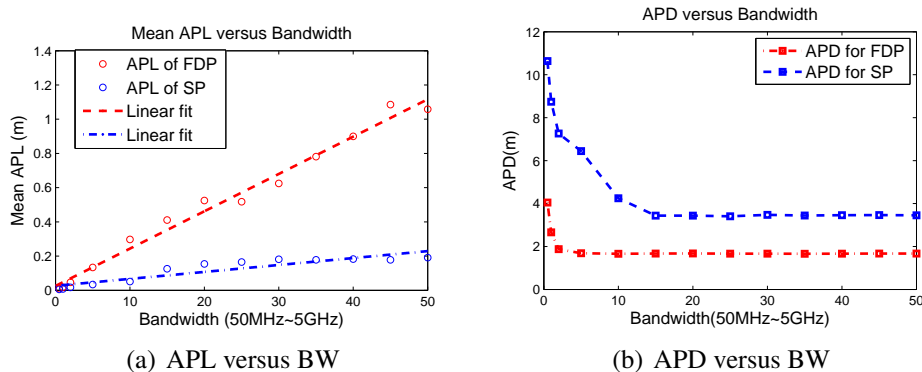
Figure 6.30: APL and APD versus bandwidth and the linear fit ($\alpha = 20dB$)

the relationship between the mean APL of SP and bandwidth can be modeled as :

$$APL = 0.0041BW + 0.0264 \tag{6.7}$$

The RMSE for this model is 0.028 m.

2. The APL of FDP is always larger than that of the SP since the power of paths suffers easily in UDP conditions causing the SP to switch to another path more often.

3. The APL and APD of the strongest path are not sensitive to α since no matter which α we choose, the power of SP is always within the α dB range of itself.

4. The APD of both the FDP and SP decreases as the bandwidth increases, but the APD of FDP and SP stays at around 1.8m for FDP and 3.5 m for SP for bandwidth greater than 0.5GHz for FDP and 1.5GHz for SP respectively.

For the corridor DDP scenario, the path persistency results are summarized in Table 6.2 and figure 6.31.

For the DDP condition we have observed that:

1. Most of the time, the APL of both FDP and SP increases with bandwidth. For the same bandwidth, the mean APL of FDP increases as the threshold value α

Table 6.2: APL(m) and APD(m) for FDP and SP for different bandwidths and α=10,20,30dB for the DDP scenario

		Bandwidth								
		100MHz		500MHz		1GHz		2GHz		5GHz
	α	APL APD	APL APD	APL APD	APL APD	APL APD
FDP	10dB	0.22 1.56	0.74 1.14	1.61 1.15	2.39 1.25	13.90 1.25
	20dB	0.22 1.49	0.73 0.79	1.87 0.80	3.00 0.78	9.23 0.79
	30dB	0.23 1.48	0.70 0.75	1.86 0.76	3.00 0.75	1.65 0.74
SP	10~30dB	0.26 2.89	0.58 3.89	1.15 4.20	1.37 4.11	1.15 4.17
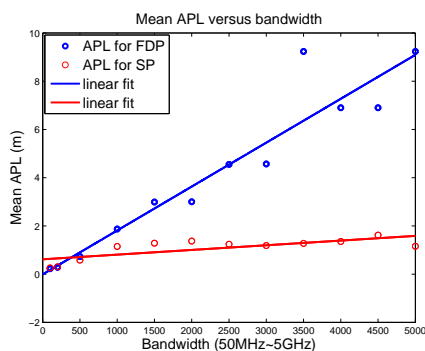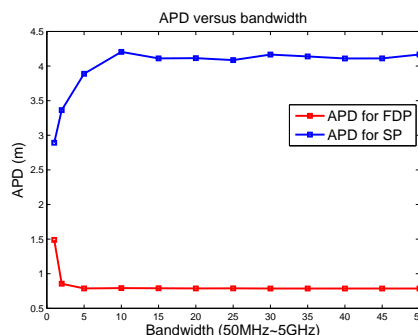
(a) APL versus BW (b) APD versus BW

Figure 6.31: APL and APD versus bandwidth and the linear fit ($\alpha = 20dB$) for DDP scenario

decreases. The relationship between the mean APL of FDP and bandwidth when $\alpha = 20dB$ can be modeled as:

$$APL = 0.182BW - 0.01 \tag{6.8}$$

where BW is the bandwidth in units of 100MHz. The RMSE for this model is 0.972 m. Choosing 20dB is reasonable since a 10dB path detection threshold would eliminate most of the multipath components, making the number of available MPCs insignificant, while if a 30dB threshold is used, the first path would be non-persistent, which is not the fact for the LOS scenario. The relationship between the mean APL

of SP and bandwidth can be modeled as

$$APL = 0.0194BW + 0.6141 \qquad (6.9)$$

The RMSE for this model is 0.274 m.

2. The APL of FDP is always larger than that of the SP which is in accordance with the results for the loop scenario.

3. The APL and APD of the strongest path are not sensitive to the threshold α for picking paths .

4. The APD of FDP in the LOS scenario decreases as the bandwidth increases. However, the APD for SP increases with bandwidth. The APD of FDP and SP stay at about 0.75 m and 4 m for the bandwidth greater than 1GHz.

For corridor NLOS (OLOS) scenario, the path persistency results are summarized in table 6.3 and figure 6.32.

Table 6.3: APL(m) and APD(m) for FDP and SP for different bandwidths and α=10,20,30dB for the NLOS scenario

		Bandwidth				
		100MHz	500MHz	1GHz	2GHz	5GHz
	α	APL APD	APL APD	APL APD	APL APD	APL APD
FDP	10dB	0.11 3.01	0.25 1.65	0.37 1.62	0.48 1.63	0.69 1.83
	20dB	0.11 3.06	0.25 1.69	0.40 1.68	0.57 1.73	0.69 1.90
	30dB	0.11 3.07	0.25 1.69	0.40 1.68	0.57 1.73	0.69 1.90
SP	10~30dB	0.12 11.35	0.20 7.58	0.25 8.32	0.47 8.02	0.55 7.93

For the OLOS scenario we have the following observations:

1. the APL of both FDP and SP increases with bandwidth. However, comparing with the results for the LOS scenario, the APL of FDP decreases due to walls and metallic objects blockage between the transmitter and receiver. For the same bandwidth,

(a) APL versus BW   (b) APD versus BW
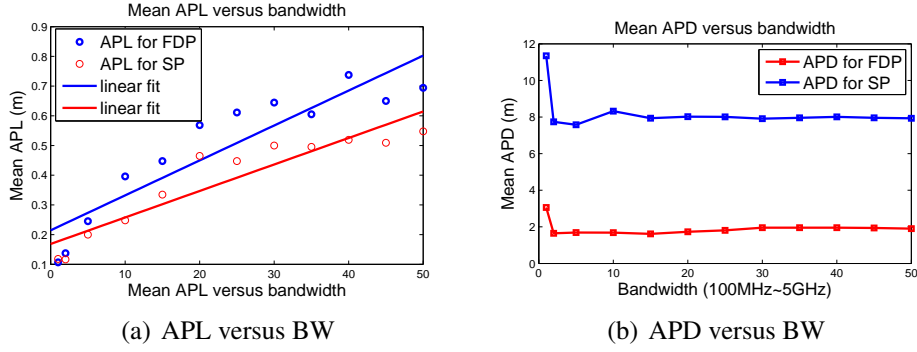
Figure 6.32: APL and APD versus bandwidth and the linear fit ($\alpha = 20dB$) for NLOS scenario

the mean APL of the FDP is not very sensitive to the threshold α. The relationship between the mean APL of FDP and bandwidth when $\alpha = 20dB$ can be modeled as

$$APL = 0.012BW - 0.215 \qquad (6.10)$$

where BW is the bandwidth in units of 100MHz. The RMSE for this model is 0.0851 m. The relationship between the mean APL of SP and bandwidth can be modeled as :

$$APL = 0.009BW + 0.169 \qquad (6.11)$$

The RMSE for this model is 0.057 m.

2. The APL of the FDP is always larger than that of the SP, which is in accordance with the results for Loop and LOS scenario.

3. The APL and APD of the strongest path are not sensitive to the threshold α for picking paths.

4. The APD of both FDP and SP decreases as the bandwidth increases. The APD of FDP and SP stay at about 2m and 8m after the bandwidth reaches 1GHz.

For the corridor UDP scenario, the path persistency results are summarized in Table

6.4 and figure 6.33.

Table 6.4: APL(m) and APD(m) for FDP and SP for different bandwidths and α=10,20,30dB for the UDP scenario

		Bandwidth				
		100MHz	500MHz	1GHz	2GHz	5GHz
	α	APL APD	APL APD	APL APD	APL APD	APL APD
FDP	10dB	0.12 3.10	0.14 1.57	0.32 1.76	0.21 1.52	0.27 1.56
	20dB	0.12 2.97	0.16 1.59	0.12 1.25	0.19 0.93	0.31 0.89
	30dB	0.12 3.12	0.20 1.65	0.15 1.38	0.18 1.07	0.33 1.02
SP	10~30dB	0.10 5.29	0.16 5.27	0.18 6.00	0.15 4.73	0.20 4.73
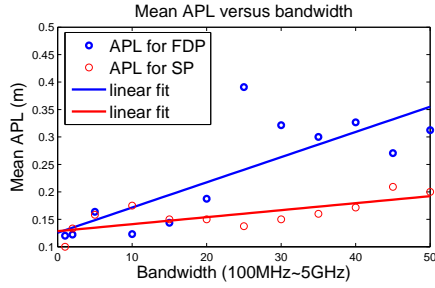
(a) APL versus BW
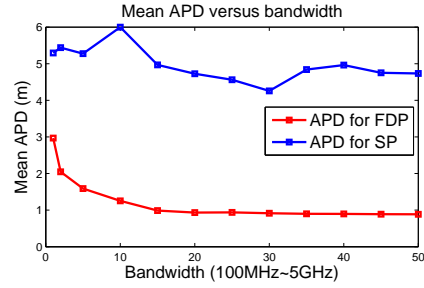
(b) APD versus BW

Figure 6.33: APL and APD versus bandwidth and the linear fit ($\alpha = 20dB$) for UDP scenario

For the UDP condition, we have observed that:

1. the APL of both FDP and SP increases with bandwidth. However, in contrast with the results for of LOS and OLOS scenario, the APL of the FDP decreased significantly due to the wall and micro-metal blockage between the transmitter and receiver, causing the FDP to jump among several different MPCs. For the same bandwidth, the mean APL of FDP is not very sensitive to the threshold value α. The relationship between the mean APL of FDP and bandwidth when $\alpha = 20dB$ can be modeled as

$$APL = 0.005BW + 0.126 \tag{6.12}$$

124

where BW is the bandwidth in units of 100MHz. The RMSE for this model is 0.057 m. The relationship between the mean APL of SP and bandwidth can be modeled as :

$$APL = 0.001BW + 0.128 \qquad (6.13)$$

The RMSE for this model is 0.019 m.

2. The APL of FDP is always larger than that of the SP but the difference between them is not as significant as that for LOS and NLOS scenarios.

3. The APL and APD of the strongest path is not sensitive to the threshold α for picking paths .

4. The APD of both FDP and SP decreases as the bandwidth increases. The APD of FDP and SP stay at about 1 m and 4 m for the bandwidth above 1GHz.

6.8 Conclusions

In this chapter we presented the results of an empirical UWB measurement campaign. Particularly we investigated the effect of system bandwidth, path detection threshold, propagation conditions and transmitter-receiver distance on MPC features such as persistency and the number of MPCs.

Chapter 7

Statistical Spatial Model for Multipath Components

In chapter 4 we introduced the concept of path persistency and how additional MPC information can be utilized to get accurate ranging information. In chapter 6 we presented the results of measurements to gain an insight to various MPC properties such as number of MPCs and persistency. In this chapter we will present our comprehensive spatial MPC model based on data we have obtained through RT simulations. This chapter draws substantially from results presented previously in: [29]–[32].

When we employ TOA based systems for precise indoor ranging and localization there are some serious challenges that we need to take into consideration. These might be listed as:

- Blockage of DP

- Limited system bandwidth

- Lack of MPC behavior study for indoor geolocation

In order to address this problem in general we have the following methods:

- Modeling the behavior of DP to be used for algorithms exploiting DP

  – This is primarily used in GPS, cooperative localization and various other algorithms. Modeling for these algorithms is provided in [23, 114]–[116].

- Modeling the behavior of multipath components to be used by algorithms exploiting multipath diversity (using indirect paths)

  – This method is used in rake receivers for communications applications

  – Channel modeling for performance evaluation of these algorithms is presented in this chapter.

7.1   Overview of Wireless Channel Models

Earlier works in indoor channel modeling focused on communication systems. Some of them used geometric models [117]–[119], and some followed statistical modeling approach based on comprehensive empirical results with emphasis on static channel where transmitter and receiver are kept fixed with respect to each other [112, 120]–[129], while some newer studies also considered the spatial channel behavior [113, 130, 131]. Consequently, a substantial amount of work has been devoted to this field and researchers obtained statistical and empirical models for the indoor environment. Although a majority of these studies focused on high data rate, short range communication applications [132, 133], studies do exist that place more importance on indoor geolocation specific features [18, 20, 59].

We can thus make a classification of wireless channel models as shown in figure 7.1.

Here we should note that there has not been an extensive research on the spatial wireless channel modeling towards geolocation applications. Hence characterization of the

127
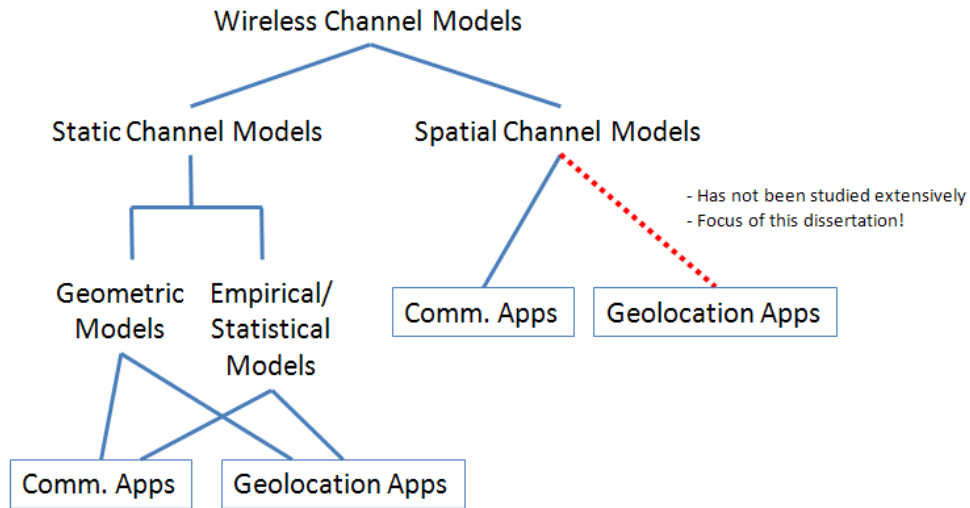
Figure 7.1: Classification of wireless channel models

spatial wireless channel keeping in mind the importance of geolocation applications is the focus of this dissertation.

Spatial channel adds an additional dimension to Turin's well known tapped-delay line model. The static dimensions can be listed as TOA, AOA, path gain as well as phase and number of MPCs. The modeling approach we will present in this chapter will address the evolution of these features over time or equivalently distance the receiver moves. Figure 7.2 shows the static and spatial channel modeling schemes.

We mentioned earlier that the existence of UDP conditions greatly hinder the performance of ranging and hence positioning systems. Under UDP conditions, spatial behavior of the MPCs caused by the dynamic movement of the receiver gains importance since they can be utilized for multipath diversity [20, 96]. When performance evaluation of algorithms using multipath diversity is needed, a modeling approach that takes geolocation related aspects into account is needed.

Hence for accurate modeling of indoor propagation for positioning applications, we would need to have as much information as possible regarding the features of MPCs. Individual TOAs of MPCs relative to the LOS arrival together with their AOAs, path
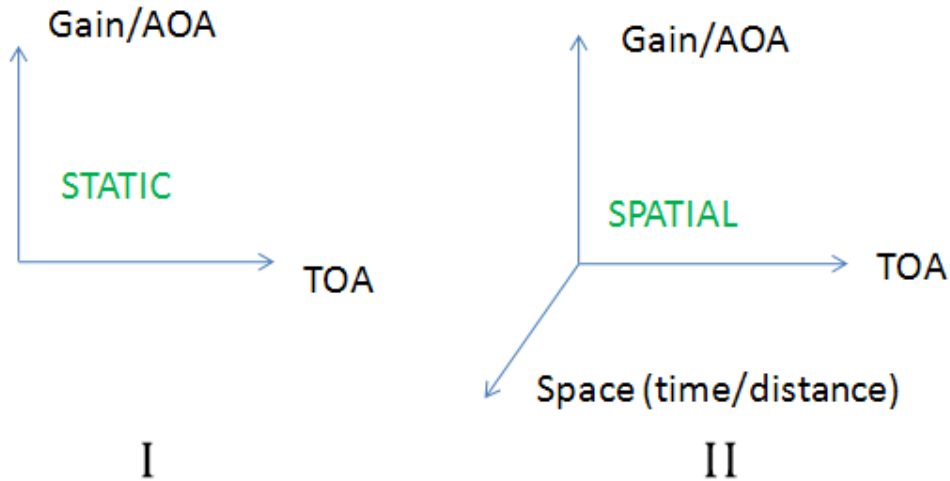
Figure 7.2: Static (I) vs Spatial Channels (II)

gains (amplitudes) and the total number of MPCs need to be known to employ channel aware precise positioning systems that can exploit multipath diversity.

Besides these channel parameters, accurate spatial MPC behavior needs to be considered for the cases of moving transmitter and/or receiver. The studies given in [113, 130, 131] do not present an elaborate solution to MPC behavior in the sense that they do not put emphasis on transmitter-receiver distance and do not consider modeling of number of paths. In this context, we propose a spatial indoor channel model based on ray optics and hence give an accurate characterization for MPCs.

Spatial behavior of the channel encompasses two important metrics. The first and most important of these metrics is the spatial path persistency, which is the lifetime of a path as the receiver is moving at a given velocity. The second is the birth rate which dictates the mechanism paths appear during the motion of the mobile. Path death is dictated by the path lifetime. The available path lifetime models in the literature are [113, 131] which were developed for communication applications. In [131] path birth/death is modeled by a marked Poisson process and hence path lifetime is exponentially distributed. The study reported in [113] follows a different approach and use multi-state Markov

model to describe path birth/death and exponential distribution for path lifetime.

In this chapter, based on an extensive database of measurement calibrated RT results in a typical office building, AK at WPI, we first propose ray optics based statistical models for the features of the MPCs taking into account geolocation aspects like the transmitter-receiver distance by extending the study in [29]. Later we derive the spatial behavior of MPCs based on ray optics and present a modified statistical path persistency and birth model which was first developed in [32] to obtain the full spatial channel model.

7.2   Extended Channel Modeling for Indoor Geolocation

Indoor multipath propagation is dictated by various interactions of the MPCs by the various types of objects such as furniture, walls, doors and windows which have varying degrees of effect on signal propagation. The two main interactions are namely the reflection and transmission. Diffraction and diffuse scattering can be ignored for indoor environments [134]. Based on the material properties, these objects will have different reflection and transmission coefficients. Metal and steel surfaces, for instance, can be considered as specular reflectors but no or very little transmission will take place. On the other hand, materials such as wood or brick, will both reflect and transmit the incoming ray after a certain loss. Each reflection and transmission has a corresponding loss coefficient and will decrease the path power accordingly.

Exact modeling of indoor channel requires tedious solution of Maxwell's wave equations for complex structures. Even though computational electrodynamics methods such as finite-difference time-domain (FDTD) are available, they are not time-efficient and require high utilization of computational resources. As an alternative there exist RT solutions, which are based on ray shooting principles. In terms of speed and conformance to real-world measurement data, RT techniques are preferred for most indoor propagation

prediction studies [135]–[137]. Given a transmitter location, rays are shot in every possible direction (with a certain discretization) and they interact with the objects through either reflection and transmission on which we will elaborate below. The rays, that can reach the receiver through geometric propagation, are considered to be the components of the CIR if they are within the detection threshold.

In RT techniques, each ray is considered to be an infinite bandwidth optical ray. This representation of MPCs is also in line with the channel model that was first proposed by Turin [70] and is well suited to describe RF propagation in multipath-rich indoor environments. We will be considering the spatial case for the receiver and hence spatial multipath channel dependent on the distance variable x can be given as

$$h(x; \tau, \theta) = \sum_{i=1}^{L_p(x)} \beta_i(x, \tau) e^{j\phi_i(x,\tau)} \delta(t - \tau_i(x)) \delta(\Theta - \theta_i(x)) \qquad (7.1)$$

where $L_p(x)$ is the number of MPCs, and β_i, τ_i, θ_i and ϕ_i represent the path gain, TOA, AOA and phase, given by $\phi_i = -2\pi\tau_i/\lambda$, of the ith path, respectively. Based on equation (7.1), we can easily see that the unique features of a single MPC can be characterized by its TOA, AOA, and path gain. Number of MPCs is also an important feature and can be an indicator of how densely cluttered a certain environment is. In the following section we will outline the details of our model and related parameters for each of these features as obtained from the RT simulations performed in AK Labs at WPI. Details of the RT simulation platform will be presented in section 7.5.

7.3   A New Statistical Ray Optical Model

This section presents the overall indoor channel modeling scheme. We first present the statistical models for the TOAs and AOAs of the MPCs. Then, based on the TOA, we obtain the path gain subject to a certain number of reflections and transmissions which

we obtain through the statistics of object interactions. Later, we obtain the number of MPCs based on a distance dependent model derived from our observations.

This statistical characterization of the channel enables us to generate an accurate indoor channel model. The spatial behavior of MPCs can be combined with this model for a complete characterization of indoor wireless channel pertinent to indoor geolocation.

Various channel models are present in the literature that either use geometrically based statistical channel models (GBSCMs) [119] or use statistical fitting methods based on empirical or simulation data [122, 124] as mentioned before. GBSCMs present an optimistic approach which is usually not encountered in real-life scenarios, such as single bounce or a circular/elliptic scatterer region assumption. On the other hand, statistical fitting methods may not be applicable to some environments, since data from measurements or simulations would be limited. However, since real propagation environments are considered, these models might represent the actual indoor RF channel better.

Here, our aim is to present a channel model that takes into account the geolocation aspects. One such aspect is the separation distance between the transmitter and receiver. Many channel models presented in the literature do not differentiate the proximity of the receiver to the transmitter, which is in fact an important factor in determining channel parameters.

The parameters for these models have been obtained through statistical best fit approaches that best represent the RT simulation results. We will give an outline for the model in this section and numerical analysis and related parameter values will be given later in the chapter along with their discussions.

7.3.1 Model for the TOA - τ_i

Based on our extensive RT simulations we propose the use of lognormal model for the distribution of relative TOAs (τ) as

$$f_\tau(\tau) = \frac{1}{\tau\sigma\sqrt{2\pi}}e^{-\frac{(ln(\tau)-\mu)^2}{2\sigma^2}} \tag{7.2}$$

where μ and σ are the mean and standard deviation of $ln(\tau)$.

We should note that this model is actually the distribution of MPC TOAs relative to the LOS distance, hence this way we are also incorporating the effect of transmitter-receiver separation distance into our model. A similar approach has been followed by [126] as they modified the model in [122] by incorporating the LOS distance. Another TOA modeling approach is the modeling of path inter-arrivals as presented in [124], however this model does not take into account the transmitter-receiver separation.

Thus the absolute TOAs can be given as:

$$\tau_{abs}(r) = r/c + \tau \tag{7.3}$$

where r is the LOS distance and c is the speed of light.

The use of lognormal modeling for the TOA has also been proposed by [138] and our findings also confirm the suitability of this model for TOAs of MPCs. Other well known distributions such as Beta and Weibull have also been considered, however, conformance in the maximum-likelihood-estimation (MLE) sense is found to be best for lognormal distribution.

7.3.2 Model for the AOA - θ_i

AOA modeling for indoor channel can be considered as a relatively recent area compared to TOA, since earlier systems were mainly omnidirectional and hence did not exploit the direction of MPC arrival. With advances in antenna technology and signal processing techniques, AOA has gained importance for MIMO systems employing spatial diversity and beam-steering techniques.

Some previous works in AOA modeling include the Geometrically Based Statistical Channel Models (GBSCMs) [119] and measurement fitted statistical models [126]. However, most of these studies are aimed at telecommunications applications. Spencer's Laplacian model [126] is particularly useful for MIMO telecommunications applications in which data rate and coverage are important factors hence relative positions of the transmitter and receiver is not of primary concern. When indoor geolocation applications are considered, AOA information can be used to increase ranging and hence positioning accuracy coupled with additional information such as TOA [24]. AOA information becomes particularly useful in tracking certain indirect MPCs when these MPCs can be used to aid in precise TOA ranging when the LOS path gets blocked due to obstructions [20, 96]. For these applications, relative positions of transmitter and receiver gain importance, since path arrivals will be affected accordingly.

Proposed AOA Model

Based on the collected database of CIRs, we observed strong dependence of the MPC AOAs on the interconnection line between the transmitter and the receiver. In other words, the MPCs tend to arrive close to LOS path. We should point out that actual LOS path might not be available due to obstructions, however the arrival of MPCs were still observed to be in the vicinity of transmitter-receiver interconnection line. In order to describe this behavior, we define the MPC AOA relative to the AOA of the LOS path which is a deterministic value given the locations of the transmitter and the receiver. This is depicted in figure 7.3. Expression of MPC AOAs relative to the LOS path takes into account the receiver and transmitter locations with respect to each other and hence allows for a more descriptive model. As a matter of fact, the placement of transmitter and receivers are generally done according to the building layout and the uniform assumption of transmitter and/or receiver locations inside a building may not be always be a realistic

assumption. Hence dependence of the AOA on transmitter/receiver placement should not be included in the modeling approach; nonetheless, its effect should be explicitly given as a separate variable.
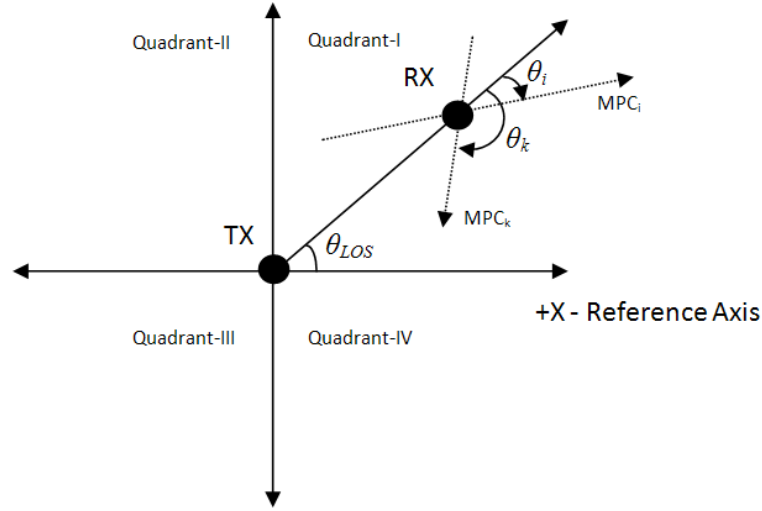
Figure 7.3: Illustration of MPC Arrivals

MPC AOAs can be uniquely identified in the range [-π, π] with respect to the LOS path which is assumed to be the reference axis for all MPC arrivals. Our observations indicated strong angle components at -π, 0, and π finally leading to a distribution model that is in the form of a classic "bathtub" model similar to Doppler power spectral density. We have found this model to show an accurate representation of AOA distribution around the LOS component.

The model for the relative AOA can thus be given as

$$f_\theta(\theta) = \begin{cases} \dfrac{1}{\pi^2 \sqrt{1-\left(\frac{\theta+\pi/2}{\pi/2}\right)^2}} & -\pi < \theta < 0 \\[3ex] \dfrac{1}{\pi^2 \sqrt{1-\left(\frac{\theta-\pi/2}{\pi/2}\right)^2}} & 0 \leq \theta < \pi \\[3ex] 0 & \text{otherwise} \end{cases} \tag{7.4}$$

With the piecewise integration of equation (7.4) we get the CDF as

135

$$F_\theta(\theta) = \begin{cases} \frac{1}{2\pi} sin^{-1}(\frac{2}{\pi}\theta + 1) + 1/4 & -\pi < \theta < 0 \\ \\ \frac{1}{2\pi} sin^{-1}(\frac{2}{\pi}\theta - 1) + 3/4 & 0 \le \theta < \pi \\ \\ 0 & \text{otherwise} \end{cases} \qquad (7.5)$$

The distribution presented in equation (7.5) is the relative AOA. The absolute AOA of a certain path with respect to a certain universal reference is thus given by

$$\theta_{abs}(\theta_{LOS}) = \theta_{LOS} + \theta \qquad (7.6)$$

In equation (7.6), θ_{LOS} is computed as

$$\theta_{LOS} = atan2\left(TX_y - RX_y, TX_x - RX_x\right) \qquad (7.7)$$

with respect to a certain universal reference. In equation (7.2), atan2 is the 4-quadrant inverse tangent and TXx, TXy, RXx, RXy denote the x,y coordinates of the transmitter and receiver respectively. 4-quadrant inverse tangent takes on values from $[-\pi, \pi]$ and is particularly useful for identifying angles with respect to a certain reference axis such as X-axis. Its formal definition is given by

$$atan2(y, x) = \begin{cases} tan^{-1}(y/x) & x > 0 \\ tan^{-1}(y/x) + \pi & x < 0, y \ge 0 \\ tan^{-1}(y/x) - \pi & x < 0, y < 0 \\ \pi/2 & x = 0, y > 0 \\ -\pi/2 & x = 0, y < 0 \\ undefined & x = 0, y = 0 \end{cases} \qquad (7.8)$$

7.3.3 Model for the Path Gain - β_i

Modeling of the path gains and total RSS have been an area of extensive research for the design and performance of wireless systems, since accurate modeling of RSS is important both for communication and geolocation systems alike. Primary focus has been on the outdoor environment for relatively narrow band systems, since earlier systems were developed for long range low rate communications. Due to the nature of narrowband signals, path gains were conveniently modeled as Rayleigh distribution which is attributed to the multipath fading. Signal components are vectorially added according to their phases and the resulting vector could exhibit drastic changes even for short periods of time. The total power for these signals can be given as

$$P_r = P_0 \left| \sum_{i=1}^{L_p} \frac{a_i}{d_i} e^{j\phi_i} \right|^2 \tag{7.9}$$

where P_0 is the power of the signal at 1m, L_p is the number of MPCs, ϕ_i and a_i are the phase and overall reflection/transmission factor for ith path after j interactions expressed as

$$a_i = \prod_j \alpha_{ij} \tag{7.10}$$

with α_{ij} being either the reflection or the transmission coefficient for the jth interaction ($\alpha_{ij} = R$ for a reflection, and $\alpha_{ij} = T$ for a transmission), and $d_i(= c\tau_{abs})$ is the total distance the MPC has traveled.

However, for wideband systems, since individual paths can be isolated to a certain degree, their phases do not contribute to amplitude characteristics of the channel. In this case, total power is found by squaring the path gain of each arriving path and summing them over all the arrivals. This can be expressed mathematically as

137

$$P_r = P_0 \sum_{i=1}^{L_p} \left| \frac{a_i}{d_i} \right|^2 = \sum_{i=1}^{L_p} |\beta_i|^2 \qquad (7.11)$$

Most studies model P_r distribution based on statistical methods similar to τ and θ. Here we are going to follow the work by [127] to obtain path gains by statistical interactions of each path with the walls either by transmission or reflection. The path gain, after a total of $m + n$ interactions (a total of m reflections and n transmissions) can be given as

$$\beta_i = \frac{A}{c\tau_{i,abs}} \prod_j \alpha_{ij} \qquad (7.12)$$

where A is the signal amplitude at 1m given by $A = \sqrt{G_t G_r} \frac{c}{4\pi f} = \sqrt{P_0}$, $\tau_{i,abs}$ is the absolute TOA of the ith path. Here G_t, G_r, c and f are the transmit and receive antenna gains, speed of light in m/s and center frequency of the signal respectively. For isotropic antennas, $G_t = G_r = 1$ and for our modeling approach we have chosen $f = 1GHz$.

For the distribution of object interactions we have observed a very good conformance to Poisson distribution which has also been observed by [127]. Furthermore, both reflections and transmissions can be modeled separately as independent Poisson distributions. We will model the distributions of number of reflections, m, and number of transmission, n, as follows

$$P(M = m) = \frac{\lambda_r^m}{m!} e^{-\lambda_r} \qquad (7.13a)$$

$$P(N = n) = \frac{\lambda_t^n}{n!} e^{-\lambda_t} \qquad (7.13b)$$

where λ_r and λ_t are the average number of reflections and transmissions respectively.

Although number of reflections and transmissions are dependent on the distance an MPC travels, this method provides a simpler and straightforward modeling. For a more

138

detailed analysis of path gain modeling one can refer to [127].

Hence, given the transmitter-receiver distance τ_{abs} as obtained from the TOA model, m and n as obtained from equations (7.13a) and (7.13b), we can use equation (7.12) to estimate path gains.

7.3.4 Model for the Number of MPCs - L_p

Number of MPCs is also an important parameter in estimating the characteristics of the indoor channel. It is related to the degree of the clutter around the transmitter and/or the receiver. Unlike the outdoor propagation medium, a large number of MPCs will be present in the indoor environment due to numerous interactions with walls and objects. There are two important quantities related to the detection of MPCs at the receiver. The first one is the sensitivity (ψ) of the receiver which determines the ability of the receiver to detect signals above noise threshold. Signals below the sensitivity of the receiver will not be detected. The second one is the dynamic range (ρ) of the receiver which determines the ability of the receiver to detect weak signals in the presence of stronger signals [12]. Hence the number of MPCs will be effected by the dynamic range of the receiver and the sensitivity. An MPC can hence be detected if the following hold

$$
\begin{aligned}
\frac{|\beta_{SP}|^2}{|\beta_i|^2} &\leq \rho \\
|\beta_i|^2 &> \psi
\end{aligned}
\tag{7.14}
$$

where β_{SP} is the path gain for the strongest path.

Dynamic range or ρ can also be thought as the threshold for picking paths in the CIR relative to the strongest path. Here we should note that we used α in the previous chapter as the path detection threshold which is identical to the dynamic range.

For small values of transmitter receiver separation we would expect the presence of strong MPCs hence the number of MPCs will be limited by the dynamic range. As the distance increases MPC powers will drop and consequently receiver sensitivity will be the limiting factor. At a certain distance, D_T and beyond, we would not expect to see any more paths since the receiver will be beyond signal detection point. We also expect that the number of MPCs will show a random behavior since at two different locations which have the same distance between the receiver and transmitter, it is possible to observe different number of MPCs due to the existence of clutter.

Based on the results of our simulations we propose the negative binomial model for the number of MPCs. The use of negative binomial distribution is well suited as compared to the widely used Poisson distribution due to overdispersion of data [139]. The probability mass function of this model for $d_{ref,\rho} < d < D_T$ can be given as

$$p(L_p = k; r_{d,\rho}, p_{d,\rho}) = \frac{\Gamma(r_{d,\rho} + k)}{k!\Gamma(r_{d,\rho})} p_{d,\rho}^{r_{d,\rho}} (1 - p_{d,\rho})^k \qquad (7.15)$$

where $r_{d,\rho}$ and $p_{d,\rho}$ are the distance and threshold dependent parameters of the distribution. The special case of $d \leq d_{ref,\rho}$ and $d \geq D_T$ will be discussed shortly.

The distance dependence of these parameters can be attributed to the distance dependent mean value of this distribution which is given by

$$\mu_{d,\rho} = r_{d,\rho} \frac{1 - p_{d,\rho}}{p_{d,\rho}} \qquad (7.16)$$

The distance dependency of the mean can be best given by

$$\mu_{d,\rho} = f_1(d) f_2(d) \qquad (7.17)$$

where $f_1(d)$ is the function governing the variation of MPCs due to dynamic range and $f_2(d)$ is the function governing variation of MPCs due to receiver sensitivity.

Hence, based on the results of our simulations, we propose the following model for $\mu_{d,\rho}$.

$$\mu_{d,\rho} = a_{1,\rho}de^{-d/a_{2,\rho}} = r_{d,\rho}\frac{1-p_{d,\rho}}{p_{d,\rho}} \tag{7.18}$$

Here $f_1(d) = a_{1,\rho}d$, a linear function accounting for the effects of dynamic range, and $f_2(d) = e^{-d/a_{2,\rho}}$, an exponential function accounting for the effects of receiver sensitivity.

In order to get the parameters of the negative binomial distribution, namely $r_{d,\rho}$ and $p_{d,\rho}$, we also need to model one of the parameters. We have chosen to model $p_{d,\rho}$ and by using (7.16) we can obtain $r_{d,\rho}$ as

$$r_{d,\rho} = \frac{\mu_{d,\rho}p_{d,\rho}}{1-p_{d,\rho}} \tag{7.19}$$

After a careful investigation of the data we propose to use the following model for $p_{d,\rho}$ for $d \in (d_{ref,\rho}, D_T)$

$$p_{d,\rho} = b_{1,\rho}e^{-log_{10}(d)/b_{2,\rho}} + b_{3,\rho}e^{-log_{10}(d_{ref,\rho}-D_T)/b_{4,\rho}} \tag{7.20}$$

where $d_{ref,\rho}$ is the ρ dependent reference distance until which the number of MPCs is assumed to be 1. For the special case of $d \leq d_{ref,\rho}$ we assume that there is only one path (the DP). In other words at such small distances the presence of the strong direct path shadows all other paths. Thus we have $p(L_p = 1|d \leq d_{ref,\rho}) = 1$. For $d \geq D_T$ we have $p(L_p = 0|d \geq D_T) = 1$.

We should also note here that since RT simulations are based on infinite bandwidth assumption, it gives us all possible rays reaching the receiver. When bandwidth restrictions are imposed, paths that are closer to each other than the MPC resolution interval will be detected as one path. Hence we expect a decrease in the number of paths as we start to decrease signal bandwidth. The effect of bandwidth on MPC count has been studied in

the previous chapter based on empirical measurements and the modeling approach differs from RT. In the previous chapter number of paths have been modeled differently under different propagation conditions.

7.4 Spatial Multipath Model Based on Geometrical Interpretation

Method of Transmitter Images (MOTI)

Indoor propagation environment can be modeled by vertical and horizontal dielectric structures (walls, furniture, windows etc.) with certain reflection and transmission coefficients. Conducting surfaces such as metallic doors or steel beams can be modeled by a reflection coefficient of 1 and a transmission coefficient of 0. The propagation path of the rays emanating from the transmitter can be expressed as a direct path between the receiver and the image of the transmitter corresponding to the last reflecting surface. Thus for each reflecting wall we will have a virtual transmitter obtained through the principles of transmitter images. Hence, the complete multipath propagation can be expressed as the combination of direct paths between all possible transmitter images and the receiver. The idea of source (transmitter) images has also been used by other researchers [140, 141]. This is depicted in a very basic 4 wall scenario given in figure 7.4. Here we have a transmitter (TX) and a receiver (RX) at the indicated positions, and we assume a rectilinear motion for the receiver composed of horizonal and/or vertical motion paths. For convenience, we choose the lower left corner of this room as the universal origin (0,0) and distances are with respect to this point. For this special scenario considering TX is located at coordinates (TX_x, TX_y) and RX is at (RX_x, RX_y) and wall distances from origin are given by d_H and d_V for the top horizontal and right vertical walls respectively, we have

$$x_m = 2jd_V \pm TX_x, j \in (-\infty, \infty) \tag{7.21}$$

$$y_m = 2kd_H \pm TX_y, k \in (-\infty, \infty)$$
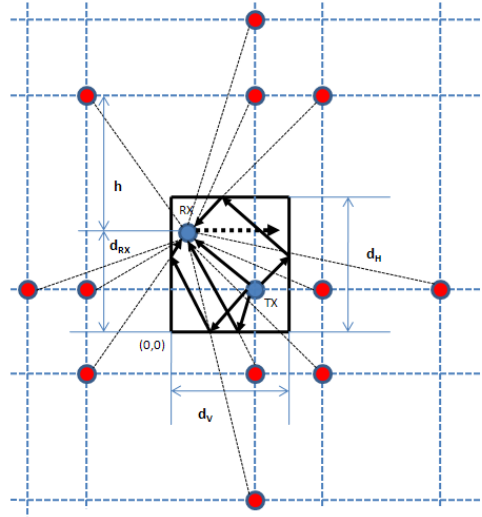
Figure 7.4: Method of transmitter images

$$h = \begin{cases} |y_m - d_{RX}| & \text{horizontal} \\ \\ |x_m - d_{RX}| & \text{vertical} \end{cases} \tag{7.22}$$

where h denotes the distance of transmitter image location to the receiver's path of motion for horizontal or vertical motion of the receiver and d_{RX} is the vertical or horizontal distance of the receiver's path of motion respectively. Theoretically speaking, infinite images will be created however, in practice, transmitter images created after a certain order of reflections can be ignored since signal will diminish after back and forth reflections and transmissions.

As we include more details in the floorplan, reflection structure will become more complicated since number of first order reflections will increase exponentially with linear

143

increase in the number of walls and when we consider higher number of reflections, the determination of image locations will demand high computation power and resources.

MOTI can be considered as a framework for explaining spatial MPC behavior by treating each path as coming from a virtual source which is created by the reflecting and transmission mechanisms inside the building. We will introduce the spatial MPC behavior in the following subsections. Section 7.4.1 will present the path birth for appearance of paths, section 7.4.2 will introduce and present the persistency or equivalently the lifetime of the paths and section 7.4.3 will give the spatial path behavior during path persistency.

7.4.1 Path Birth Rate

During the course of the receiver movement, many paths will appear and disappear. Path appearance is the formation of a new reflection mechanism so that an MPC can reach the receiver by this propagation scenario. Path disappearance, on the other hand, is the loss of a reflection mechanism since an MPC cannot reach the receiver via the same propagation scenario anymore. The disappearance or "death" of paths will be governed by the path persistency since a path will be assumed dead at the end of its persistency which will be discussed next. However, we need to have a certain model for the generation or "birth" of new paths. The mechanism by which these paths are born has been studied through various models in the literature [113, 131] as mentioned before. Based on our observations, we propose a Poisson birth model for the number of paths that are born. One previous study [123] proposed a Poisson model for the arrival of paths in the static case. In that study, experiments and simulations were performed at predefined transmitter or receiver locations and a number of CIRs were collected. Hence these models are actually valid for the τ axis. Our model is defined in the spatial dimension, x, describing the spatial evolution of paths as the receiver moves. Figure 7.5 gives an overall structure for the spatial model and shows various parameters used in the model.
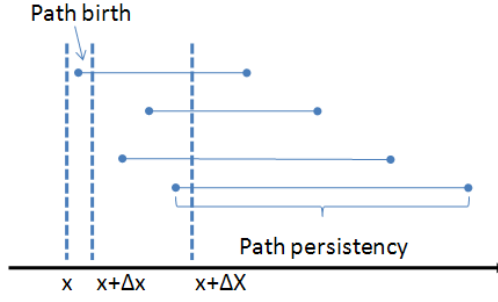
144

Figure 7.5: Path birth and persistency

The model can be briefly given as

$$p(N(\Delta X) = n_b) = \frac{(\mu_{B,\rho}\Delta X)^{n_b}}{n_b!}e^{-\mu_{B,\rho}\Delta X} \qquad (7.23)$$

where $\mu_{B,\rho}$ is the threshold dependent birth rate, n_b is the number of births in a given spatial interval, ΔX. We have observed that the path detection threshold (ρ) has an effect on the Poisson parameter, μ_B, since the probability of having higher path birth rate increases with increasing threshold and more paths being included in the CIR.

The Poisson modeling approach that we have adopted is actually based on a Bernoulli trial in which we assume either a "zero" or a "single" birth in an interval small enough to make our assumption valid. In this small interval, Δx, we assign a probability of p_0 for a no-birth case and a p_1 for a single birth. Our choice of the Poisson model stems from the fact that this simple yet powerful model can describe multiple stochastic occurrences of certain events in a given time. Hence the probability of occurrence of n paths in a given interval $\Delta X = m\Delta x$ can be computed as

$$p_n = \binom{m}{n}p_1{}^n p_0{}^{m-n} \qquad (7.24)$$

When m tends to a large number and p_1 to a small number, the overall probability can be approximated by the Poisson random variable with the parameter $\mu_B = mp_1$.

145

7.4.2 Path Persistency

As the receiver is moving steadily on a given route its TOA and AOA will exhibit differential changes as long as there is no major change in the propagation scenario. Propagation scenario is tightly related to the internal structure of the indoor environment, and is primarily dependent on the reflection mechanism. Referring to figure 7.6, we can express the reflection mechanism as a vector whose elements are an ordered set of surface/wall indices. For instance, a path that goes through 2 reflections at walls w_1 and w_2 respectively would have a reflection mechanism $[w_1 w_2]$. Changing the order of reflections would create a different reflection mechanism hence a different propagation scenario. We will use the notation $P_{i,x} = [w_1 w_2 ... w_n]$ to denote the propagation scenario of the ith MPC at position x after getting reflected at the walls $w_1, w_2 ... w_n$.
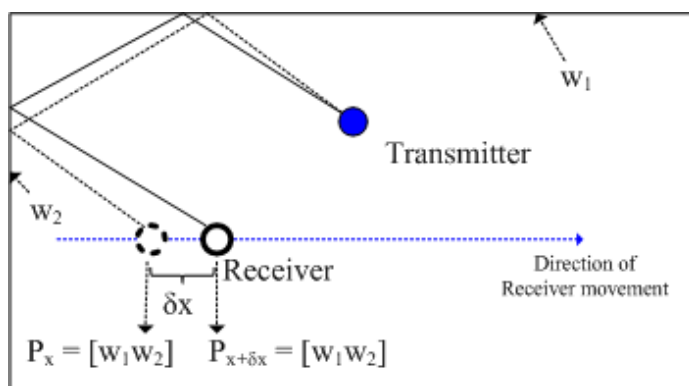
Figure 7.6: A sample persisting path in interval δx

Persistency of a certain MPC is the time interval expressed in number of discrete time steps (or equivalently the distance that the receiver moves given its speed) in which the propagation scenario stays intact. In other words, having $P_{i,x} = [w_1 w_2 ... w_n]$ at position x and $P_{i,x+\delta x} = [w_1 w_2 ... w_n]$ at position $x + \delta x$ would indicate a persistency of δx for the ith path.

The persistency of MPCs has not been studied extensively in the literature. The studies in [131] and in [113] are some previous and early works that model the duration for

which MPCs stay active. Authors in [131] propose a Poisson birth/death process for multipath duration, hence the lifetime is modeled as an exponential random variable. The study in [113] similarly propose an exponential path lifespan based on experimental data obtained with a system bandwidth of 120 MHz. The exponential model with parameter λ is given as

$$f_{x_P}(x) = \lambda e^{-\lambda x} \tag{7.25}$$

Although an exponential form is also a valid approach for modeling persistency, it is not adequate [142, 143]. Hence other modeling schemes need to be considered. One such method is the Weibull modeling approach written as

$$f_{x_P}(x) = (b/a)(x/a)^{(b-1)} e^{-(x/a)^b} \tag{7.26}$$

where a, b are the scale and shape parameters respectively. However, based on our observations from the RT simulations, Weibull scheme would still not be able to provide an accurate representation of lifetime data. Hence, we are proposing log-logistic distribution for the persistency of a MPC. The use of log-logistic has been considered in other disciplines [144] as a statistical lifetime model. The log-logistic model is written as

$$f_{x_P}(x) = \frac{e^{\frac{ln(x)-\mu}{\sigma}}}{\sigma x [1 + e^{\frac{ln(x)-\mu}{\sigma}}]^2} \tag{7.27}$$

where μ, σ are the scale and shape parameters, respectively, and x is the distance receiver moves. Equivalently path persistency can be interpreted as the time duration, t_P; it persists through the relation $t_P = x_P/v$.

Among the three modeling schemes, namely exponential, Weibull and log-logistic, our observations indicate a better conformance to the log-logistic method. Since path persistency is directly related to the propagation scenario, the distribution of the interior

wall lengths of the building has a direct impact on the distribution of path persistency. The log-logistic model can describe longer path persistencies that are produced by longer walls such as corridors better. The Exponential and Weibull models decay too quickly to describe this behavior.

Thus the complete spatial path behavior is modeled by the combination of the log-logistic path persistency and the Poisson birth model. Results in terms of cumulative hazard function and a two-sample K-S test will be presented in section 7.5 for a quantitative comparison of the aforementioned models and the suitability of our proposed model.

7.4.3   Spatial Path Behavior During Path Persistency

Now that we have discussed how paths appear/disappear and how their persistencies can be modeled, we will now focus on how MPC parameters change during its persistency. The derivations will follow the ray-optical geometric approach.

Since each path can be represented as a direct line between the transmitter image and the receiver, differential changes on any path can be expressed in terms of geometric relations. Each parameter of the MPC exhibits a differential change throughout its lifetime.

Before introducing the discrete and continuous models for path behavior, we will at this point define the angle notations. In our modeling approach there are 3 different angles that we consider. These are θ_{LOS}, the absolute LOS angle, θ, the relative angle wrt to the LOS and w, the acute angle that is between the direction of receiver motion and the MPC. The spatial equations will be based on w, however it will be straightforward to obtain θ_{abs} using basic trigonometric relations as given in figure 7.7.

In order to present the derivation of the model we will focus on the 4th quadrant of figure 7.7 wrt to virtual TX axes as shown in figure 7.8. For the spatial model we will use the notation τ corresponding to the absolute TOA, τ_{abs}, as mentioned earlier in the TOA model.
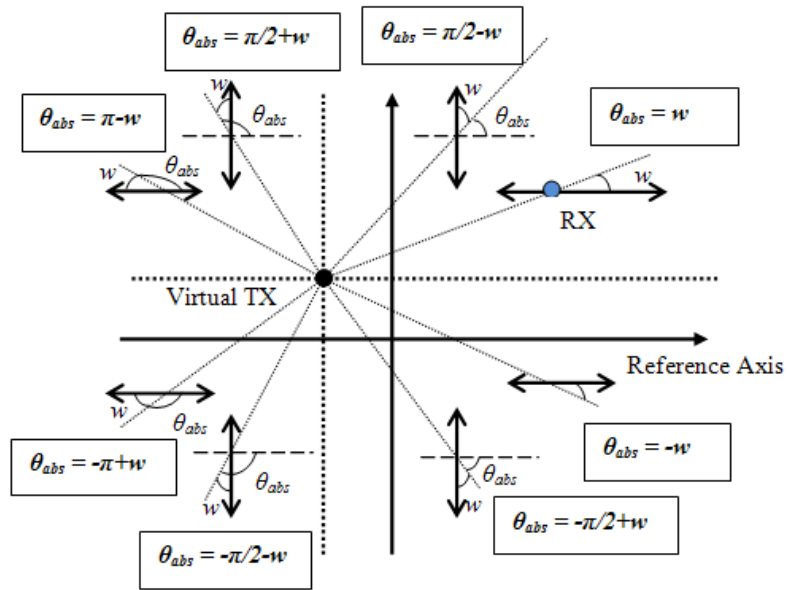
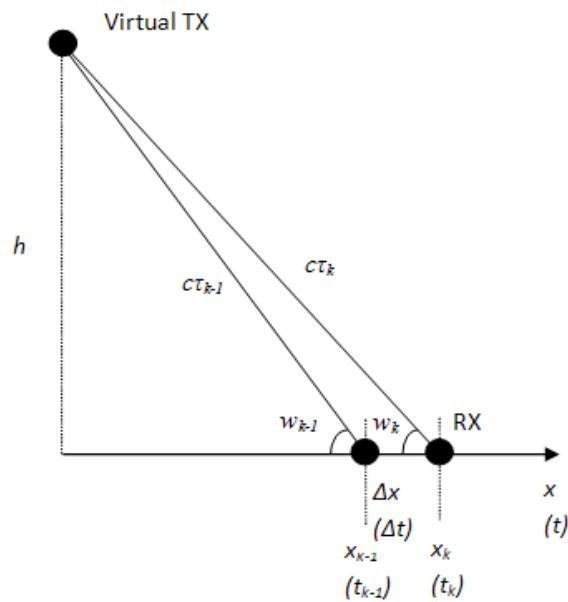Figure 7.7: Relation between w and θ_{abs}

Figure 7.8: Geometry for differential feature update

Employing the cosine rule for the triangle indicated, we can write the discrete time difference equations for $\tau_{i,k}, \omega_{i,k}, \beta_{i,k}$ as:

149

$$\tau_{i,k} = \frac{\sqrt{(c\tau_{i,k-1})^2 + (\Delta x)^2 + Y}}{c} \tag{7.28}$$

$$\omega_{i,k} = cos^{-1} \left(\frac{(c\tau_{i,k})^2 - (c\tau_{i,k-1})^2 + (\Delta x)^2}{Z} \right) \tag{7.29}$$

$$\beta_{i,k} = \frac{A}{c\tau_{i,k}} \prod_j \alpha_{ij} \tag{7.30}$$

where Δx is the differential distance that the receiver moves in time Δt which is also the interval between consecutive time steps, and $A = \sqrt{G_t G_r (c/4\pi f)^2}$. When the receiver is moving away from transmitter $Y = -2c\tau_{i,k-1}\Delta x cos(\omega_{i,k-1})$, $Z = 2\Delta x c\tau_{i,k}$ respectively and when the receiver is moving towards the virtual transmitter $Y = 2c\tau_{i,k-1}\Delta x cos(\omega_{i,k-1})$, $Z = -2\Delta x c\tau_{i,k}$ respectively.

Although we assume Δx is relatively very small when compared to actual path distances, it may be of importance to present these results in their most general continuous differential form. Again referring to figure 7.8 we can represent the path length hence the τ in terms of the distance receiver moves (x) and the vertical distance (h) of the transmitter image to the path of motion through a basic relation

$$c\tau = \sqrt{x^2 + h^2} \tag{7.31}$$

The differential change in τ with respect to x is thus

$$d\tau/dx = \frac{x}{c\sqrt{x^2 + h^2}} \tag{7.32}$$

For the w we observe the relation

$$w = tan^{-1}(h/x) \tag{7.33}$$

150

Hence the differential change in w with respect to x is

$$dw/dx = \frac{1}{\sqrt{1 + h^2/x^2}} \qquad (7.34)$$

For the differential change in amplitude we refer to the path gain expression given as:

$$\beta_i = \frac{A}{c\tau_i} \prod_j \alpha_{ij} \qquad (7.35)$$

As we will discuss later the path loss associated with multiple reflection and transmissions given by $\prod_j \alpha_{ij}$ is also distance hence τ dependent. We will represent the loss with a τ dependent function, $f_L(\tau)$ and the differential change in β with respect to τ is thus given by

$$d\beta/dx = \frac{d\beta}{d\tau}\frac{d\tau}{dx} = \left(\frac{A}{c\tau}\frac{df_L(\tau)}{d\tau} - \frac{f_L(\tau)}{\tau^2} \right) \left(\frac{x}{c\sqrt{x^2 + h^2}} \right) \qquad (7.36)$$

The spatial changes in the TOA and AOA of the paths have been previously discussed in [113] but the variations during a path lifespan have been modeled using a basic best line fit approach which does not accurately capture the changes in path features.

Through these simple geometric relations we can mathematically define the exact motion of a certain ray. Here we see the dependance of differential TOA and AOA change on both the distance traveled by the receiver and the perpendicular distance of the transmitter image to the receiver motion direction.

Since a path is considered to belong to a certain propagation scenario during its persistency, we do not expect abrupt changes in the TOA and AOA. The existence of abrupt changes beyond a certain threshold indicate reception of a new path arising from a different propagation scenario.

7.5 RT Simulation Platform and Results

For the simulations, we utilized a calibrated RT tool [145], and developed realistic indoor floorplans of the AK Labs at WPI. Ray tracing methods have proven to be efficient for most studies [131, 135, 146]. For the purposes of this study we have developed two simulation scenarios in order to derive and verify the proposed models. In the first scenario, we have produced an extensive database of CIRs for 3 different transmitter locations (denoted as TX-n, n=1,2,3) and about 13500 receiver locations for each transmitter location for a total of more than 40000 CIRs. Each CIR is composed of all relevant path parameters such as TOA, AOA, and path gain. Floorplan consists of the rectilinear layout of the 3rd floor of AK with metallic doors and dielectric walls. Elevator shaft and the anechoic RF chamber in room 320 have been modeled like metallic doors as almost perfect conductors, and hence giving us a more realistic propagation environment. The floorplan with the transmitter and receiver locations is depicted in figure 7.9. We have used this scenario to obtain the statistical model parameters for our proposed model.
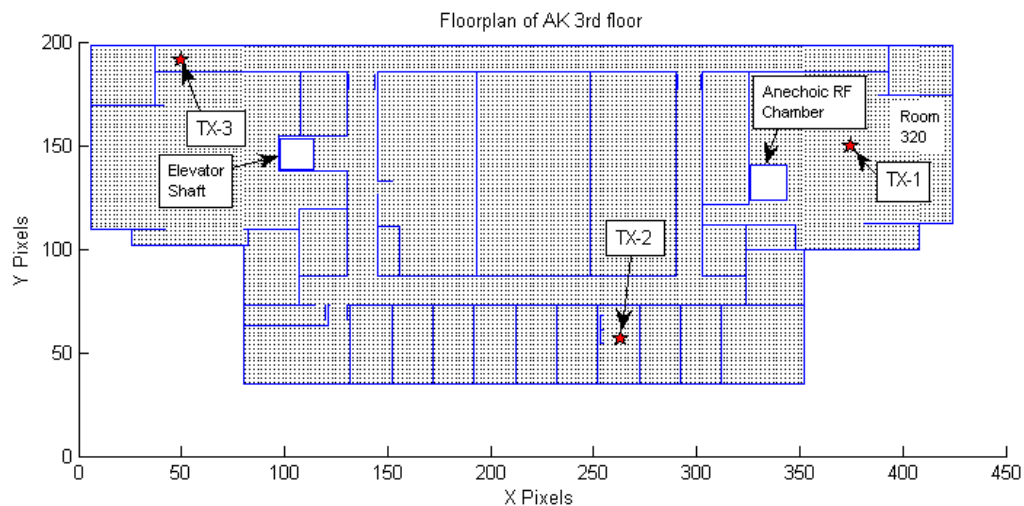
Figure 7.9: Map of AK 3rd floor showing transmitter/receiver locations and floorplan features

Figures 7.10 and 7.11 show the CDF and histogram of the TOAs relative to the first

arriving path. We can see a close match with the RT data. Beta and Weibull distributions can also describe relative TOA to a certain degree accuracy, however lognormal distribution has been found to be the best performing model.

Figure 7.10: Cumulative distribution for the relative TOA, τ

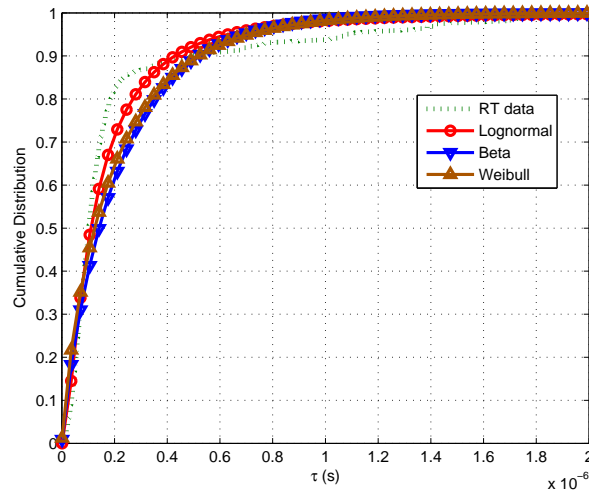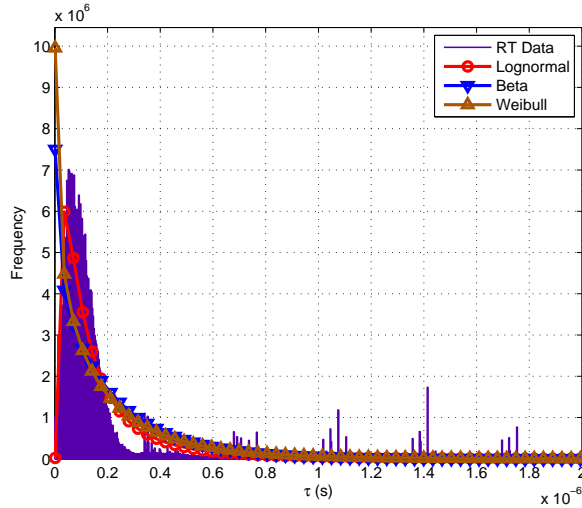Figure 7.11: Histogram for the relative TOA, τ

Since in one of the scenarios, transmitter (TX-3) is located at one end of a 50 m long corridor on the 3rd floor of AK, results also show the presence of higher order reflections occurring at the ends of the corridor. This can be seen in the histogram of the relative TOAs in figure 7.11.

Figures 7.12 and 7.13 show the CDF and PDF of the AOAs relative to LOS component. Here, we can see the strong dependence of the multipath arrivals on the LOS path since most paths tend to arrive around $-\pi$, 0, and π radians around the LOS.

Figure 7.14 shows the CDF of path gain, β, obtained using the proposed model vs the path gain from RT data. We see a very close match between the model and the observed data. The threshold for path power has been fixed at -56 dB for the RT. The small fraction of paths that are below -56 dB can be attributed to the design of the RT software which checks for threshold at each object interaction rather than a continuous check during propagation. Hence a path might have incurred additional path loss since the last object interaction at which point it might have had higher power than the threshold.

Figure 7.15 shows the CDFs for the number of reflections and transmissions for the proposed Poisson models vs the RT data. From this figure we see the suitability of the
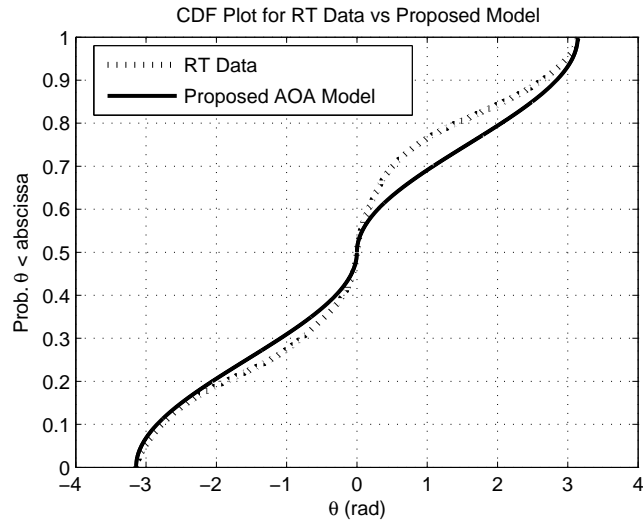
Figure 7.12: Cumulative distribution for the relative AOA, θ
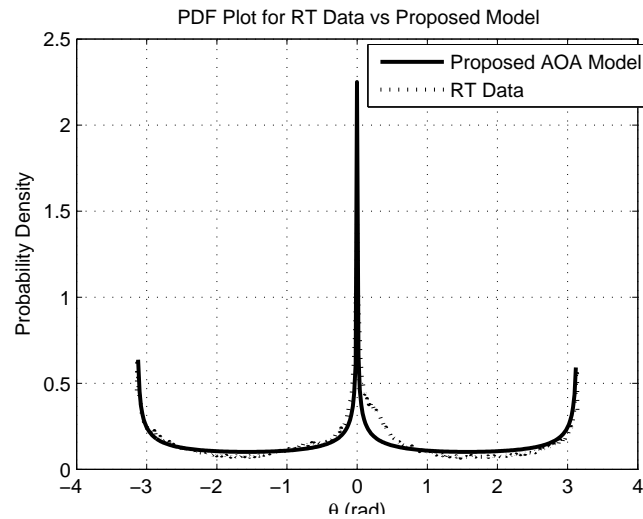
Figure 7.13: Probability density for the relative AOA, θ

Poisson Model for the number of object interactions. For the coefficients of reflection and transmission we have used an average reflection coefficient of $R = 0.7$ and a transmission coefficient of $T = 0.5$. These values have been taken from [127].

Figure 7.16 shows the dependence of number of paths, L_p, to distance. From this figure, we can see the distance dependence of L_p for varying thresholds. For smaller values of transmitter-receiver distances, we can see the dominance of dynamic range in

155
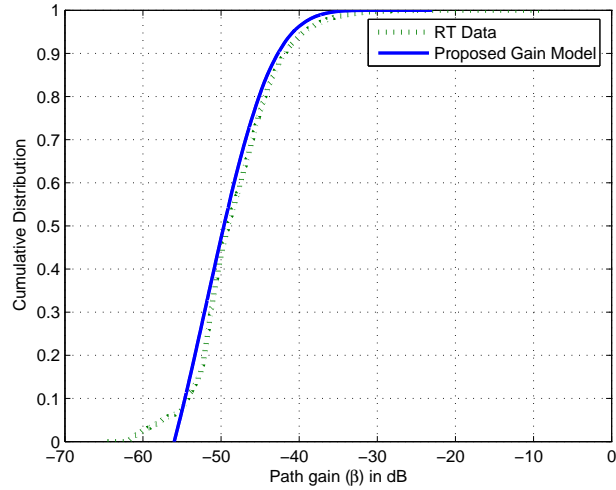
Figure 7.14: CDF for path gains using the proposed model vs RT Data
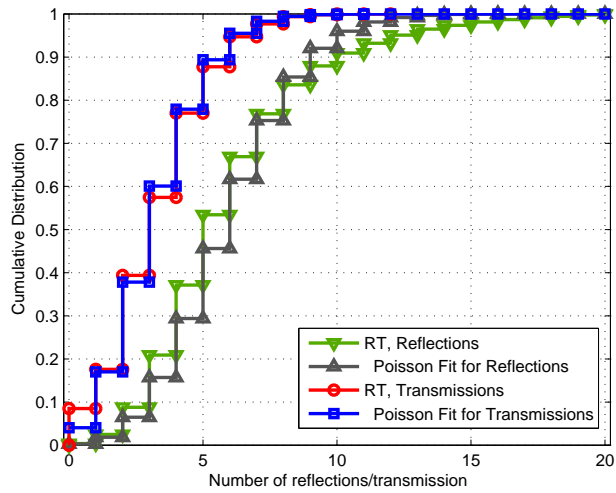
Figure 7.15: CDFs for the number of reflections/transmissions for Poisson model vs RT data

MPC count and for higher distances receiver sensitivity becomes dominant hence leading to less paths. This is an expected result since more and more paths will be below the detection threshold with increasing distance.

The existence of high order reflections for the corridor points leads to almost fixed number of MPCs starting at a distance of around 25m and going up to about 50m which

156
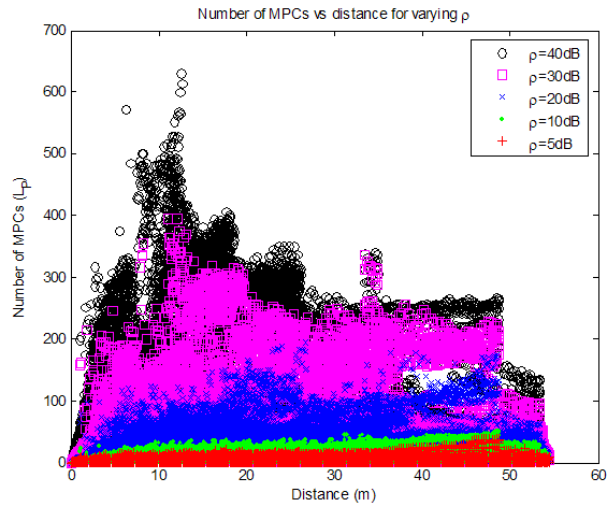
Figure 7.16: Number of paths (L_p) vs distance

can also be seen in figure 7.16. The waveguiding effect of the corridor actually needs a separate modeling approach, however it has been included in our simulations to emphasize the variety of possible scenarios in a typical indoor environment.

Figures 7.17 and 7.18 show the mean value and p for the negative binomial model for varying distance and ρ values. D_T as mentioned in the model has been found to be 56 m specific to our case.
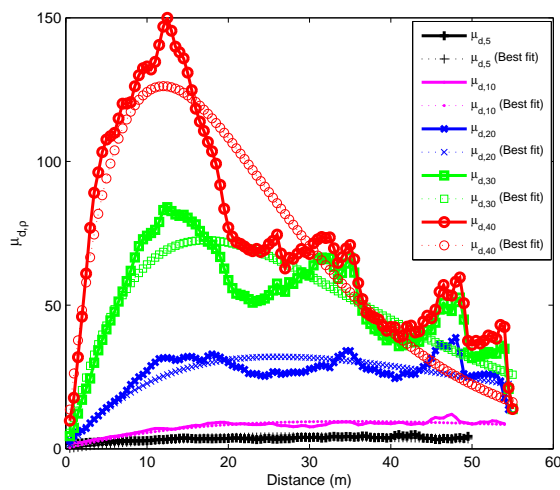
Figure 7.17: Distance and ρ dependent μ
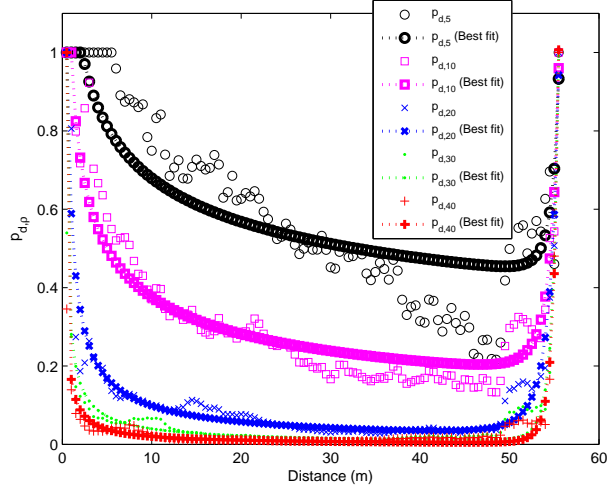
Figure 7.18: Distance and ρ dependent p

The second scenario has been used to obtain the spatial path characteristics of the indoor channel. The setup for the this scenario is shown in figure 7.19. The choice of the receiver loop chosen also presents a diversified RF environment with mixed DDP/UDP conditions due to both macro and micro metallic obstructions including the anechoic RF chamber and the metallic vertical beam. Receiver motion is simulated by obtaining consecutive CIR responses at locations 5 cm apart from each other on the loop on the 3rd floor of AK. Hence the CIR results have been obtained with a spatial resolution of 5 cm corresponding to the floorplan scale of 20 pixels/m. This spacing also corresponds to the ΔX as described in the path birth model.

For the modeling of path birth, we have two free variables p_1 and m. By assigning a small probability value to p_1 we can obtain all the other related parameters. Specific to our case we have chosen $p_1 = 0.01$. Based on the RT simulation results and fixing ρ at 30dB, μ_B is calculated as 2 and thus $m = 200$. Hence $\Delta x = \Delta X/m = 0.025cm$. Figure 7.20 shows the CDF for net path birth/death using the combined Poisson path birth and log-logistic path persistency model. Different values of m and Δx can be calculated from $\mu_{B,\rho}$ for varying ρ values as will be given in table 7.2.

158
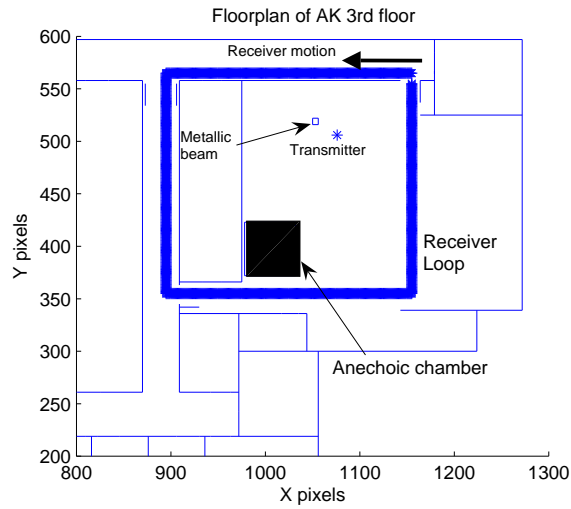
Figure 7.19: Test loop on AK 3rd floor
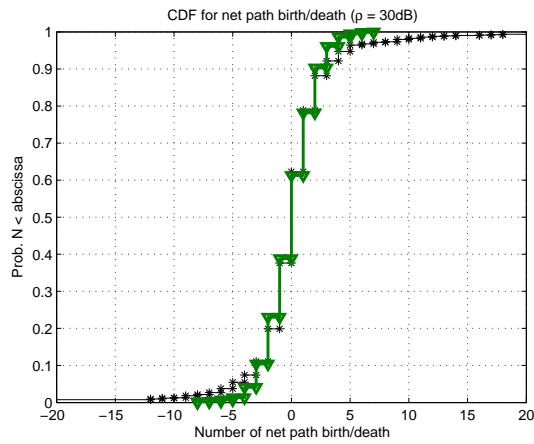
Figure 7.20: CDF for net path birth/death

A two sample K-S test is used to test the suitability of the selected model. The D statistic, given as:

$$D = \sup_x |F(x) - S(x)| \tag{7.37}$$

where F(x) denotes the fitted distribution with estimated parameters and S(x) denotes the experimental data, can be interpreted as the greatest vertical distance between these two distributions and is a measure of how closely the proposed model describes empirical

results. A smaller D indicates a better overall fit. Comparison of this value against a tabulated critical value determines if the proposed (hypothesized) model can be accepted at 5% significance level, which is a common value used in statistical tests. Based on this test and at 5% significance, our proposed Poisson birth model is acceptable.

In order to obtain the persistency of a single path, a path tracking algorithm is employed. A version of this algorithm is discussed in [24]. For the comparison of persistency results, we have chosen the cumulative hazard function which is a common method used in survival analysis [143]. The cumulative hazard function can be written as:

$$H(x) = -logS(x) \tag{7.38}$$

where $S(x)$ is the survivor function expressed as:

$$S(x) = Pr(x_P \geq x) \tag{7.39}$$

which gives the probability that path persistency, x_P, is greater than x. As we can see from figure 7.21, log-logistic modeling for path persistency is a more accurate approach following the cumulative hazard of the empirical results more closely. In this graph, x axis is the lifetime in meters and y axis is the $H(x)$. The KS results for the models (for a representative ρ value of 30 dB) based on D statistic are also given in table 7.1 for a quantitative comparison.

Table 7.1: K-S comparison for different persistency models

Persistency Models (ρ=30dB)	D	Model Parameters
Exponential	0.1497	$\lambda = 1.247$
Weibull	0.1427	$a = 0.722, b = 0.855$
Log-logistic	0.0767	$\mu = $ -0.934, $\sigma = 0.606$

The KS test yields the minimum D value for the log-logistic model when compared to Weibull and exponential for path persistency indicating a better overall conformance
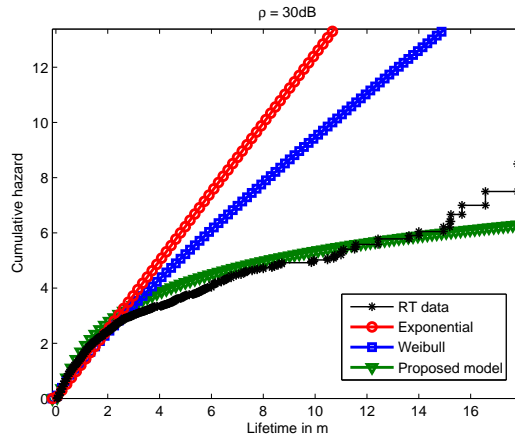
Figure 7.21: Cumulative hazard comparison for path persistency

to this model. The results of the calibrated RT tool show a good agreement with the proposed log-logistic path persistency model coupled with Poisson path birth model. For different values of ρ log-logistic still exhibits the best performance, however due to space limitations parameters for $\rho = 30$dB have been presented only.

Figure 7.22 shows sample spatial path behavior for the first segment of the test loop (top part of the rectangular loop) processed at $\rho = 30$ dB. As we can clearly note in the graph, the TOA of each detectable path exhibits a smooth geometric behavior throughout its persistency. We can also observe the persistent higher order paths in the UDP region which we can use for accurate ranging.

Figure 7.23 shows the complete loop spatial behavior of τ and θ given for ρ=10,20,30,40dB. z-axis is the path gain, β, in dB and x-axis is the spatial distance (time) in terms of pixels.

7.6 Conclusions

In this chapter we have introduced a spatial model for the behavior of MPCs that rely on geometric optics and presented statistical characterization of key MPC components, namely TOA, AOA, path gain and number of MPCs. Based on an extensive set of em-
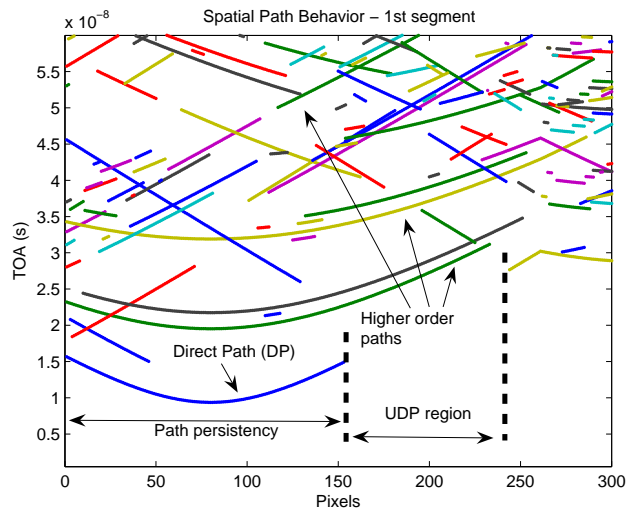
Figure 7.22: Sample spatial path behavior for the first segment of the test loop

pirical measurements we proposed a log-normal model for relative TOA, bathtub density for relative AOA, negative binomial model for the number of MPCs, log-logistic model for path persistency and poisson model for path birth. Table 7.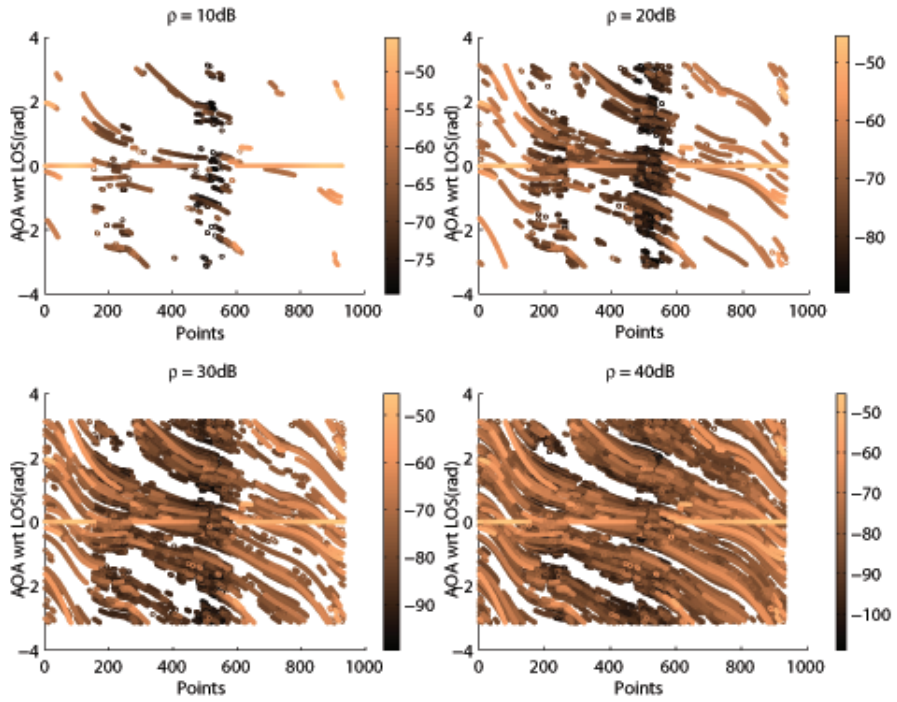2 summarizes the models chosen for the characterization of MPC behavior along with their parameters obtained through our simulations.

Table 7.2: Overall model summary

MPC feature	Proposed Model	Model Parameters
TOA	$\tau_{abs} = r/c + \tau$ $f_\tau(\tau) = \frac{1}{\tau\sigma\sqrt{2\pi}}e^{-\frac{(ln(\tau)-\mu)^2}{2\sigma^2}}$	$\mu = -16.02$ and $\sigma = 1.06$
AOA	$\theta_{abs}(\theta_{LOS}) = \theta_{LOS} + \theta$ $f_\theta(\theta) = \begin{cases} \frac{1}{\pi^2\sqrt{1-\left(\frac{\theta+\pi/2}{\pi/2}\right)^2}} & -\pi < \theta < 0 \\ \frac{1}{\pi^2\sqrt{1-\left(\frac{\theta-\pi/2}{\pi/2}\right)^2}} & 0 \le \theta < \pi \\ 0 & \text{otherwise} \end{cases}$	$\theta_{LOS} = atan2\left(TX_y - RX_y, TX_x - RX_x\right)$ $atan2(y,x) = \begin{cases} tan^{-1}(y/x) & x > 0 \\ tan^{-1}(y/x) + \pi & x < 0, y \ge 0 \\ tan^{-1}(y/x) - \pi & x < 0, y < 0 \\ \pi/2 & x = 0, y > 0 \\ -\pi/2 & x = 0, y < 0 \\ undefined & x = 0, y = 0 \end{cases}$
Path gain	$\beta_i = \frac{A}{c\tau_{abs}}\prod_j \alpha_{ij}$ $P(M = m) = \frac{\lambda_r^m}{m!}e^{-\lambda_r}$ $P(N = n) = \frac{\lambda_t^n}{n!}e^{-\lambda_t}$	$A = \sqrt{G_t G_r}\frac{c}{4\pi f}$ $\alpha_{ij} = \begin{cases} R = 0.7 & \text{if reflection} \\ T = 0.5 & \text{if transmission} \end{cases}$ $\lambda_r = 5.94$ $\lambda_t = 3.21$

Number of paths:

$$p(L_p = k; r_{d,\rho}, p_{d,\rho}) = \frac{\Gamma(r_{d,\rho}+k)}{k!\Gamma(r_{d,\rho})}p_{d,\rho}^{r_{d,\rho}}(1-p_{d,\rho})^k$$

$$\mu_{d,\rho} = a_{1,\rho}de^{-d/a_{2,\rho}} = r_{d,\rho}\frac{1-p_{d,\rho}}{p_{d,\rho}}$$
$$p_{d,\rho} = b_{1,\rho}e^{-log_{10}(d)/b_{2,\rho}} + b_{3,\rho}e^{-log_{10}(d_{ref,\rho}-D_T)/b_{4,\rho}}$$

ρ(dB)	a_1	a_2	b_1	b_2	b_3	b_4	$d_{ref,\rho}$(m)
5	0.40	28.66	1.23	1.69	172.7	0.09	2.23
10	0.75	34.64	0.98	1.05	107.4	0.11	0.94
20	3.33	26.13	0.59	0.56	92.8	0.12	0.50
30	11.47	17.20	0.28	0.51	1208.7	0.08	0.22
40	28.50	12.04	0.17	0.47	2733.9	0.07	0.14

$D_T = 56$m

MPC feature	Proposed Model	Model Parameters
Path persistency	$f_{x_P}(x) = \frac{e^{\frac{ln(x)-\mu}{\sigma}}}{\sigma x[1+e^{\frac{ln(x)-\mu}{\sigma}}]^2}$	$\mu = -0.934, \sigma = 0.606$ ($\rho = 30$dB)

Path birth:

$$p_n = \binom{m}{n}p_1^n p_0^{m-n}$$

$$\Delta X = m\Delta x, \mu_B = mp_1$$

ρ(dB)	$\mu_{B,\rho}$	KS Statistic D
5	0.06	0.0065
10	0.1	0.0142
20	0.5	0.0475
30	2	0.0405
40	7	0.0243

$p_1 = 0.01, m = 200$
$\Delta X = 5$cm, $\Delta x = 0.025$cm ($\rho = 30$dB)

Figure 7.23: (a) TOA vs spatial distance (b) AOA (wrt LOS) vs spatial distance for ρ=10,20,30,40dB

Chapter 8

Conclusion and Future Directions

8.1 Conclusion

This chapter provides an overall conclusion and discussion of some possible directions for the research that has been the focus of this dissertation.

Indoor wireless channel presents unique challenges for system researchers and system developers, especially those working on indoor geolocation systems. The existence of a cluttered environment is the main reason for a CIR that is composed of many closely arriving paths. Additionally, since there is a high chance of frequent obstructions between the transmitter and receiver, the amplitude of the DP will most of the time be diminished to a level not detectable by the receiver. This results in the so called UDP condition and causes large ranging errors. A combination of multiple UDP measurements will eventually lead to an erroneous position estimation for indoor geolocation, which will be unacceptable for most applications.

The work presented in this dissertation has addressed the indoor geolocation problem from a channel modeling point of view given the existence of harsh UDP conditions.

Chapter 2 presented background information on RF geolocation techniques from the

system engineering and channel modeling points of view. Special attention has been given to TOA based systems since the major challenge involved in high precision ranging and positioning systems is the frequent absence of the DP, causing the UDP condition. Two studies have also been presented in this chapter demonstrating the effect of UDP conditions on typical geolocation systems.

In Chapter 3 we introduced a study on UDP identification since identification is the first step and plays an important role in obtaining precise ranging measurements.

In Chapter 4 we introduced the path persistency and demonstrated how we can utilize this information to get precise ranging in the absence of DP. UDP error mitigation is the second step in obtaining precise ranging and consequently localization.

In Chapter 5 we presented a study that shows the effect of building architecture on path persistency and we introduced a concept called floorplan complexity, which was used as a measure of the complexity of the propagation environment.

In Chapter 6 we presented the results of an empirical measurement campaign to analyze the effect of bandwidth, peak detection threshold and propagation condition (DDP/UDP) on some key MPC parameters such as path persistency and the number of MPCs. The effect of transmitter and receiver distance has also been studied through these measurements.

In Chapter 7 we presented our comprehensive spatial multipath model based on ray optics and a statistical modeling approach. We created an extensive RT database and based on our observations we proposed a wireless channel model keeping in mind the indoor geolocation applications. We proposed statistical models for TOA, AOA, amplitude of the MPCs. A distance dependent model is also introduced for the number of MPCs. The appearance and disappearance of the MPCs have been modeled through path persistency (equivalently path lifetime) and path birth. The spatial behavior of MPCs has been investigated using the ray optics model.

Development of such a model is particularly important for indoor geolocation applications utilizing multipath diversity in the absence of DP. Therefore accurate characterization of multipath behavior is essential for indoor areas.

8.2   Future Directions

This study can be extended in several possible directions. One possible direction is the investigation of the actual indoor geolocation performance of the proposed model by combining the ranging information from multiple transmitters as obtained by using this model. Another direction would be the development of a 3D propagation model. Thus a more realistic assessment of positioning algorithms can be made especially for multi-story buildings. A third extension to this study could be the integration and comparison of path number modeling approach based on measurements and RT. Yet another direction would be the quantitative modeling of the dependence of path persistency on building specific parameters such as mean wall length, number of walls, mean wall reflection/transmission coefficients, etc.

Appendix A

Geometric Derivation for Path Persistency-Wall Length Dependency

In this appendix we will show geometrically the dependence of path persistency on the length of the walls. For this purpose we consider 2 walls, 1 horizontal (w_1) and 1 vertical (w_2) wall as shown in figure A.1. Transmitter (TX) is at (0,0). Receiver (RX) moves in the indicated direction at the y coordinate S_y. The entities of interest and their coordinates are given in table A.1.

Table A.1: Entities of interest

Entities	Coordinates (x,y)
Wall 1 (w_1)	$(w_{1,x1}, w_{1,y}) - (w_{1,x2}, w_{1,y})$
Wall 2 (w_2)	$(w_{2,x}, w_{2,y1}) - (w_{2,x}, w_{2,y2})$
Transmitter (TX)	(0,0)
Virtual TX1 (VTX_1)	$(0, 2w_{1,y})$
Virtual TX2 (VTX_2)	$(2w_{2,x}, 2w_{1,y})$

Table A.2 shows the geometries of interest. Here our aim is to find the line segments $c_{11} - c12$ and $c_{21} - c22$ which represent the persistency of the corresponding reflected paths. We assume that walls allow transmission of the paths.

For the horizontal wall w_1:
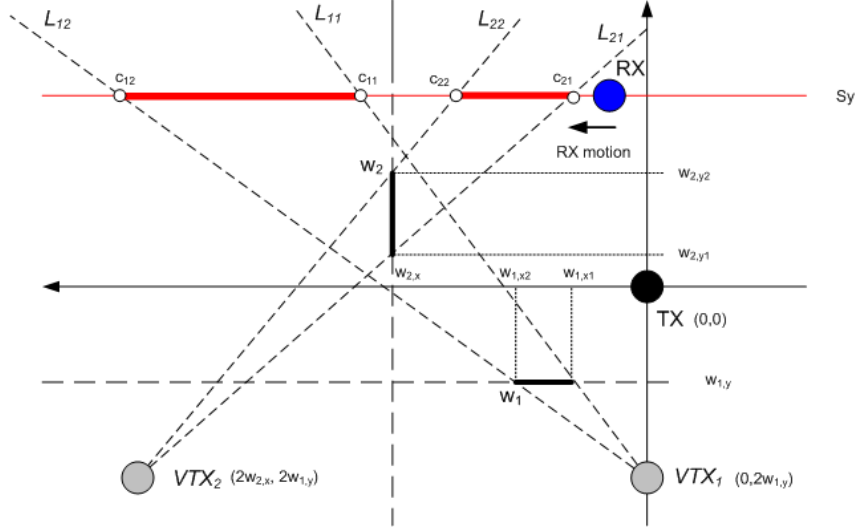
Figure A.1: Sample scenario for showing path persistency dependence on wall lengths

Table A.2: Geometries of interest
w_1-VTX_1 intersection line 1 (L_{11})
w_1-VTX_1 intersection line 2 (L_{12})
w_2-VTX_2 intersection line 1 (L_{21})
w_2-VTX_2 intersection line 2 (L_{22})
L_{11} and RX motion path intersection point (c_{11})
L_{12} and RX motion path intersection point (c_{12})
L_{21} and RX motion path intersection point (c_{21})
L_{22} and RX motion path intersection point (c_{22})

The equation for L_{11} is given as

$$\frac{y - 2w_{1,y}}{w_{1,y} - 2w_{1,y}} = \frac{x - 0}{w_{1,x1} - 0} \tag{A.1}$$

The equation for L_{12} is given as

$$\frac{y - 2w_{1,y}}{w_{1,y} - 2w_{1,y}} = \frac{x - 0}{w_{1,x2} - 0} \tag{A.2}$$

We obtain the x-coordinate of c_{11} by substituting S_y in L_{11} equation:

$$c_{11x} = \frac{-w_{1,x1}}{w_{1,y}}(S_y - 2w_{1,y}) \tag{A.3}$$

and likewise we obtain the the x-coordinate of c_{12} by substituting S_y in L_{12} equation:

$$c_{12x} = \frac{-w_{1,x2}}{w_{1,y}}(S_y - 2w_{1,y}) \tag{A.4}$$

For the vertical wall w_2:

The equation for L_{21} is given as

$$\frac{y - 2w_{1,y}}{w_{2,y1} - 2w_{1,y}} = \frac{x - 2w_{2,x}}{w_{2,x} - 2w_{2,x}} \tag{A.5}$$

The equation for L_{22} is given as

$$\frac{y - 2w_{1,y}}{w_{2,y2} - 2w_{1,y}} = \frac{x - 2w_{2,x}}{w_{2,x} - 2w_{2,x}} \tag{A.6}$$

We obtain the x-coordinate of c_{21} by substituting S_y in L_{21} equation:

$$c_{21x} = \frac{S_y - 2w_{1,y}}{w_{2,y1} - 2w_{1,y}}(-w_{2,x}) + 2w_{2,x} \tag{A.7}$$

and likewise we obtain the the x-coordinate of c_{22} by substituting S_y in L_{22} equation:

$$c_{22x} = \frac{S_y - 2w_{1,y}}{w_{2,y2} - 2w_{1,y}}(-w_{2,x}) + 2w_{2,x} \tag{A.8}$$

Now we can write the segment lengths (or equivalently path persistencies) $x_{p_1} = |c_{11} - c_{12}|$ and $x_{p_2} = |c_{21} - c_{22}|$ as

$$\begin{aligned}
x_{p_1} = |c_{11x} - c_{12x}| &= \frac{S_y - 2w_{1,y}}{w_{1,y}}|w_{1,x1} - w_{1,x2}| \\
&= K_1|w_{1,x1} - w_{1,x2}| \qquad\qquad\qquad\qquad\qquad\text{(A.9)} \\
x_{p_2} = |c_{21x} - c_{22x}| &= -\frac{S_y - 2w_{1,y}}{w_{2,y1} - 2w_{1,y}}\frac{w_{2,x}}{w_{2,y2} - 2w_{1,y}}|(w_{2,y1} - 2w_{1,y}) - (w_{2,y2} - 2w_{1,y})| \\
&= K_2|w_{2,y2} - w_{2,y1}| \qquad\qquad\qquad\qquad\qquad\text{(A.10)}
\end{aligned}$$

Here we can easily see that since wall coordinates and virtual TX locations are known (constant), the path persistencies represented by the segment lengths are only dependent on the wall lengths.

Assuming wall lengths are represented by a random variable, we expect that the path persistencies will follow the same family of distribution as the wall lengths up to a certain constant. Considering wall lengths are denoted by the random variable L then the CDF for L is $F_L(l) = Pr\{L < l\}$. Since the path persistency (X_p) for a particular path can be shown as $X_p = KL$ the CDF for the random variable X_p will be $F_{X_p}(x_p) = Pr\{X_p < x_p\} = Pr\{KL < x_p\} = Pr\{L < x_p/K\} = F_L(x_p/K)$.

Appendix B

Slicing Tree Floorplaning

In this appendix we will present the slicing tree algorithm to create a slicing floorplan. The starting point is a rectangular layout. This layout is recursively sliced by either horizontal or vertical slices into rectangular blocks which denote the rooms on the floorplan. A pseudocode for this algorithm is given below:

Algorithm 1 Slicing Floorplan
---
   for $i = 1$ **to** $MAXDEPTH$ **do**
     for $k = 1$ **to** 2^i **step** 2 **do**
       if Min room dimension $< THR$ **then**
         continue for
       else
         Slice vertically or horizontally (with probability $p = 0.5$)
       end if
     end for
   end for

In our algorithm we applied a threshold (THR) in order to have rooms with reasonable sizes. For our purpose, we chose 3 m as the minimum room dimension (vertical or horizontal). The probability of either vertical or horizontal slice has been chosen as $p = 0.5$ as to eliminate bias towards one kind of slicing. $MAXDEPTH$ specifies the maximum depth of the slicing tree.

Figure B.1 shows a sample 20m by 20m floorplan with its corresponding slicing tree. **H** denotes a horizontal slice and **V** denotes a vertical slice. In this example $MAXDEPTH = 4$.

(a)   (b)
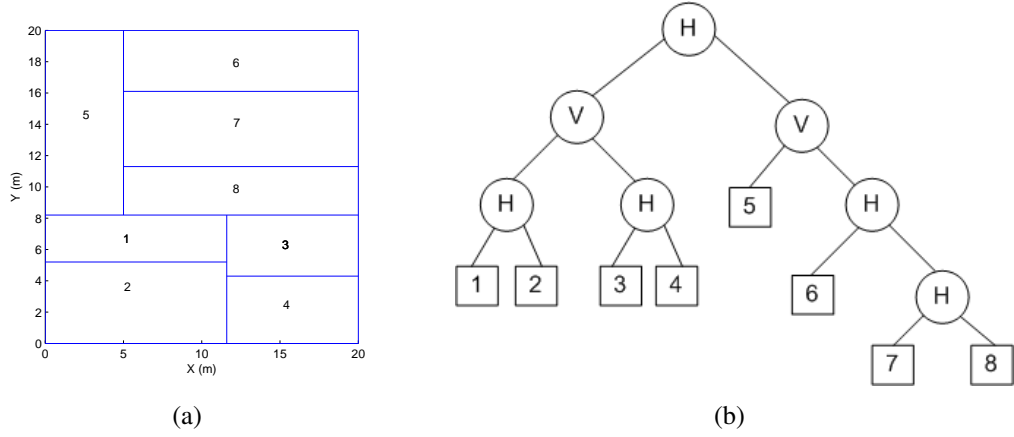
Figure B.1: (a) Sample 20m by 20m floorplan with numbered rooms (children) (b) Corresponding slicing tree

Appendix C

Cellular Positioning

In this appendix we present a study on outdoor cellular based positioning and it is presented based on the following published paper: [33]. Some parts of this appendix have been presented earlier in the thesis, but they are left intact for the completeness of this study.

C.1   Introduction

The world is fast moving towards an era of seamless networking as mobile devices are becoming smaller, smarter and more affordable. Ubiquity of such devices is also the key enabler for location based services. The first serious attempt for localization came in the form of a US military initiated project, the GPS. In its 40 years of development and maturity, GPS has become a reliable location finding and tracking system for use not only by military but also by civilians in numerous applications.

Although GPS is a proven and reliable technology, it falls short of expectations for some terrestrial applications where the GPS signals cannot be detected due to obstructions. Satellite signals are attenuated heavily through the atmosphere and further obstruc-

tion by trees, heavy fog or manmade structures such as building tops prevent this system to be useful especially for densely populated urban settlements and inside buildings. In order to overcome this issue, researchers turned their attention to land-based positioning and tracking systems for situations that cannot make use of satellite signals. The two widely available technologies suitable for this purpose are the Wi-Fi (WLAN) and cellular networks.

The proliferation of cellular based radio communications systems made them also potential candidates for ground-based positioning applications. Following the availability and the wide footprint of these systems, FCC mandated mobile phones be located within a certain accuracy in the US [7]. Accordingly mobile operators should be able to locate phones with 50m accuracy 67% of the time and 150m accuracy 95% of the time for handset based positioning, and 100m accuracy 67% of the time and 300m 95% of the time for network based positioning. Thus, positioning using cellular networks became feasible and provided operators with quick deployment opportunities for location based services (LBS).

On the other hand, rapid adoption of WLAN technology throughout the world especially in densely populated areas made it another compelling choice for localization. Figure C.1 summarizes the capabilities and operational coverage of these different technologies in terms of localization performance. As we can see, a hybrid solution combing all these technologies is clearly needed for the most effective coverage and localization performance.

In this part, we will focus on the use of cellular localization for typical positioning applications and evaluate its effectiveness using a real life test bed. In section C.2 we will give a brief overview of location metrics that can be used to obtain position information, and in section C.3 we will introduce basic concepts for cellular positioning. Section C.3 will also present the testbed that we have used to obtain our results. Results and perfor-

175
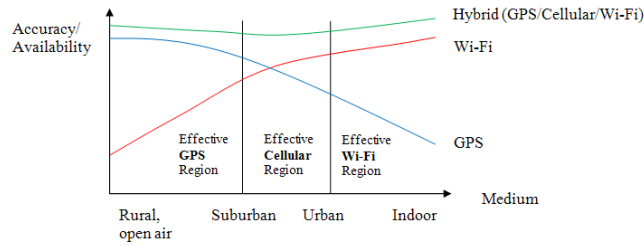
Figure C.1: Different localization technologies

mance evaluation will be given in section C.4. Finally, we will conclude this appendix in section C.5. We shall point out that the words localization, positioning and geolocation are used interchangeably throughout this paper.

C.2 Overview of a Localization System

A typical localization system consists of mobile terminals that need to be located/tracked, beacon or anchors serving as reference points, a central processing station that implements the positioning algorithm and keeps track of all the terminals as well coordinates data communications and a higher layer system that shows the results of positioning or tracking like an LCD panel. Figure C.2 shows the components of such a localization system. The system might use different ranging metrics for obtaining the position information. The most common of these metrics are received signal strength (RSS) and time-of-arrival (TOA). RSS and TOA might be considered as ranging metrics since ranging information can be obtained from these signal parameters. The nodes will need at least three ranging estimates from different anchors to be able to obtain a position fix.

In the following section, we will briefly introduce the distance or equivalently ranging estimation metrics and present some theoretical performance bounds.
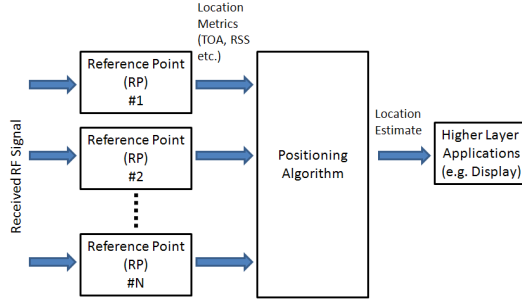
Figure C.2: High level architecture of a typical positioning system

Distance Estimation Metrics

RSS: After the RF signal is transmitted by a transmitter, its energy experiences loss that is proportional to the distance signal travels. A common model based on single-path radio propagation is given by

$$P_r(dB) = P_t(dB) - 10\alpha log_{10}(d) \qquad (C.1)$$

where P_r (dB) and P_t (dB) denote the received and transmitted signal powers in dB. α is the distance-power gradient and is dependent on the propagation environment. For free space, α is considered to be equal to 2. A wide range of values are possible for α, i.e. for a brick construction office environment α is reported to be 3.9 or for a laboratory environment with metal-faced partitioning it is found to be 6.5 [14].

Other empirical models have also been developed based on extensive measurements in various environments. The author in [34] proposed a path-loss model for multi-floor buildings. Technical working group of TIA/ANSI JTC recommended an indoor path loss model [147] for PCS applications. Apart from the indoor model, the same group proposed micro and macro-cellular models for outdoor applications. Other popular models for outdoor environments are the Okumura [36], Hata [37] and COST231 [38] models.

Either by using the simple radio-propagation or the more complicated empirical mod-

els, distance information can be obtained from the received signal power given the transmitted signal power. This method can be easily applied since almost all RF wireless devices can report received signal strength however its accuracy may not always be acceptable due to the stochastic variation of the channel.

The path loss models discussed above are deterministic models that do not consider the fading and shadowing effects. At any time instant, the signal level experiences slow and fast fading caused by local scatterers and the movement of the receiver node. Due to this fluctuating behavior of received signal power, accurate ranging measurements are not always possible hence leading to lower accuracy position estimation. In fact, the accuracy of such estimation is lower bounded by its Cramer-Rao lower bound (CRLB). CRLB basically specifies the lower bound on the variance of estimation. For the simplistic RSS model this bound has been given in [39] as:

$$\sigma^2_{d_{RSS}} \geq (ln10\sigma_{sh}d/(10\alpha))^2 \tag{C.2}$$

Here, $\sigma^2_{d_{RSS}}$ is the variance of estimation, σ^2_{sh} is the variance for shadow fading, d is the actual distance between the transmitter and the receiver and α is the power-distance gradient.

TOA: Another distance estimation method is the TOA method in which the range is estimated based on the time the signal spends traveling from the transmitter to the receiver. Since the speed of RF propagation is very well known in both free space and air, it gives a direct estimation of the distance between the transmitter and the receiver once the travel time is estimated. When TOA systems are considered, the only important parameter that needs to be estimated correctly in a multipath propagation environment is the TOA of the LOS path or the DP. Other multipath components are not important for ranging and localization purposes except for the cases when the DP is not available. The basic equation needed to obtain the distance is given as

178

$$d = \tau_{DP}c \qquad\qquad (C.3)$$

where d is the distance estimate, τ_{DP} is the TOA of the DP and c is the speed of light. Accurate TOA estimation needs perfect synchronization between the clocks of the transmitter and the receiver. Clock synchronization might be achieved by regular data exchange between the transmitter and the receiver or an additional anchor for correcting the clock bias. Although 3 anchors are necessary to obtain position, a 4th anchor will be needed for time correction. This method is readily applied for the GPS in which a 4th satellite is used to compensate for the receiver clock bias. The TOA location estimation is depicted in figure C.3 where a perfect synchronization is assumed between the transmitters and the receiver. Same procedure also applies to the RSS method in which individual distance estimates are also used for position fixing. The dotted circles denote the uncertainty in range estimation hence leading to an area for the possible location of the receiver between the three estimation circles, rather than a single point.
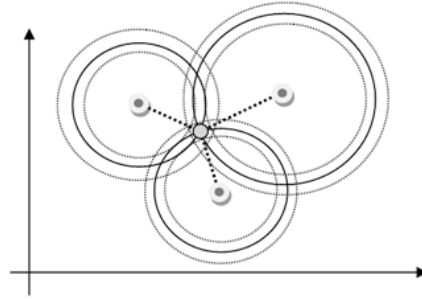
Figure C.3: Trilateration of a node by three anchors (RSS and TOA)

In the case of single path TOA estimation, CRLB is computed to be [55]

$$\sigma^2_{d_{TOA}} = \frac{1}{8\pi^2(SNR)(BT_0)(f_0^2 + B^2/12)} \qquad\qquad (C.4)$$

where σ^2_d is the variance of TOA estimate, $B = f2 - f1$, $f0 = (f2 + f1)/2$ and T_0 is

the observation time. From C.4, it is easy to see that the bound is inversely proportional to the SNR, the signal bandwidth and observation time.

Besides perfectly synchronized RPs, TOA positioning requires advanced signal processing techniques to achieve highly accurate position estimates and it suffers greatly from blockage of direct path [75]. Hence other methods might be considered for ease and practicality at the cost of inferior position estimate.

In the next sections we will focus on RSS based positioning and present empirical results obtained by using a commercial cellular network in both urban and suburban areas in MA, USA.

C.3   Cellular positioning

Cellular positioning can be considered as a complementary approach to both GPS and WiFi based solutions. Worldwide availability of cellular systems make them an ideal platform for deploying location based services and hence they have also been studied by other researchers for LBS [148], [149]. Even though the accuracy of these systems can be considered inferior to that of GPS, the penetration of cellular signals is much better since they are land based systems. This provides better indoor availability for location based services. GPS on the other hand falls short of expectations in dense urban areas and inside buildings. Some services available through cellular positioning are zone-based billing, location aware social networking, tracking, personnel, asset or fleet management and location specific traffic, news, and advertisement.

C.3.1   Cellular positioning methods

There are a number of methods available for deploying a cellular based positioning system. These methods can be briefly given as:

1. CID

2. Geometric Methods such as TOA, TDOA and AOA

3. Fingerprinting

CID: CID method is the simplest method that can be used to determine location. It is based on the cell tower location the mobile handset is connected to. For this method to be applicable, a database consisting of ground truth coordinates of cell tower is needed. This database can either be obtained from the operator for which this application is to be deployed, or extensive scanning can be done to estimate cell tower locations based on maximum signal strength.

Each GSM cell tower usually carries three 120 degree sectors usually pointing in northeast, south and northwest directions respectively. Each sector has a unique CID and the sectors on the same tower are numbered sequentially based on their operating band.

Geometric Methods: Geometric methods rely on the availability of metrics (TOA, RSS) from multiple BSs. If TOA information is available from 3 BSs, it becomes possible to trilaterate handset position. This method is also used for GPS. The specific parameter available in GSM for timing is called the timing advance (TA). It takes on values in the range [0, 63] with each step representing one symbol advance, which is 3.69 us. Hence each change in this value approximately corresponds to a round trip distance of 1100m or one way distance of 550m. Although this is much worse compared to GPS standards, it can be combined with other methods such as RSS and CID to obtain better accuracy.

TDOA is an alternative to TOA and it does not need perfect synchronization between the MS and the BS. Time difference of the signal is calculated between the MS and 2 BSs. The time difference is constant on a hyperbola. Hence two hyperbolas are obtained and the intersection of these two hyperbolas gives the position fix.

RSS is another option to get distance estimate. As previously mentioned, there are numerous path loss models available in the literature obtained through various real-world measurements in urban/suburban areas. These models relate the path loss to distance, hence once a signal measurement is made, we can obtain the corresponding distance. However, since these models are considered to be deterministic models, they are not flexible to cover a wide range of signal variations due to obstructions hence might easily give erroneous results. When multiple erroneous distance readings are used for position estimation (i.e via least-squares or a similar algorithm), resulting position error might be unacceptable for most cases.

Specific to GSM, RSS is reported in a RxLev format taking values in the range [0, 63] [150]. These values can be mapped directly to dBm values as follows:

$$P(dBm) = RxLev - 110 \tag{C.5}$$

Hence the maximum and minimum values that can be reported are $Max = 63 - 110 = -47$ dBm and $Min = 0 - 110 = -110$ dBm.

AOA can also be used for position determination and only two readings (from two distinct BSs) would theoretically be enough to obtain a position fix. However, for this method to be useful, MS should be able to detect the angle the signal is received at. This brings additional cost to handsets. Also, LOS signals are needed to avoid angle confusion.

Fingerprinting: Also known as database correlation or nearest-neighbor (NN), this is a method of scanning the landscape for all relevant signal information coupled with GPS data representing the coordinates of the parameters obtained at that location. This method requires intensive scanning in a given area but captures all channel related information. Hence, once a reading is taken, it is compared to all the possible entries in the database in the least squares sense and the GPS coordinates of the entry whose signal parameters are the closest is returned as the location estimate. This method requires periodic scanning

for keeping an up-to-date database. Mathematical details on this method will be presented later in this part.

C.3.2   Practical RSS positioning - A Real life testbed

RSS is fast becoming the choice for many positioning applications due to its ease of implementation and reasonable accuracy especially in fingerprinting methods.

For the purposes of this study, we have collected cellular information from AT&T's GSM network. To analyze the effectiveness of this method we have constructed an extensive RSS database in two different cities in MA, USA. Details on these areas will follow after a brief introduction to the scanning platform.

C.3.3   Scanning Platform

For the evaluation of the GSM positioning system, a platform developed by Skyhook Wireless has been used. The platform consists of 1 GSM/GPRS modem from Multitech (MTCBA-G-U-F4), 1 Globalsat USB GPS Unit (BU-353) with SiRF Star III and 1 ASUS EEE PC as the controller. Figure C.4 shows the setup for mobile data collection.
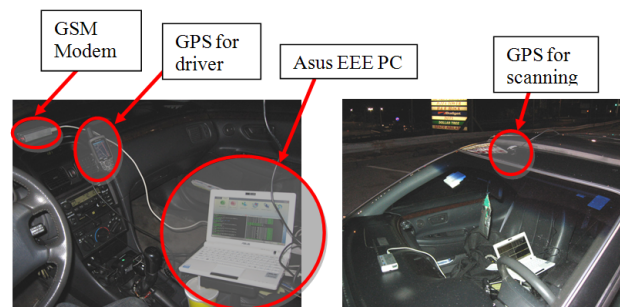
Figure C.4: Car setup for scanning

The scanning software written for this purpose runs on Linux on the ASUS PC and queries the GPS unit and the GSM modem at 1sec intervals. It then saves the data in two
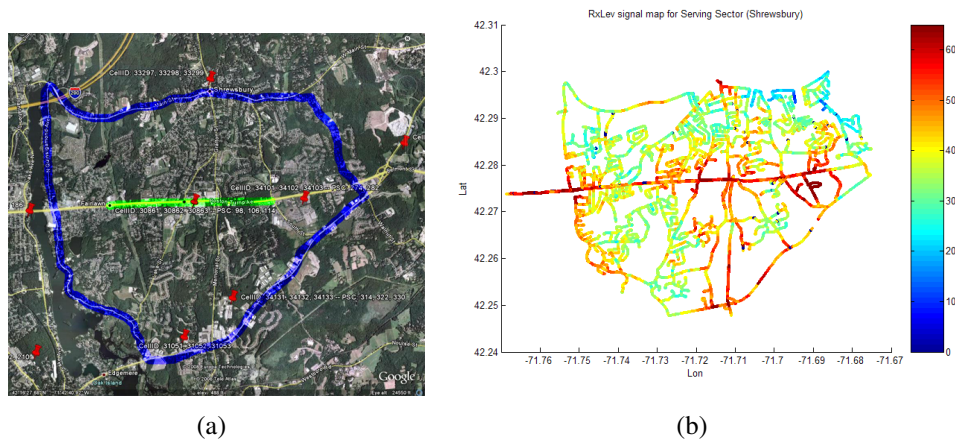
Figure C.5: (a) Shrewsbury, MA scan area - (b) Signal intensity map

separate log files time-stamped by PCs CPU time. The data is later analyzed for evaluation of different algorithms, which is explained in the performance evaluation section.

C.3.4 Scanned Areas

For the purpose of determining GSM positioning accuracy, we have chosen two different areas representing sparse suburban and densely populated urban test areas in MA, USA. Suburban area is chosen in Shrewsbury, MA and the urban area has been chosen to be in Boston (Backbay), MA.

The scanned area in Shrewsbury is given in figure C.5(a). The outer blue line represents the border of the scanned area and the straight green line represents the test route. This area can be considered as suburban since residences are usually spread out, and BSs are usually located at the top of cellular masts (marked with red pins in figure C.5(a)). This way, a large area can be serviced and the number of BSs is relatively low. The total scan area is approximately 26 km^2 and is serviced by about 8 cell towers corresponding to 24 CIDs. Figure C.5(b) shows the signal intensity map for the serving sector. It can also be interpreted as the coverage map for this area.

The scanned area in Boston (Backbay) is given in figure C.6(a). Similar to Shresbury
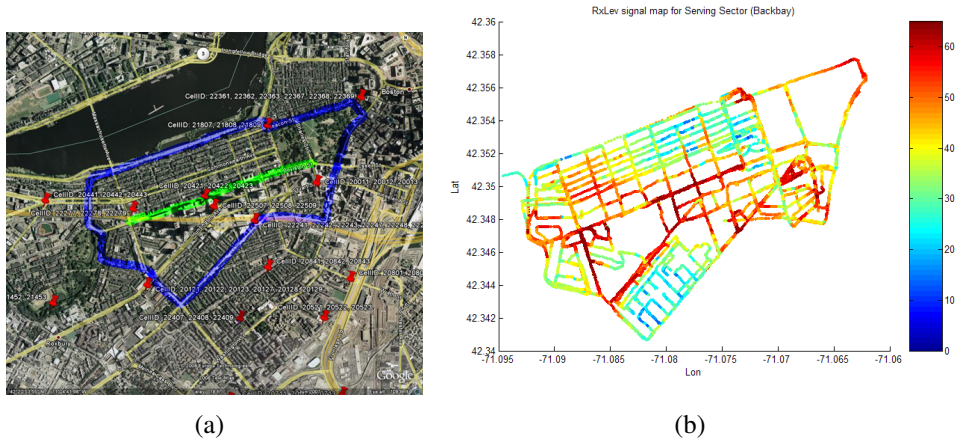
Figure C.6: (a) Boston (Backbay), MA scan area - (b) Signal intensity map

case, the outer blue line represents the border of the scanned area and the straight green line represents the test route. This area can be considered as dense urban with high rise buildings, shopping malls and stores concentrated in a relatively small area. BSs are usually located at the top of buildings or at the exterior walls to service street canyons (marked with red pins in figure C.6(a)). The total scan area is approximately 2.6 km^2 and is serviced by about 14 cell towers corresponding to 42 CIDs. Similar to Shrewsbury signal map, figure C.6(b) gives the signal intensity map for this area.

C.4   Performance Evaluation and Results

After obtaining synchronized GPS/GSM data for the aforementioned areas, we have investigated the performance of two cellular positioning algorithms. Namely, these algorithms are centroid and NN.

Centroid: Centroid is the simplest positioning algorithm and easiest to employ. When a mobile phone detects a certain number of sectors, its position is estimated as the geometric center of all the detected (L of them) and known tower locations. Mathematically this can be expressed as:

$$P_{est} = \frac{1}{L} \sum_{i=1}^{L} P_i \tag{C.6}$$

where P_{est} is the estimated mobile location and $P_i = [LonLat]$ is the GPS coordinates of the ith sector. The only information needed for this type of estimation is the CID readings from the mobile phone. If neighbor CIDs are not available, the coordinates of the serving sector is returned as the position estimate. This method can also be considered an improvement over the CID only method since averaging is done over multiple available cell towers.

Nearest Neighbor(NN): Also called as closest neighbor (CN), NN is an extensive database solution where we compare the signal print of the mobile terminal against a prerecorded database of signal prints. Each print has specific GPS coordinates and associated CIDs together with received signal powers associated with each of these CIDs. After a full scan is performed in an area of interest, related parameters are stored in the database. Whenever a fix is requested, CIDs and corresponding signal powers are sent from the mobile station to the database server and server returns the coordinates of the print which is closest to the submitted parameters. This is essentially the fingerprinting method as mentioned earlier and can be expressed as:

$$P_{est} = \left[P_s | s = \underset{n}{\operatorname{argmin}} \sum_{i=1}^{ } (f_i - g_i(n))^2 \right] \tag{C.7}$$

Here f_i is the RSS for the ith CID and $g_i(n)$ is the RSS of the ith CID for nth reference fingerprint. P_s is the GPS coordinate for the fingerprint s with the lowest argument.

A version of nearest neighbor is the K-NN in which we select K reference prints with minimum argument and take the average of their database coordinates as the estimate instead of just choosing the minimum. For Shrewsbury we have chosen $K = 50$ and $K = 30$ for Boston for minimum mean error. K values need to be adjusted for different
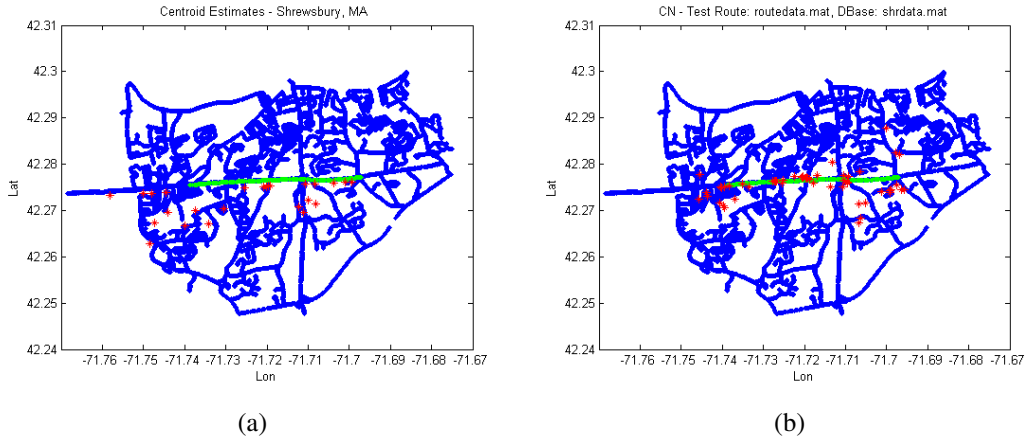
Figure C.7: Shrewsbury, MA (a) Centroid Estimation - (b) Nearest-Neighbor Estimation, K = 50

areas and for different requirements.

Figure C.7(a) and figure C.7(b) show the comparative centroid and K-NN estimation results for Shrewsbury. Likewise C.8(a) and figure C.8(b) show the centroid and K-NN estimation results for Boston.

Figure C.9(a), and C.9(b) show the comparative CDF for centroid and NN for Shrewsbury and Boston respectively. We can see from the figures that K-NN is an effective solution for both urban and suburban areas compared to centroid, although its suburban performance might not be acceptable for some applications. In the suburban Shrewsbury we observe about 316m of error for the NN and about 1km for the centroid for 50 percentile. When we consider the dense urban area of Backbay in Boston we see about 70m error at the 50 percentile using NN whereas it is about 296m for centroid for the same percentile. Urban results are much better since the deployment of cellular towers are denser and hence allows for a more refined signal map. This might particularly be useful for situations for which GPS fails to work like in urban canyons or indoors.
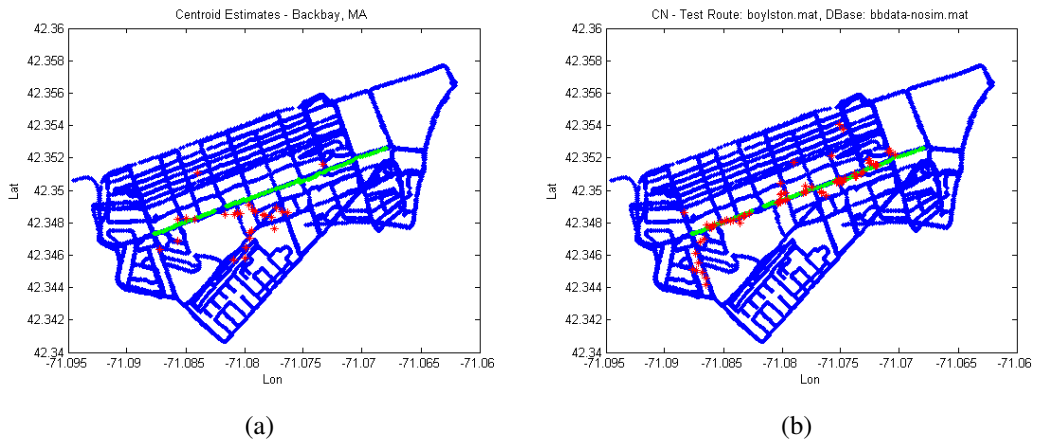
Figure C.8: Boston (Backbay), MA (a) Centroid Estimation - (b) Nearest-Neighbor Estimation, K = 30
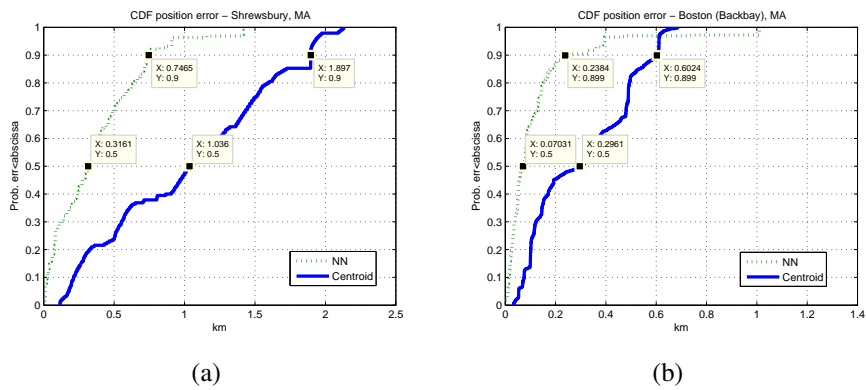
Figure C.9: (a) CDF for Shrewsbury NN and Centroid Estimation - (b) CDF for Boston NN and Centroid Estimation

C.5   Conclusions

In this appendix we have studied the effectiveness of cellular positioning by investigating two common positioning methods namely centroid and nearest neighbor. Our findings show that, in dense urban environments cellular positioning can be quite accurate and hence can be a good enough complement to GPS. Hence LBS using everyday mobile phones can easily be realized using the commercial cellular networks.

Bibliography

[1] R. Schroer, "Navigation and landing [a century of powered flight 1903-2003]," *IEEE Aerospace and Electronic Systems Magazine*, vol. 18, no. 7, pp. 27–36, 2003.

[2] E. D. Kaplan, *Understanding GPS Principles and Applications*. Boston: Artech House Publishers, 1996.

[3] H. Blomenhofer, G. Hein, E. Blomenhofer, and W. Werner, "Development of a real-time dgps system in the centimeter range," in *IEEE Position, Location, and Navigation Symposium*, (Las Vegas, NV), pp. 532–539, Oct 1994.

[4] D. Kim and R. B. Langley, "Gps ambiguity resolution and validation: Methodologies, trends and issues," in *7th GNSS Workshop-International Symposium on GPS/GNSS*, (Seoul, Korea), 2000.

[5] T. C. Poling and A. Zatezalo, "Interferometric gps ambiguity resolution," *Journal of Engineering Mathematics*, vol. 43, pp. 135–151, 2002.

[6] A. S. Zaidi and M. R. Suddle, "Global navigation satellite systems: A survey," in *International Conference on Advances in Space Technologies*, pp. 84–87, Sept. 2006.

[7] US Federal Communications Commission, "Fcc announcement of commision action. acts to promote competition and public safety in enhanced wireless 911 services." http://www.fcc.gov/Bureaus/Wireless/News_Releases/1999/nrwl9040.html, 1999.

[8] B. V. Dasarathy, *Nearest Neighbor (NN) Norms: NN Pattern Classification Techniques*. Los Alamitos, CA: IEEE Computer Society, Dec. 1991.

[9] M. Kanaan and K. Pahlavan, "Algorithm for toa-based indoor geolocation," *IEE Electronics Letters*, vol. 40, pp. 1421–1422, Oct 2004.

[10] C. Nerguizian, C. Despins, and C. Affs, "Geolocation in mines with an impulse fingerprinting technique and neural networks," *IEEE Transactions on Wireless Communications*, vol. 5, pp. 603–611, Mar 2006.

[11] M. Heidari, F. O. Akgul, N. Alsindi, and K. Pahlavan, "Neural network assisted identification of the absence of the direct path in indoor localization," in *IEEE Globecom 2007*, pp. 387–392, 2007.

[12] K. Pahlavan, P. Krishnamurthy, and J. Beneat, "Wideband radio propagation modeling for indoor geolocation applications," *IEEE Commun. Mag.*, April 1998.

[13] J. Werb and C. Lanzl, "Designing a positioning system for finding things and people indoors," *IEEE Spectrum*, vol. 35, pp. 71–78, Sept. 1998.

[14] K. Pahlavan and A. Levesque, *Wireless Information Networks*. New York: Wiley, 2nd ed., 2005.

[15] P. Bahl and V. N. Padmanabhan, "Radar: An in-building rf-based user location and tracking system," in *Proc. IEEE INFOCOM*, (Tel Aviv, Israel), pp. 775–784, 2000.

[16] R. Fontana, "Advances in ultra wideband indoor geolocation systems," in *3rd IEEE Wksp. WLAN*, (Boston, MA), Sept. 2001.

[17] S. Gezici et al., "Localization via ultra-wideband radios," *IEEE Signal Process. Mag.*, vol. 22, pp. 79–84, July 2005.

[18] B. Alavi and K. Pahlavan, "Modeling of the distance measure error using uwb indoor radio measurement," *IEEE Communication Letters*, vol. 10, pp. 275–277, April 2006.

[19] B. Fidan and G. Mao, eds., *Localization Algorithms and Strategies for Wireless Sensor Networks*, pp. 54–95. IGI Global, first ed., 2009.

[20] K. Pahlavan et al, "Indoor geolocation in the absence of direct path," *IEEE Wireless Communications Magazine*, vol. 13, pp. 50–58, December 2006.

[21] M. Kanaan, F. O. Akgul, B. Alavi, and K. Pahlavan, "Performance benchmarking of toa-based uwb indoor geolocation systems using mse profiling," in *IEEE VTC*, (Montreal, Canada), Sept. 2006.

[22] M. Kanaan, F. O. Akgul, B. Alavi, and K. Pahlavan, "A study of the effects of reference point density on toa-based uwb indoor positioning systems," in *IEEE PIMRC*, (Helsinki, Finland), Sept. 2006.

[23] M. Heidari, *Dynamic Behavior and Detection of Direct Path for Indoor Geolocation*. PhD thesis, Worcester Polytechnic Institute, Worcester, MA, 2008.

[24] F. O. Akgul and K. Pahlavan, "Aoa assisted nlos error mitigation for toa-based indoor positioning systems," in *IEEE MILCOM*, (Orlando, FL), 2007.

[25] F. O. Akgul and K. Pahlavan, "High precision ranging using temporal tdoa and multipath tracking in the absence of direct path," in *ION GNSS*, (Fort Worth, TX, USA), Sept. 2007.

[26] F. O. Akgul and K. Pahlavan, "Path persistency for high precision ranging in different building architectures," in *IEEE PIMRC*, (Athens, GR), Sept. 2007.

[27] Y. Ye, F. Akgul, and K. Pahlavan, "Dynamic behavior of uwb channel pertinent to indoor geolocation," in *IEEE ICUWB*, (Vancouver, Canada), Sept. 2009.

[28] Y. Ye, F. Akgul, and K. Pahlavan, "Effect of bandwidth, path detection threshold and udp occurrence on multipath parameters pertinent to indoor geolocation," in *IEEE WAMICON*, (Clearwater, FL), April 2009.

[29] F. O. Akgul and K. Pahlavan, "A new ray optical statistical model for multipath characteristics pertinent to indoor geolocation," in *IEEE WCNC*, (Budapest, Hungary), April 2009.

[30] F. O. Akgul and K. Pahlavan, "A novel statistical aoa model pertinent to indoor geolocation," *Journal of Geographic Information System*, vol. 2, pp. 45–48, Jan 2010.

[31] F. O. Akgul and K. Pahlavan, "Model for spatial behavior of multipath components pertinent to indoor geolocation using ray optics," *Submitted to IEEE Vehicular Transactions*, 2009.

[32] F. O. Akgul and K. Pahlavan, "A new spatial path persistency model for toa-based indoor geolocation," *IEEE Communications Letters*, vol. 13, pp. 248–250, April 2009.

[33] F. Akgul and K. Pahlavan, "Location awareness for everyday smart computing," in *ICT*, (Marrakech, Morocco), May 2009.

[34] A. J. Motley, "Radio coverage in buildings," in *Proc. National Communications Forum*, (Chicago, IL), pp. 1722–1730, 1988.

[35] Joint Technical Committee for PCS T1 R1P1.4, Technical Report on RF Channel Characterization and System Deployment Modeling, JTC (AIR)/94.09.23-065R6.

[36] Y. Okumura et al., "Field strength and its variability in vhf and uhf land-mobile radio service," *Review of the Electrical Communication Laboratory*, vol. 16, no. 9-10, 1968.

[37] M. Hata, "Empirical formula for propagation loss in land mobile radio services," *IEEE Trans. in Veh. Technology*, vol. 29, pp. 317–325, Aug. 1980.

[38] COST 231, "Urban transmission loss models for mobile radio in the 900- and 1,800 mhz bands (revision 2)." COST 231 TD(90)119 Rev. 2, 1991.

[39] Y. Qi and H. Kobayashi, "On relation among time delay and signal strength based geolocation methods," in *IEEE Global Telecommunications Conference*, (Chicago, IL), pp. 4079–4083, 2003.

[40] M. Cedervall and R. L. Moses, "Efficient maximum likelihood doa estimation for signals with known waveforms in the presence of multipath," *IEEE Transactions on Signal Processing*, vol. 45, no. 3, pp. 808–811, 1997.

[41] H. Krim and M. Viberg, "Two decades of array signal processing research: The parametric approach," *IEEE Signal Processing Magazine*, vol. 13, pp. 67–94, 1996.

[42] R. R. Kumaresan and D. W. Tufts, "Estimating the angles of arrival of multiple plane waves," *IEEE Trans. Aerosp. Electron. Syst.*, vol. AES-19, no. 1, pp. 134–139, 1983.

[43] J. Li, B. Halder, and P. Stoica, "Computationally efficient angle estimation for signals with known waveforms," *IEEE Transactions on Signal Processing*, vol. 43, no. 9, pp. 2154–2163, 1995.

[44] P. Stoica and K. Sharman, "Novel eigenanalysis method for direction of arrival estimation," *Proc. IEE*, vol. 137, pp. 19–26, Feb. 1990.

[45] A. H. Tewfik and W. Hong, "On the application of uniform linear array bearing estimation techniques to uniform circular arrays," *IEEE Transactions on Signal Processing*, vol. 40, pp. 1008–1011, 1992.

[46] S. A. Schelkunoff, "A mathematical theory of linear arrays," *Bell System Technical Journal*, vol. 22, pp. 80–107, 1943.

[47] R. Schmidt, "Multiple emitter location and signal parameter estimation," *IEEE Transactions on Antennas and Propagation*, vol. AP-34, no. 3, pp. 276–280, 1986.

[48] R. Roy and T. Kailath, "Esprit-estimation of signal parameters via rotational invariance techniques," *IEEE Transactions on Signal Processing*, vol. 37, no. 7, pp. 984–995, 1989.

[49] B. D. Rao and K. V. S. Hari, "Performance analysis of root-music," *IEEE Transactions on Acoustics, Speech and Signal Processing*, vol. 37, pp. 1939–1949, Dec. 1989.

[50] B. Ottersten, M. Viberg, and T. Kailath, "Performance analysis of the total least squares esprit algorithm," *IEEE Trans. on Signal Processing*, vol. 39, pp. 1122–1135, May 1991.

[51] A. Kuchar, M. Tangemann, and E. Bonek, "A real-time doa-based smart antenna processor," *IEEE Transactions on Vehicular Technology*, vol. 51, pp. 1279–1293, Nov. 2002.

193

[52] R. Tingley, *Time-Space Characteristics of Indoor Radio Channel*. PhD thesis, Worcester Polytechnic Institute, Worcester, MA, 2000.

[53] J. Lee and R. Scholtz, "Ranging in a dense multipath environment using an uwb radio link," *IEEE J. Sel. Areas Commun.*, vol. 20, no. 9, pp. 1677–1683, 2002.

[54] Y. Qi, H. Suda, and H. Kobayashi, "On time-of arrival positioning in a multipath environment," in *IEEE 60th Vehicular Technology Conf.*, vol. 5, (Los Angeles, CA), pp. 3540–3544, 2004.

[55] X. Li, *Super-Resolution TOA Estimation with Diversity Techniques for Indoor Geolocation Applications*. PhD thesis, Worcester Polytechnic Institute, Worcester, MA, 2003.

[56] C. Knapp and G. Carter, "The generalized correlation method for estimation of time delay," *IEEE Transactions on Acoustics, Speech and Signal Processing*, vol. 24, no. 4, pp. 320–327, 1976.

[57] X. Li and K. Pahlavan, "Super-resolution toa estimation with diversity for indoor geolocation," *IEEE Transactions on Wireless Communications*, vol. 3, no. 1, pp. 224–234, 2004.

[58] L. Dumont, M. Fattouche, and G. Morrison, "Super-resolution of multipath channels in a spread spectrum location system," *IEE Electronic Letters*, vol. 30, no. 19, pp. 1583–1584, 1994.

[59] B. Denis, J. Keignart, and N. Daniele, "Impact of nlos propagation upon ranging precision in uwb systems," in *IEEE Conference on Ultra Wideband Systems and Technologies*, 2003.

[60] I. Oppermann, M. Hamalainen and J. Linatti (Eds.), *UWB Theory and Applications*. England: John Wiley and Sons, 2004.

[61] C. Steiner, F. Althaus, F. Troesch, and A. Wittneben, "Ultra-wideband geo-regioning: A novel clustering and localization technique," *EURASIP Journal on Advances in Signal Processing*, Nov. 2008.

[62] A. Hatami and K. Pahlavan, "A comparative performance evaluation of rss-based positioning algorithms used in wlan networks," in *Proceedings of the IEEE Wireless Communications and Networking Conference*, (New Orleans, LA), pp. 2331–2337, 2005.

[63] T. Roos, P. Myllymaki, and H. Tirri, "A statistical modeling approach to location estimation," *IEEE TRANSACTIONS ON MOBILE COMPUTING*, vol. 1, no. 1, pp. 59–69, 2002.

194

[64] R. E. Kalman, "A new approach to linear filtering and prediction problems," *Transactions of the ASME - Journal of Basic Engineering*, vol. 82, pp. 35–45, 1960.

[65] S. Haykin, *Adaptive Filter Theory - 4th Ed.* Prentice-Hall, 2001.

[66] S. J. Julier and J. K. Uhlmann, "A new extension of the kalman filter to nonlinear systems," in *Proc. SPIE*, vol. 3068, (Orlando, FL), pp. 182–193, 1997.

[67] S. Beauregard, "A helmet-mounted pedestrian dead reckoning system," in *Proceedings of the 3rd International Forum on Applied Wearable Computing*, (Bremen, Germany), pp. 79–89, 2006.

[68] C. Randell, C. Djiallis, and H. Muller, "Personal position measurement using dead reckoning," in *Proceedings of the Seventh International Symposium on Wearable Computers*, (White Plains, NY, USA), pp. 166–173, Oct.

[69] M. P. Wylie and J. Holtzman, "The non-line of sight problem in mobile location estimation," in *5th IEEE International Conference on Universal Personal Communications*, (Cambridge, MA, USA), pp. 827–831, Sep.

[70] G.L. Turin et al., "A statistical model of urban multipath propagation," *IEEE Transactions on Vehicular Technology*, vol. 21, pp. 1–9, Feb 1972.

[71] B. Alavi and K. Pahlavan, "Indoor geolocation distance error modeling with UWB channel measurements," in *IEEE Personal Indoor Mobile Radio Communications Conference (PIMRC)*, 2005.

[72] W. H. Foy, "Position-location solutions by Taylor-series estimation," *IEEE Trans. Aerospace and Elect. Sys.*, March 1976.

[73] D. Torrieri, "Statistical theory of passive location systems," *IEEE Trans. Aerospace and Elect. Sys.*, vol. AES-20, March 1984.

[74] P. Deng and P. Fan, "An AOA assisted TOA positioning system," in *IEEE WCC-ICCT2000*, 2000.

[75] K. Pahlavan, X. Li, and J. Makela, "Indoor geolocation science and technology," *IEEE Commun. Mag.*, February 2002.

[76] B. Alavi and K. Pahlavan, "Studying the effect of bandwidth on performance of UWB positioning systems," in *Proceedings of the IEEE Wireless Communications and Networking Conference (WCNC)*, 2006.

[77] B. Alavi and K. Pahlavan, "Bandwidth effect of distance error modeling for indoor geolocation," in *IEEE Personal Indoor Mobile Radio Communications Conference (PIMRC)*, 2003.

195

[78] M. Unbehaun, *On the Deployment of Unlicensed Wireless Infrastructure*. PhD thesis, Royal Institute of Technology,Department of Signals, Sensors & Systems, Stockholm, 2002.

[79] M. Kanaan and K. Pahlavan, "Algorithm for TOA-based indoor geolocation," *IEE Electronics Letters*, vol. 40, October 2004.

[80] M. Kanaan and K. Pahlavan, "CN-TOAG: A new algorithm for indoor geolocation," in *IEEE Personal Indoor Mobile Radio Communications Conference*, 2004.

[81] W. C. Davidon, "Variance algorithm for minimization," *Computer Journal*, vol. 10, 1968.

[82] US Federal Communications Commission, "Revision of part 15 of the commissions rules regarding ultra-wideband transmission systems." FCC 02-48, First Report & Order, April 2002.

[83] M. Kanaan and K. Pahlavan, "A comparison of wireless geolocation algorithms in the indoor environment," in *IEEE Wireless Communications and Networking Conference*, 2004.

[84] C. Savarese, J. Rabaey, and J. Beutel, "Locationing in distributed ad-hoc wireless sensor networks," in *IEEE International Conference on Acoustics Sensors and Signal Processing (ICASSP)*, 2001.

[85] K. Chintalapudi et al, "Ad-hoc localization using ranging and sectoring," in *IEEE INFOCOM*, 2004.

[86] R. Stoleru and J. A. Stankovic, "Probability Grid: A location estimation scheme for wireless sensor networks," in *IEEE SECON*, 2004.

[87] S. Gezici, H. Kobayashi, and H. V. Poor, "Nonparametric non line-of-sight identification," in *IEEE Vehicular Technology Conference*, vol. 4, pp. 2544–2548, October 2003.

[88] M. Heidari and K. Pahlavan, "A model for dynamic behavior of ranging errors in TOA-based indoor geolocation systems," in *IEEE Vehicular Technology Conference*, pp. 1–5, September 2006.

[89] M. Heidari and K. Pahlavan, "A new statistical model for the behavior of ranging errors in TOA-based indoor localization," in *IEEE Wireless Communications and Networking Conference*, March 2007.

[90] A. F. Molisch, "Statistical properties of the RMS delay-spread of mobile radio channels with independent rayleigh-fading paths," *IEEE Transactions on Vehicular Technology*, vol. 45, pp. 201–204, February 1996.

[91] H. Hashemi and D. Tholl, "Analysis of the RMS delay spread of indoor radio propagation channels," in *IEEE International Conference on Communciations*, vol. 43, pp. 110–120, February 1994.

[92] T. S. Rappaport, S. Y. Seidel, and R. Singh, "900-MHz multipath propagation measurements for US digital cellular radiotelephone," *IEEE Transactions on Vehicular Technology*, vol. 39, pp. 132–139, May 1990.

[93] M. Kanaan et al, "Technical aspects of localization in indoor wireless networks," *Bechtel Telecommunications Technical Journal*, vol. 5, pp. 47–58, December 2006.

[94] P.-C. Chen, "A non-line-of-sight error mitigation algorithm in location estimation," in *IEEE Wireless Communications and Networking Conference*, 1999.

[95] J. Elwell, "Reliable geolocation through partial environment modeling," in *15th Virginia Tech/MPRG Symp. Wireless Pers. Commun.*, (Blacksburg, VA, USA), June 2005.

[96] D. E. Gustafson, J. M. Elwell, and J. A. Soltz, "Innovative indoor geolocation using rf multipath diversity," in *IEEE/ION Position, Location, And Navigation Symposium*, 2006.

[97] J. Dowdle, D. Gustafson, and J. Elwell, "Geographical navigation using multipath wireless navigation signals." US Patent no. 6,693,592, Feb. 2004.

[98] E. Falletti, L. L. Presti, and F. Sellone, "Sam lost smart-antennas based movable localization system," *IEEE Trans. Vehicular Technology*, vol. 55, no. 1, pp. 25–42, 2006.

[99] C. R. Rao, C. R. Sastry, and B. Zhou, "Tracking the direction of arrival of multiple moving targets," *IEEE Trans. Signal Processing*, vol. 42, pp. 1133–1144, May 1994.

[100] R. H. J. M. Otten, "Automatic floorplan design," in *Proc. 19th ACM/IEEE Design Automation Conf.*, pp. 261–267, 1982.

[101] D. F. Wong and C. L. Liu, "A new algorithm for floorplan design," in *Proceedings of the 23rd ACM/IEEE Design Automation Conference*, (Las Vegas, NV, USA), pp. 101–107, May 1986.

[102] W. Shi, "An optimal algorithm for area minimization of slicing floorplans," in *ACM/IEEE International Conference on Computer-Aided Design (ICCAD)*, (Denton, TX, USA), pp. 480–484, Nov. 1995.

[103] E.-C. Liu, M.-S. Lin, J. Lai, and T.-C. Wang, "Slicing floorplan design with boundary-constrained modules," in *Proceedings of the 2001 International Symposium on Physical Design*, (Sonoma, CA, USA), pp. 124–129, Nov. 2001.

197

[104] J. Berntsson and M. Tang, "A slicing structure representation for the multi-layer floorplan layout problem," in *Lecture Notes in Computer Science*, (Coimbra, Portugal), pp. 188–197, Apr. 2004.

[105] M. G. D. Rio-Cidoncha, J. E. Iglesias, and J. Martinez-Palacios, "A comparison of floorplan design strategies in architecture and engineering," *Automation in Construction*, vol. 16, pp. 559–568, Aug. 2007.

[106] B. Alavi et al, "Indoor geolocation distance error modeling using UWB technology," in *Proceedings of IASTED, 2nd International Conference on Communication and Computer Networks*, 2004.

[107] E. D. Zand, K. Pahlavan, and J. Beneat, "Frequency domain measurement for indoor geolocation," in *IEEE Personal Indoor Mobile Radio Communications Conference (PIMRC)*, vol. 3, pp. 2213–2217, Sep. 2003.

[108] J. Beneat, K. Pahlavan, and P.Krishnamurthy, "Radio channel characterization for indoor and urban geolocation at different frequencies," in *Proc. IEEE PIMRC*, (Osaka, Japan), Sept. 1999.

[109] "ER1 Personal Robot System." `http://www.evolution.com/er1/`.

[110] R. B. Blackman and J. W. Tukey, *The Measurement of Power Spectra, From the Point of View of Communications Engineering*. New York: Dover, 1958.

[111] T. Rappaport, S. Seidel, and K. Takamizawa, "Statistical channel impulse response models for factory and openplan building radio communicate system design," *IEEE Trans. Communications*, vol. 39, pp. 794–807, May 1991.

[112] H. Hashemi, "Impulse response modeling of indoor radio propagation channels," *IEEE J. on Sel. Areas in Comm.*, vol. 11, pp. 967–978, Sep 1993.

[113] Chia-Chin Chong et al., "A novel wideband dynamic directional indoor channel model based on a markov process," *IEEE Trans. Wireless Communications*, vol. 4, Jul 2005.

[114] P. Krishnamurthy, *Analysis and Modeling of the Wideband Radio Channel for Indoor Geolocation Applications*. PhD thesis, Worcester Polytechnic Institute, Worcester, MA, 1999.

[115] B. Alavi, *Distance Measurement Error Modeling for Time-of-Arrival Based Indoor Geolocation*. PhD thesis, Worcester Polytechnic Institute, Worcester, MA, 2006.

[116] N. Alsindi, *Indoor Cooperative Localization for Ultra Wideband Wireless Sensor Networks*. PhD thesis, Worcester Polytechnic Institute, Worcester, MA, 2008.

[117] J. C. Liberti and T. S. Rappaport, "A geometrically based model for line-of-sight multipath radio channels," in *IEEE Veh. Tech. Conf.*, pp. 844–848, 1996.

198

[118] R. B. Ertel and J. H. Reed, "Angle and time of arrival statistics for circular and elliptical scattering models," *IEEE JSAC*, vol. 17, pp. 1829–1840, November 1999.

[119] P. Petrus, J. Reed, and T. Rappaport, "Geometrical-based statistical macrocell channel model for mobile environments," *IEEE Transactions on Communications*, vol. 50, pp. 495–502, March 2002.

[120] H. Suzuki, "A statistical model for urban radio propogation," *IEEE Transactions on Communications*, vol. 25, pp. 673–680, July 1977.

[121] H. Suzuki, "Simulation of the urban radio propagation channel," *IEEE Transactions on Vehicular Technology*, vol. 28, pp. 213–225, Aug 1979.

[122] A. Saleh and R. A. Valenzuela, "A statistical model for indoor multipath propagation," *IEEE Journal on Selected Areas in Comm.*, vol. 5, Feb 1987.

[123] R. Ganesh and K. Pahlavan, "Statistical modeling and computer simulation of indoor radio channel," *IEE Proceedings on Communications, Speech and Vision*, vol. 138, Jun 1991.

[124] P. Yegani and C. D. McGillem, "A statistical model for the factory radio channel," *IEEE Transactions on Communication*, vol. 39, pp. 1445–1454, October 1991.

[125] Q. Spencer, M. Rice, B. Jeffs, and M. Jensen, "A statistical model for angle of arrival in indoor multipath propagation," in *IEEE 47th Vehicular Technology Conf.*, vol. 3, (Phoenix, AZ), pp. 1415–1419, May 1997.

[126] Quentin Spencer et al., "Modeling statistical time and angle of arrival characteristics of an indoor multipath channel," *IEEE Journal on Selected Areas in Comm.*, vol. 18, Mar 2000.

[127] M. Hassan-Ali and K. Pahlavan, "A new statistical model for site-specific indoor radio propagation prediction based geometric optics and geometric probability," *IEEE Trans. Wireless Communications*, vol. 1, Jan 2002.

[128] D. Cassioli, M. Win, and A. Molisch, "The ultra-wide bandwidth indoor channel: From statistical model to simulations," *IEEE Journal in Selected Areas in Comm.*, vol. 20, pp. 1247–1257, August 2002.

[129] S. Ghassemzadeh, R. Jana, C. Rice, W. Turin, and V. Tarokh, "Measurement and modeling of an ultra-wide bandwidth indoor channel," *IEEE Transactions on Communications*, vol. 52, pp. 1786–1796, Oct 2004.

[130] Nielsen et al., "A dynamic model of the indoor channel," *Wireless Personal Communications*, vol. 12, Nov 2001.

199

[131] Thomas Zwick et al., "A stochastic multipath channel model including path directions for indoor environments," *IEEE Journal on Selected Areas in Comm.*, vol. 20, Aug 2002.

[132] H. Lee et al., "Multipath characteristics of impulse radio channels," in *Proc. IEEE VTC 2000*, pp. 2487–2491, 2000.

[133] M. Z. Win and R. A. Scholtz, "On the robustness of ultra- wide bandwidth signals in dense multipath environments," *IEEE Communication Letters*, vol. 2, pp. 51–53, February 1998.

[134] H. Bertoni, W. Honcharenko, L. R. Maciel, and H. Xia, "Uhf propagation prediction for wireless personal communications," *Proceedings of the IEEE*, vol. 82, pp. 1333–1359, Sep 1994.

[135] R. Valenzuela, "A ray tracing approach to predicting indoor wireless transmission," in *Proc. IEEE VTC 1993*, pp. 214–218, 1993.

[136] S. Y. Seidel and T. S. Rappaport, "A ray tracing technique to predict path loss and delay spreadinside buildings," in *IEEE Global Telecommunications Conference*, (Orlando, FL), pp. 649–653, Dec 1992.

[137] F. A. Agelet, F. P. Fontan, and A. Formella, "Fast ray-tracing for microcellular and indoor environments," *IEEE Trans. Magn.*, vol. 33, pp. 1484–1487, Mar 1997.

[138] Y.-H. Jo, J.-Y. Lee, D.-H. Ha, and S.-H. Kang, "Accuracy enhancement for uwb indoor positioning using ray tracing," in *Proc. IEEE/ION PLANS 2006*, (San Diego, CA), pp. 565–568, 2006.

[139] Z. Yang, J. W. Hardin, and C. L. Addy, "A score test for overdispersion in poisson regression based on the generalized poisson-2 model," *Journal of Statistical Planning and Inference*, vol. 139, no. 4, pp. 1514 – 1521, 2009.

[140] S. F. Mahmoud and J. R. Wait, "Geometrical optical approach for electromagnetic wave propagation in rectangular mine tunnels," *Radio Sci.*, vol. 9, pp. 1147 – 1158, December 1974.

[141] W. Q. Malik, C. J. Stevens, and D. J. Edwards, "Spatio-temporal ultrawideband indoor propagation modelling by reduced complexity geometric optics," *IET Communications*, vol. 1, pp. 751 – 759, August 2007.

[142] A. Papoulis and S. U. Pillai, *Probability, Random Variables and Stochastic Processes*. New York: McGraw-Hill, 4th ed., 2002.

[143] J. F. Lawless, *Statistical models and methods for lifetime data*. New York: Wiley, 1982.

[144] R. C. Gupta, O. Akman, and S. Lvin, "A study of log-logistic model in survival analysis," *Biometrika Journal*, vol. 41, pp. 431–443, August 1999.

[145] T. Holt, K. Pahlavan, and J. Lee, "A graphical indoor radio channel simulator using 2d ray tracing," in *IEEE PIMRC*, (Boston, USA), pp. 411–416, Oct 1992.

[146] G. German, Q. Spencer, A. Swindlehurst, and R. Valenzuela, "Wireless indoor channel modeling: Statistical agreement of ray tracing simulations and channel sounding measurements," in *IEEE Intl. Conf. Acoustics, Speech, Signal Processing*, vol. 4, (Salt Lake City, UT), pp. 778–781, May 2001.

[147] JTC (Joint Technical Committee for PCS T1 R1P1.4). (1994). Technical Report on RF Channel Characterization and System Deployment Modeling, JTC(AIR)/94.09.23-065R6.

[148] M. Chen et al., "Practical metropolitan-scale positioning for GSM phones," in *Proceedings of Ubicomp*, (Orange County, CA, USA), 2006.

[149] A. LaMarca et al., "Place lab: device positioning using radio beacons in the wild," in *Proceedings of the third international conference on pervasive computing*, (Munich, Germany), 2005.

[150] 3GPP TS05.08 V8.23.0, Radio subsystem link control (Release 1999), 2005-11.